

BNL-NUREG 28707

INFORMAL REPORT

~~LIMITED DISTRIBUTION~~

7/1/80

OFFICIAL FILE COPY

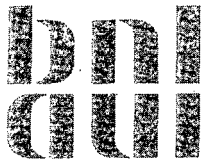
ORECA CODE ASSESSMENT

PETER G. KROEGER

~~LIMITED DISTRIBUTION~~

JULY 1980

DEPARTMENT OF NUCLEAR ENERGY BROOKHAVEN NATIONAL LABORATORY
UPTON, NEW YORK 11973



Prepared for the U.S. Nuclear Regulatory Commission
Office of Nuclear Regulatory Research
Contract No. DE-AC02-76CH00016

NOTICE

This report was prepared as an account of work sponsored by the United States Government. Neither the United States nor the United States Nuclear Regulatory Commission, nor any of their employees, nor any of their contractors, subcontractors, or their employees, makes any warranty, express or implied, or assumes any legal liability or responsibility for the accuracy, completeness or usefulness of any information, apparatus, product or process disclosed, or represents that its use would not infringe privately owned rights.

7/10/80

ORECA Code Assessment

Peter G. Kroeger

July 1980

HTGR Safety Division
Department of Nuclear Energy
Brookhaven National Laboratory
Associated Universities, Inc.
Upton, New York 11973

NOTICE: This document contains preliminary information and was prepared primarily for interim use. Since it may be subject to revision or correction and does not represent a final report, it should not be cited as reference without the expressed consent of the author(s).

ABSTRACT

Results of an assessment of the ORECA code are being presented. In particular it was found that in the case of loss of forced flow circulation the predicted peak core temperatures are very sensitive to the mean gas temperatures used in the evaluation of the pressure drop terms. Some potential shortcomings of the conduction algorithm for some specific applications are discussed.

The results of these efforts have been taken into consideration in the current version of the ORECA code.

TABLE OF CONTENTS

	<u>Page</u>
ABSTRACT	ii
1. INTRODUCTION	1
2. GENERAL OBSERVATIONS	1
3. RESULTS OF ORECA CODE EVALUATION	2
3.1 Temperature Dependence of Pressure Drop	2
3.2 Pressure Drop Equation.	4
3.3 Internodal Heat Conduction Algorithm.	4
4. CONCLUSION	5
APPENDIX A	7
APPENDIX B	11
APPENDIX C	63
NOTATION	73
REFERENCES	75

1. INTRODUCTION

An assessment of the ORECA code has been completed as part of our ongoing effort, to review the features and limitations of existing HTGR safety codes. The ultimate objective of the effort is to enhance confidence in these codes and increase their utility for licensing applications.

An earlier draft of this report was transmitted to Oak Ridge National Laboratory (ORNL) and its results have already been considered in current versions of the ORECA code. This report serves primarily as documentation of our code assessment efforts.

The ORECA version obtained from ORNL is written for the Fort St. Vrain reactor, and is documented in Reference 1. The code was reviewed primarily with the test case with which it was received: loss of forced flow circulation (LOFC) followed by firewater cooldown (FWCD).

Section 2 of this report contains some general observations. Section 3 summarizes the major results of this review effort. The sequence of code evaluations and local modifications which were made is given in essentially chronological sequence in Appendix A. Plots of some results are given in Appendix B. Appendix C describes some separate evaluations solving a specific idealized conduction problem in the ORECA HTGR core configuration.

None of the comments of this informal report are in any way meant to be critical of the authors of the ORECA code. Every code, having advanced to a given level, in response to specific problems, will have further restrictions and shortcomings when applied to new problems. This report will primarily outline areas where significant further code improvements can be obtained with little or moderate programming efforts, and outline situations, where application of the code in its present form can result in substantial uncertainties, due to its current modelling assumptions and limitations.

2. GENERAL OBSERVATIONS

The ORECA (Fort St. Vrain) code presents a three dimensional model of an HTGR core. The core is divided into 37 hexagonal refueling regions and 18 side reflectors. Each of these 55 regions is divided axially into nine nodes; one top reflector, seven active core nodes, one bottom reflector, and one core support block.

Inlet flow rate, inlet temperature, and inlet pressure to the core are prescribed functions of time (to be supplied as function type subroutines).

The code solves for the flow distribution to the 55 lateral regions, the overall pressure drop, and the coolant temperature change due to convection in each axial node of each flow channel. The temperature within the composite solid of each node is considered to be constant. The solid temperature change of each node due to internal heat generation, heat flow to the coolant, and due to conduction between nodes is being computed.

Most of the design and operating parameters are "hard wired" into the code and cannot be changed readily. For instance, the coolant passage diameter is neither an input, nor a constant given somewhere in the code, but is embedded in numerous numerical constants occurring in various executable statements. Without a detailed list, where this parameter is embedded in numerical constants it would be a major undertaking to change it, for instance, in order to evaluate the effect of such a design change. Such "hard wiring" increases computation speed, but it significantly reduces the flexibility of the code, and does not offer the generality of a general purpose code.

The desirability of program structure changes, to accept such basic design and operating parameters as input data or at least as one individual constant, depends on the envisioned future applications of the code.

3. RESULTS OF ORECA CODE EVALUATION

The most significant results of our evaluations of various aspects of the ORECA code are summarized in this section. A more complete and essentially chronological description of the code evaluations is given in Appendix A.

3.1 Temperature Dependence of Pressure Drop

The pressure drop and flow distribution are obtained from Equation 20 of Reference 1, which expresses the pressure drop of each channel and can be written as follows:

$$\begin{aligned} \Delta p_i &= \Delta p_{or_i} + \Delta p_{fr_i} + \Delta p_{accel_i} + \Delta p_{buoy_i} \\ &= K_{or_i} \frac{G_i |G_i|}{\rho_{i,inlet}} + \frac{4 \tilde{f}_i L}{D} \frac{G_i |G_i|}{2 \tilde{\rho}_i} \\ &\quad + \left(\frac{1}{\rho_{i,exit}} - \frac{1}{\rho_{i,inlet}} \right) G_i^2 - g \tilde{\rho}_i L \end{aligned} \quad (1)$$

The quantities \tilde{f} and $\tilde{\rho}$ are to be averaged over the coolant channel. For the evaluation of the coolant densities $\tilde{\rho}_i$ the code, in the version received, uses the solid node temperatures $[X(I,J)]$ rather than an average of the coolant temperatures $[T0(I,J)]$.

Within the code assumption of constant core temperature in each node the coolant temperatures will approach the core temperature exponentially as follows:

$$T_{fl}(x) = T_s + (T_{fl,in} - T_s) e^{-\left(\frac{A'U}{Wc_p}\right)x} \quad (2)$$

i.e. for large A and U or low W the coolant temperature will essentially reach the core temperature. However, the integrated average coolant temperature remains generally different from the solid temperature.

To assess the effect of the coolant temperatures via coolant densities on the channel pressure drop and the flow redistribution, and thus ultimately on core temperature, a set of three runs was made, all in the mode FINDEX (described in Appendix A). In the first run the solid temperature was used as average gas temperature; in the second run an arithmetic average of coolant inlet and exit temperature was used; and in the third run integrated average gas temperatures were used as follows:

For the friction term, where the temperature appears in the numerator:

$$T_{avg_{fr}} \equiv \frac{1}{L} \int_0^L T(x) dx = T_s + \frac{T_{fl_{in}} - T_{fl_{ex}}}{sL} \quad (3)$$

for the buoyancy term, where the temperature appears in the denominator:

$$\frac{1}{T_{avg_b}} \equiv \frac{1}{L} \int_0^L \frac{dx}{T(x)} = \frac{1}{T_s} \left[1 + \frac{1}{sL} \ln \left(\frac{T_{fl_{ex}}}{T_{fl_{in}}} \right) \right] \quad (4)$$

where

$$sL \equiv \frac{A'UL}{Wc_p} \quad (5)$$

For practical purposes these two logarithmic average temperatures were very close to each other.

The three runs are compared in Figures B-31 to B-50, giving results for channel 19, which is one of the two high temperature and low flow channels (No. 6 and 19) as well as for the maximum flow channel No. 28.

In the downward flow of a fluid being heated in various parallel channels at different rates, an unstable situation is incurred as the hotter channels will tend to get less flow, thereby becoming even hotter, and getting even less coolant flow, etc. With the use of average gas temperature, arithmetic or log mean, this effect is further strengthened, resulting in less flow in the hot channels (see Figures B-31), increased gas temperatures (Figures B-33 to 37) and ultimately in increased core temperatures (Figures B-41 to 45). The peak core temperatures shown in Figure B-50 are about 600°F higher towards the end of the transient if log mean gas temperatures are used, rather than solid temperatures, in the evaluation of the densities in the pressure drop terms. This appears to indicate, that due to the unstable flow situation, the flow distribution over the various parallel channels, and the ultimate core

temperature distributions depend very strongly on the fluid temperature distribution, and it may be warranted to use the more appropriate log mean temperature differences, even though their evaluation would slightly increase computer run times.

3.2 Pressure Drop Equation

The overall pressure drop and the flow distribution over the 37 parallel channels - each representing one refueling region - is obtained iteratively by solving Equation 1, the momentum equation, for each channel. It is important to note that in this equation the orifice and friction pressure drop terms will change sign ($\propto G|G|$), as the flow direction changes, while the momentum pressure drop term does not change sign, regardless of flow direction ($\propto G^2$). In the ORECA code, as received, all three terms were changing sign, i.e. were treated as $G|G|$. Thus, the momentum pressure drop is not accounted for properly during reverse flow. This provides for a much simpler solution algorithm, but is not strictly correct. The code subroutine SUMW was, therefore, modified, considering a change in sign in the friction and orifice pressure drop terms only. For the sample case the resulting changes were very minor, i.e. the momentum pressure drop always remained small with respect to the orifice and friction pressure drop terms. However, in transients in which low flow rates and large channel temperature rises persist for longer time periods, the momentum pressure drop would not remain negligible, and a corresponding code modification could become very essential.

3.3 Internodal Heat Conduction Algorithm

Considering the solid of each node as being at uniform temperature the energy equation for heat transfer between nodes can be expressed after lumping or spatial discretization as

$$M_{i,j} c_p(T_{i,j}) \frac{d}{dt} T_{i,j} = \sum_{\substack{\text{all} \\ \text{neighbors}}} \frac{k(T)A}{\Delta x} (T_{\text{neighbor}} - T_{i,j}) + Q_{\text{gen}} - Q_c$$

(6)

In this equation c_p and k are temperature dependent, as indicated.

Solution in the code is effected through an exponential algorithm (Equation 26 of Reference 1) rather than through conventional finite difference techniques. This exponential technique is, for instance, discussed for linear problems, i.e. for the case of constant material properties in Reference 2. As shown there it can be of some advantage in problems where heat conduction is of less importance than internal heat generation or convective heat transfer to the coolant.

The time constant for heat conduction in an HTGR reactor core is of the order of months: To reach a Fourier number of unit order

$$Fou = \frac{\alpha t}{L^2} \approx 1$$

with $k \approx 10 \frac{\text{BTU}}{\text{ft} \cdot \text{hr} \cdot \text{F}}$ and $c_p \approx .3 \frac{\text{BTU}}{\text{lb} \cdot \text{F}}$

and $L \approx 25 \text{ ft}$, as used in ORECA one requires a time of

$$t \approx \frac{L^2}{\alpha} = \frac{L^2 \rho c_p}{k} = \frac{625 \times 90 \times .3}{10} \approx 1900 \text{ hrs!}$$

This implies that temperature relaxation due to conduction within a core without coolant flow could require times of the order of 2000 hrs. Or, alternatively, that internal heat generation and heat transfer to the coolant within each node are significantly more essential than conduction for transients lasting several hours or even a few days. For such cases, the exponential method should give good results for linear problems (constant material properties), as discussed in Reference 2. However, in typical HTGR transients the temperature dependence of the specific heat and the thermal conductivity remains essential. This effect is only partially considered in the exponential algorithm as used in the ORECA code, where the local thermal conductivity was used at each node $k(T_{i,j})$, rather than an average value between the node and its respective neighbor, $k(T_{\text{avg}})$. Thus, the computed conduction heat flux between two nodes i_1 and i_2 will be different when used for the computation of nodal temperatures i_1 and i_2 , respectively.

For the test transient a corresponding code modification to use conductivities evaluated at an arithmetic average temperature between nodes resulted in core temperature changes of up to 180°F, as shown in Figures B-28 to B-30, and described in more detail in Section 4 of Appendix A. For a longer term idealized transient it is shown in Appendix C that the exponential algorithm in its present form cannot conserve energy and approaches a steady state solution more than 200°F lower than the correct solution.

The conductivity evaluation as currently used is much simpler and results in faster code execution than the algorithm using average temperatures between nodes. It might, therefore, be desirable to retain the current procedure for most runs, especially those of an exploratory nature. However, it would be desirable to permit as an option, with corresponding decrease in computational speed, the use of an alternate algorithm which uses an energy conserving average conductivity between nodes.

4. CONCLUSION

The ORECA code has been reviewed and tests performed on several of its algorithms. The resulting observations have been communicated to the original author for his consideration, as appropriate.

Appendix A

Sequence of ORECA Code Evaluation Runs

A.1 BASE

The ORECA code as received, with minor initialization changes, was executed at BNL. The output results were identical to those given for the ORNL sample test case. These results are labelled as "BASE" in this study.

A.2 MOD-BASE

The following changes were made to the BASE-version before prior code evaluations:

A.2.1 Reverse Flow Coolant Temperature

Subroutine CFLØW uses as coolant temperature at the upper end of the first node (j=1) the upper plenum temperature TIP. This is appropriate for downward flow, but not for the case of reverse flow. The code was modified to use in the case of reverse flow the outlet temperature of node j=1 in this position. Significant changes in results were only observed during flow reversal, with no major long term effects.

A.2.2 Reverse Flow in Inlet Flow Path

The code includes computations for the temperature rise in the inlet flow path from the steam generator outlet (TSGØ) to the upper plenum inlet (TINP). These computations were found to produce erroneous results in the case of reverse inlet flow (FT<0). The code was modified to account for reverse flow in the inlet flow path. Significant changes in results were only observed during flow reversal with no major long term effect. However, in using ORECA as part of a systems simulation, the resulting higher values of the steam generator outlet position temperature (TSGØ) could effect the steam generator performance.

A.2.3 Pressure Drop Algorithm

As described in the body of this report, the pressure drop algorithm was modified to retain the appropriate sign in the momentum pressure drop term. For the sample test case used here, no significant changes were observed. Nevertheless, as pointed out above, this change can lead to significant deviations in some transients of interest.

A.2.4 Convergence Tolerance in Flow Distribution Loop

Tightening of the convergence parameters in the loop for pressure drop and flow distribution from

absolute error = .1
relative error = .5%

to

absolute error = .001
relative error = .005%

resulted in some long term temperature changes of about 10°F and in some more significant short-time changes during flow reversal time.

The runs with the above four program modifications are labelled as MOD-BASE in this study. Their comparison to the BASE run is included in Figures B-1 to B-27. For the sample test case the MOD-BASE results differ from the BASE results only slightly in core and coolant temperatures, in particular in the long term response. Significant differences occur for short time periods only during reverse flow at the steam generator outlet position and at the upper plenum inlet position due to the modified reverse flow computations, see Figure B-23 and B-24.

A.3 MOD-REV

The temperatures used in the evaluation of the coolant densities were changed for the friction and buoyancy terms from the node solid temperature $X(I,J)$ to the average node coolant temperature $[1/2(TO(I,J) + T\emptyset(I,J-1))]$. At the same time in the orifice pressure drop the upper plenum temperature TIP was replaced by the coolant temperature at the top of the first node (see A.2.1). Execution of the sample test case with these modifications, was labelled MOD-REV.

Some of the output data are being compared to those of the BASE and MOD-BASE cases in Figures B-1 to B-27. Significant long term temperature changes are now being observed, exceeding 400°F in the core and coolant temperatures in the center of the hottest channel (see Figures B-6 and B-15 for the coolant and core temperatures of channel 19, node $j=5$). The peak core temperature rises by more than 200°F (see Figure B-27).

A.4 TEMPS Modifications

To compare the non-conservative exponential algorithm for heat conduction of the ORECA code with a conventional finite difference algorithm, modifications were made to solve for the solid temperature distribution in a subroutine which uses either the exponential algorithm as provided in the code (Mode=EXPO), or a conservative finite difference algorithm (Mode=FINDIM), or a slightly non-conservative but faster finite difference algorithm (Mode=FINDEX). The code as received considered property variations with temperature in the refueling regions using constant properties only in the side reflectors. An option was provided to either retain this procedure (IOPT=1) or to consider the properties to be temperature dependent in all nodes (IOPT=2).

The TEMPS runs Mode=EXPO, IOPT=1 did duplicate the MOD-REV results. Applying IOPT=2 vs IOPT=1, i.e. considering the temperature dependence of k and c_p , everywhere changes in the reflector temperatures of about 30°F were observed (Mode=EXPO). Decreasing the time step interval from $\Delta t=.5$ sec to $\Delta t=.1$ sec resulted in maximum temperature changes of about 30°F in the EXPO mode as well as in the FINDIM mode.

Much more significant temperature changes were observed when comparing runs made in the EXPO mode vs runs in the FINDIM or FINDEX mode (also referred to as FINDIF) both with IOPT=2 and $\Delta t=.1$. These changes are primarily due to the fact that the EXPO version evaluates all heat fluxes at a specific node based on the thermal conductivity at the temperature of that node. Thus, in this mode, as in the ORECA code received, the heat flux from node i to node j , used when computing temperature T_i is different from the flux between i and j used when computing T_j . This leads to non-conservation of energy and to the following temperature deviations.

The core and coolant outlet temperatures of channel 6, node 6, change by 180°F, as does the peak core temperature. These results are shown in Figures B-28 to 30.

A.5 Conduction Area Ratio in Axial Direction

The code, in the version received, uses an area ratio multiplier for thermal conduction in axial correction. As implemented with the current exponential algorithm this option would yield incorrect results for any value of AR other than 1.0. (In the current EXPO test runs only AR=1.0 was used.) The error arises as in an integration of Equation 6, leading to an equation similar to Equation 26 of Reference 1, the effect of $AR \neq 1$ would also be reflected in the first term on the right hand side of Equation 26, and not only in the second term, as it is currently implemented in the code.

The Fort St. Vrain core geometry would suggest that an area ratio of about 2.5 would be appropriate. One such run using the FINDIF mode, where the use of $AR \neq 1$ has been incorporated appropriately yielded only about 30°F in peak temperature changes, indicating that axial conduction was not very essential in the test case used. However, before future problems can be investigated in which axial conduction is expected to be more essential, the appropriate code modifications should be made.

Appendix B

In this appendix some of the results of the ORECA evaluations are shown. Figures B-1 to B-27 cover the cases BASE, MOD-BASE and MOD-REV of Appendix A. Typically, results are shown for the following characteristic channels*:

Channel No.	Radial Power Factor QR	Channel Flow Rate (lb/min)		Core Maximum Temperature and Axial Position (F)	
		t=0 min	t=240 min	t=0 min	t=240 min
6	1.83	2132	3.9	1905/7	2556/7
19	1.83	2132	2.8	1905/7	2603/7
20	.99	1153	.86	1848/7	2272/7
28	.56	1465	68	1269/7	930/9

Thus, the channels have the following characteristics:

6 and 19: Highest Q_R , highest temperatures at t=0 and t=240.
Highest flow at t=0; relatively low flow rate at t=240.

20 : Lowest flow rate at t=240.

28 : Highest flow rate at t=240.

Figures B-28 to B-30 give some results from the EXPO vs FINDIF runs. Figures B-31 to B-51 show results for the gas temperature variation in the pressure drop density terms of Equation 20 of Reference 1 (see Section 3 of this memorandum).

*Summary data from a typical run (FINDEX, log any gas temp., t=.1).

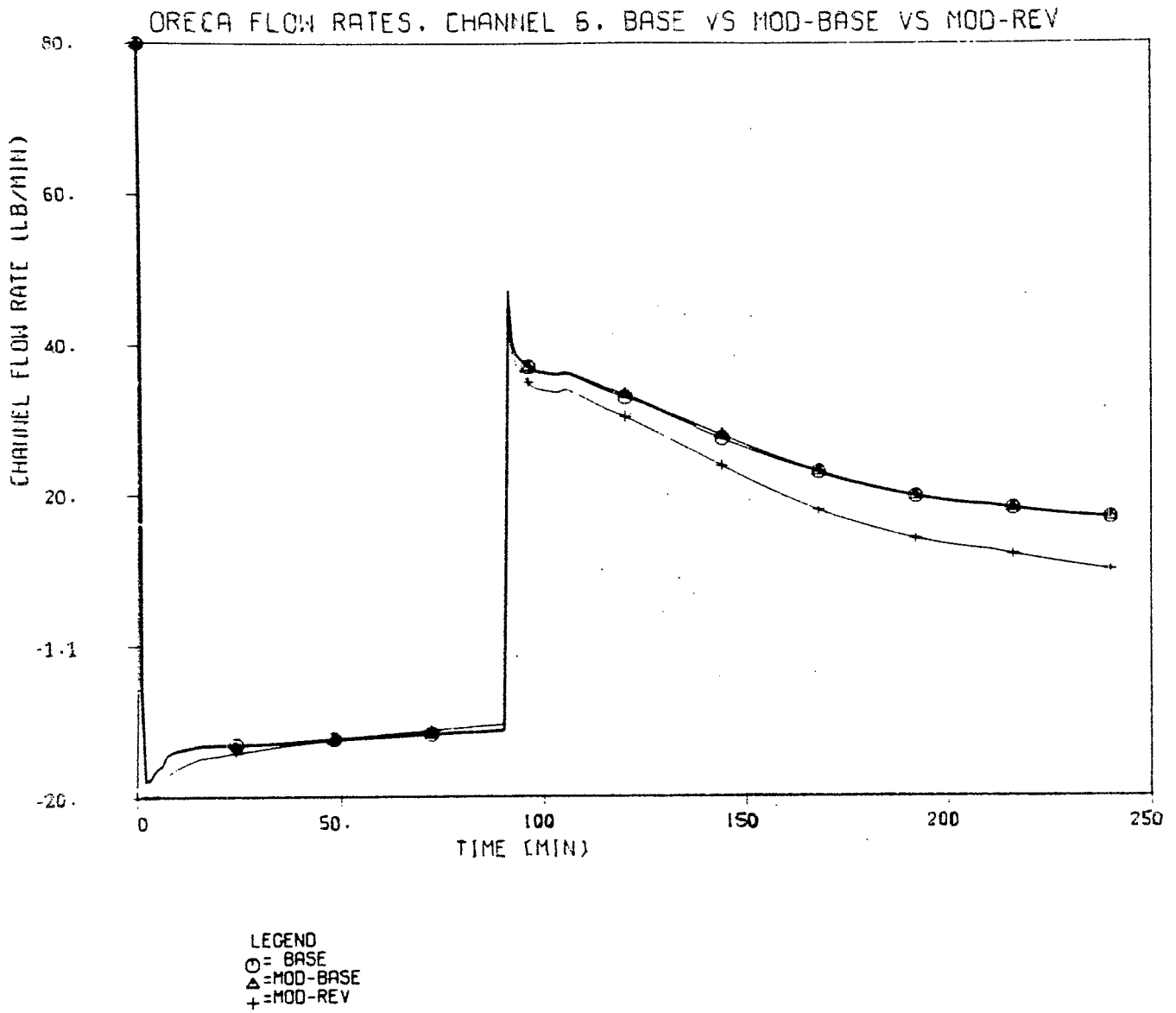


Figure B-1. Channel 6 flow rate for cases BASE, MOD-BASE, and MOD-REV.

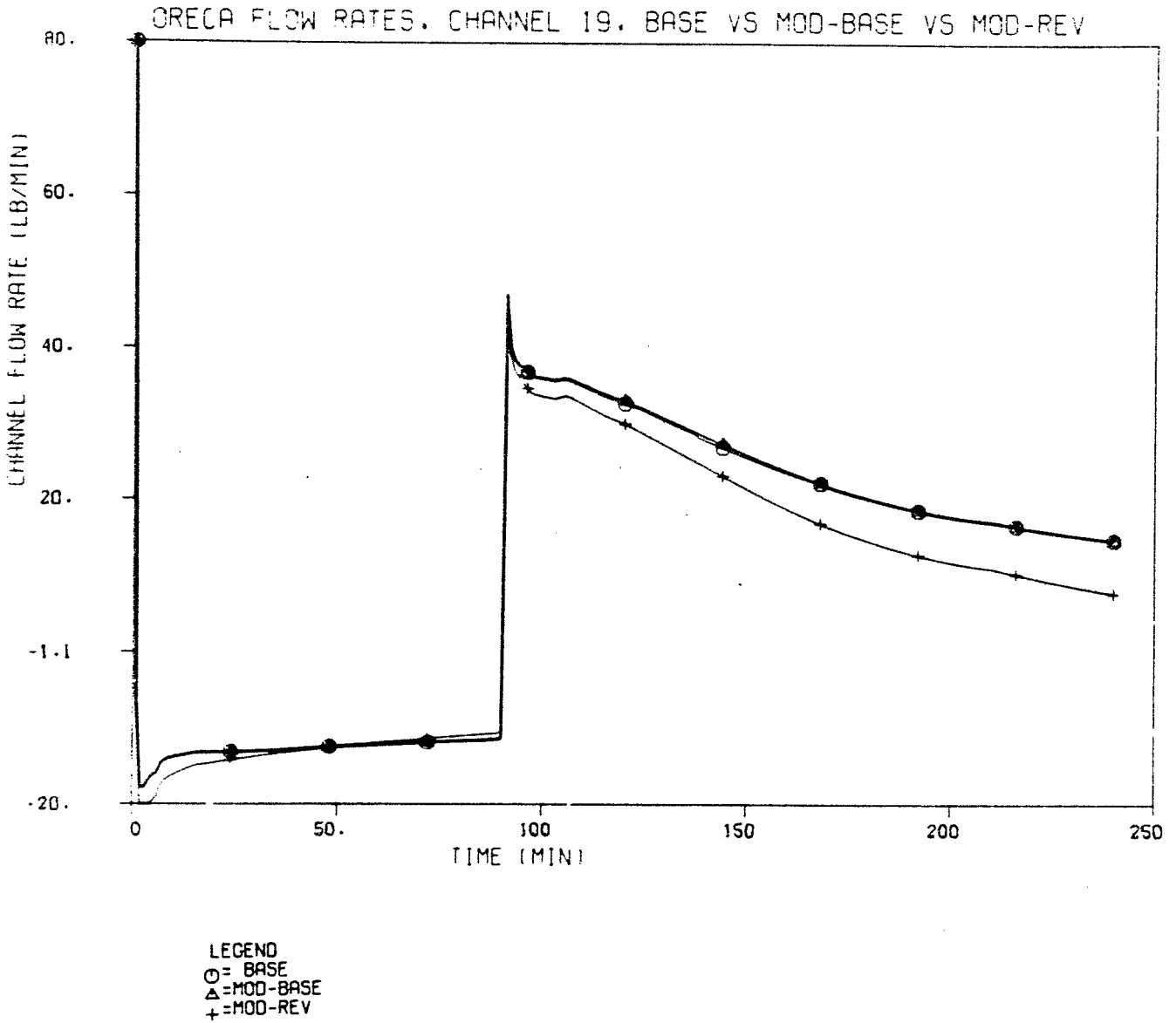


Figure B-2. Channel 19 flow rate for cases BASE, MOD-BASE, and MOD-REV.

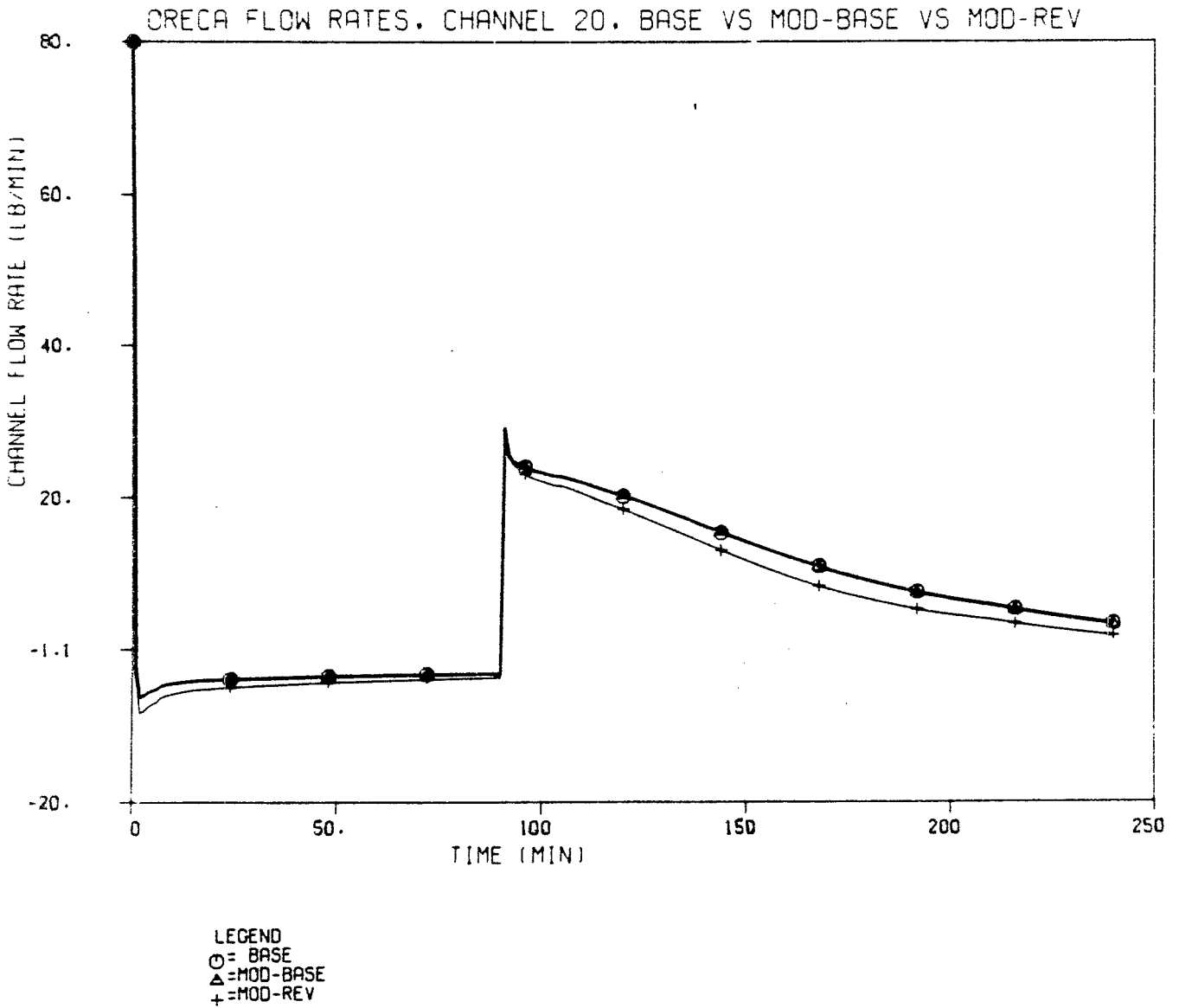


Figure B-3. Channel 20 flow rate for cases BASE, MOD-BASE, and MOD-REV.

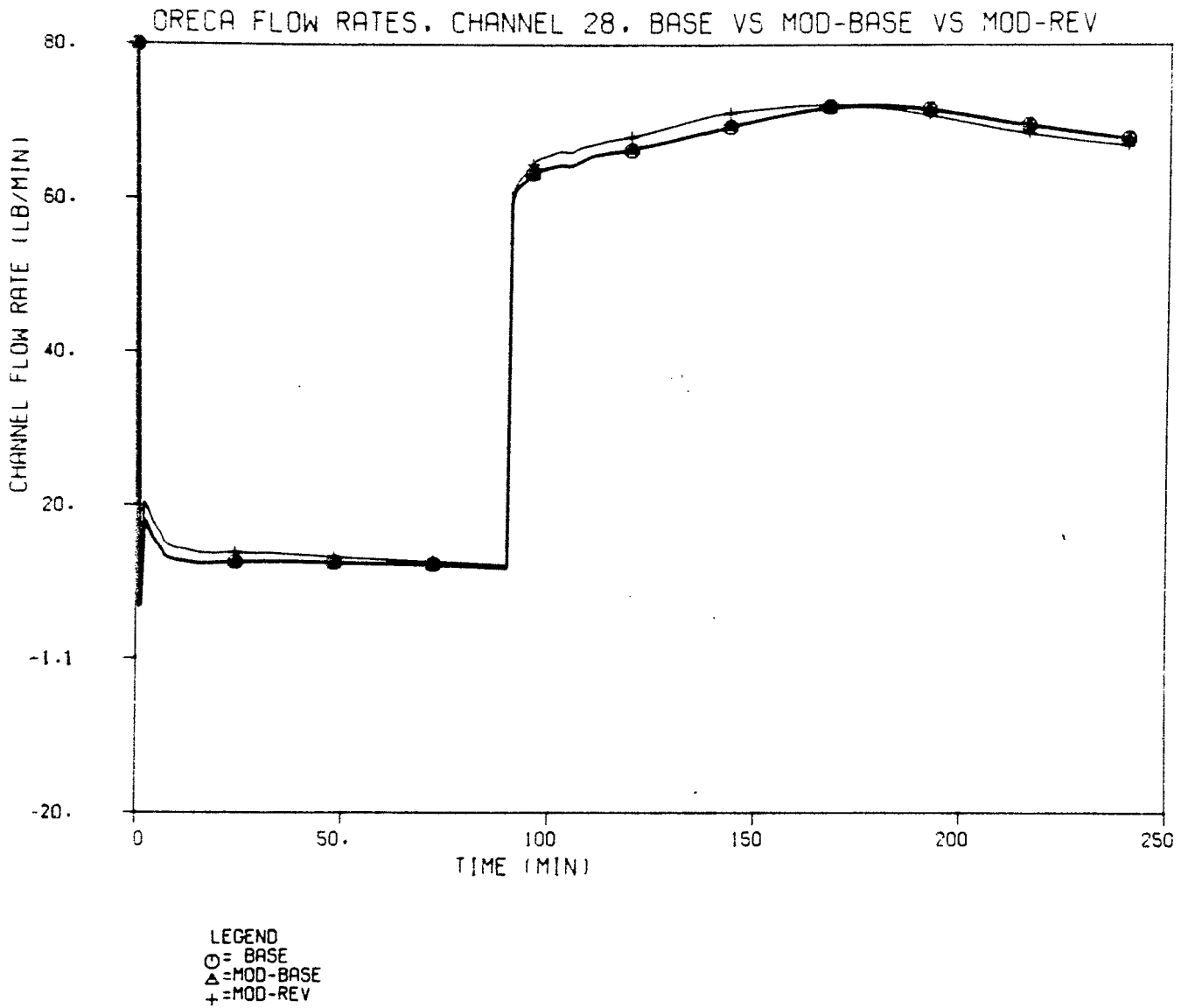


Figure B-4. Channel 28 flow rate for cases BASE, MOD-BASE, and MOD-REV.

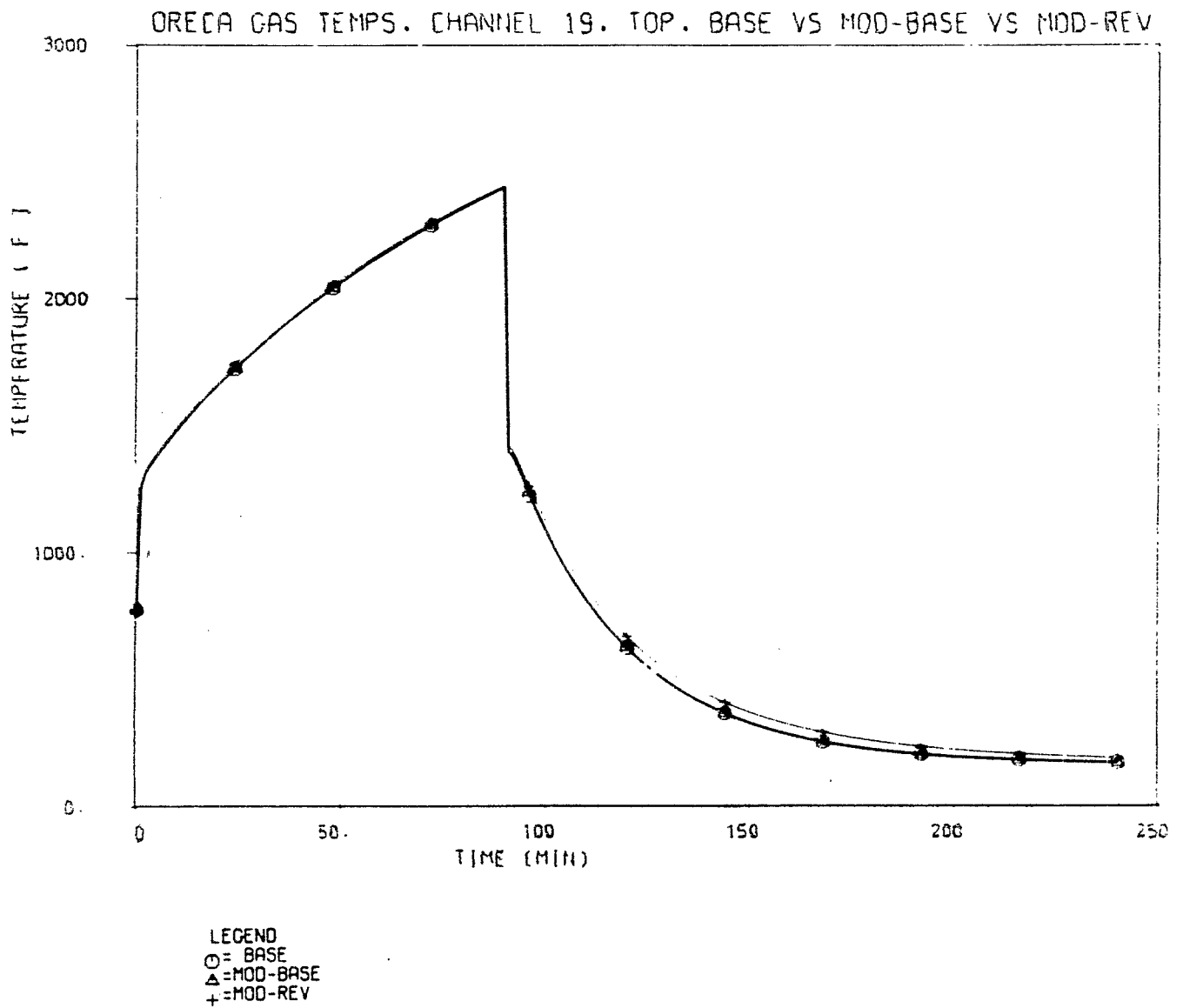
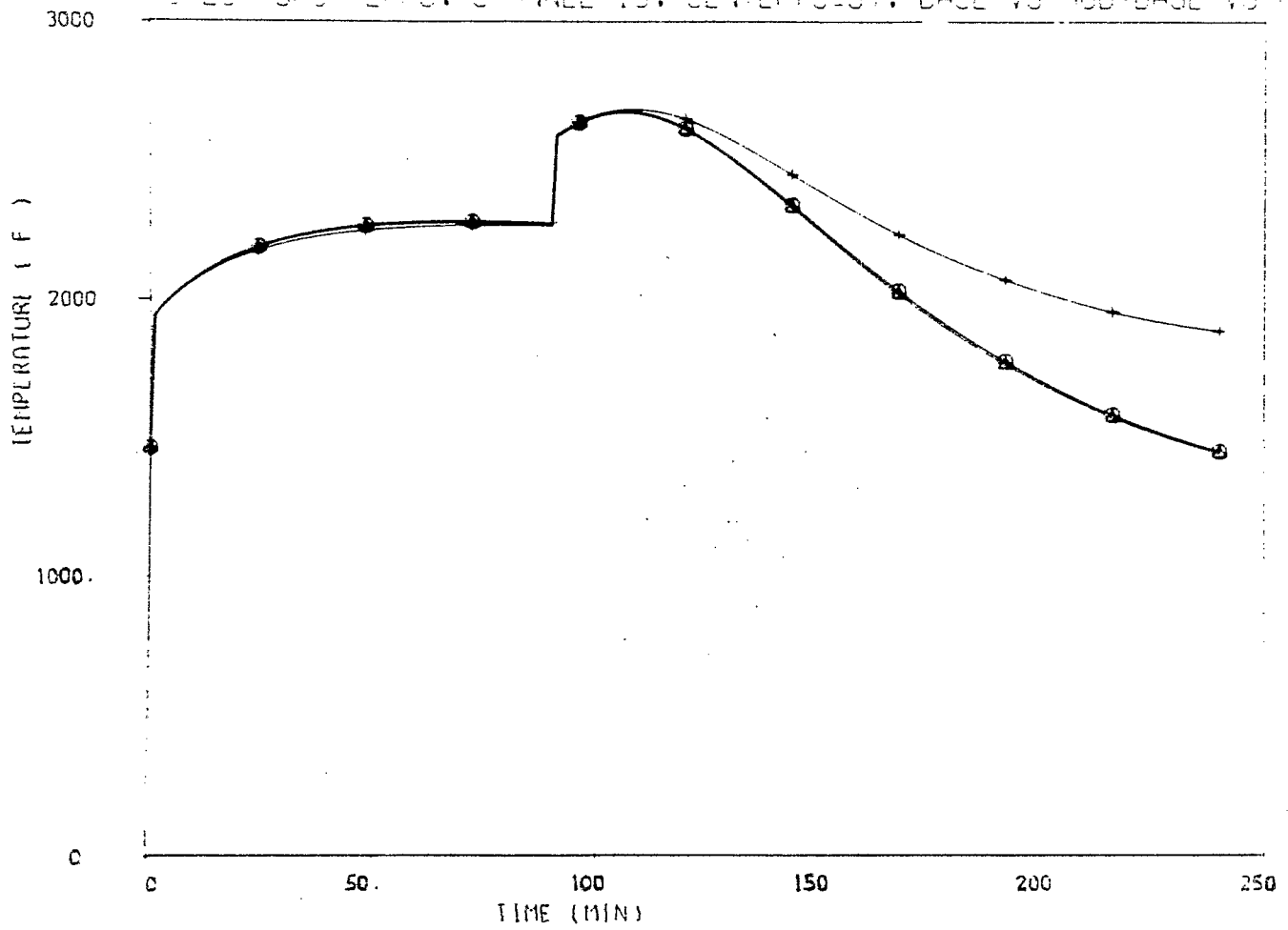


Figure B-5. Channel 19 gas outlet temperature at top node (J=1) for cases BASE, MOD-BASE, and MOD-REV.

OPERA GAS TEMPS. CHANNEL 19, CENTER (J=5), BASE VS MOD-BASE VS MOD-REV



LEGEND
 ○ = BASE
 △ = MOD-BASE
 + = MOD-REV

Figure B-6. Channel 19 gas outlet temperature at center node (J=5) for cases BASE, MOD-BASE, and MOD-REV.

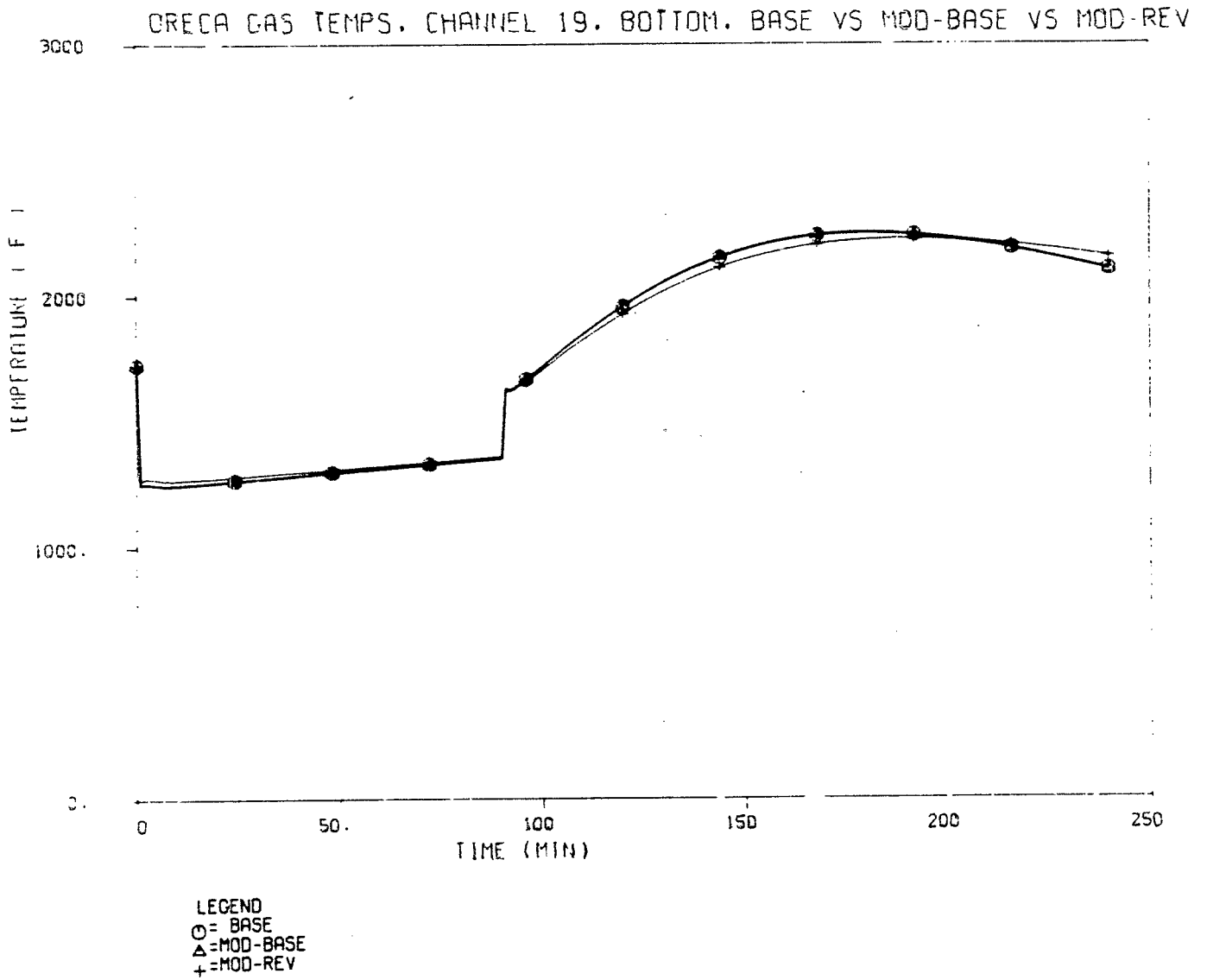


Figure B-7. Channel 19 gas outlet temperature at bottom node (J=8) for cases BASE, MOD-BASE, and MOD-REV.

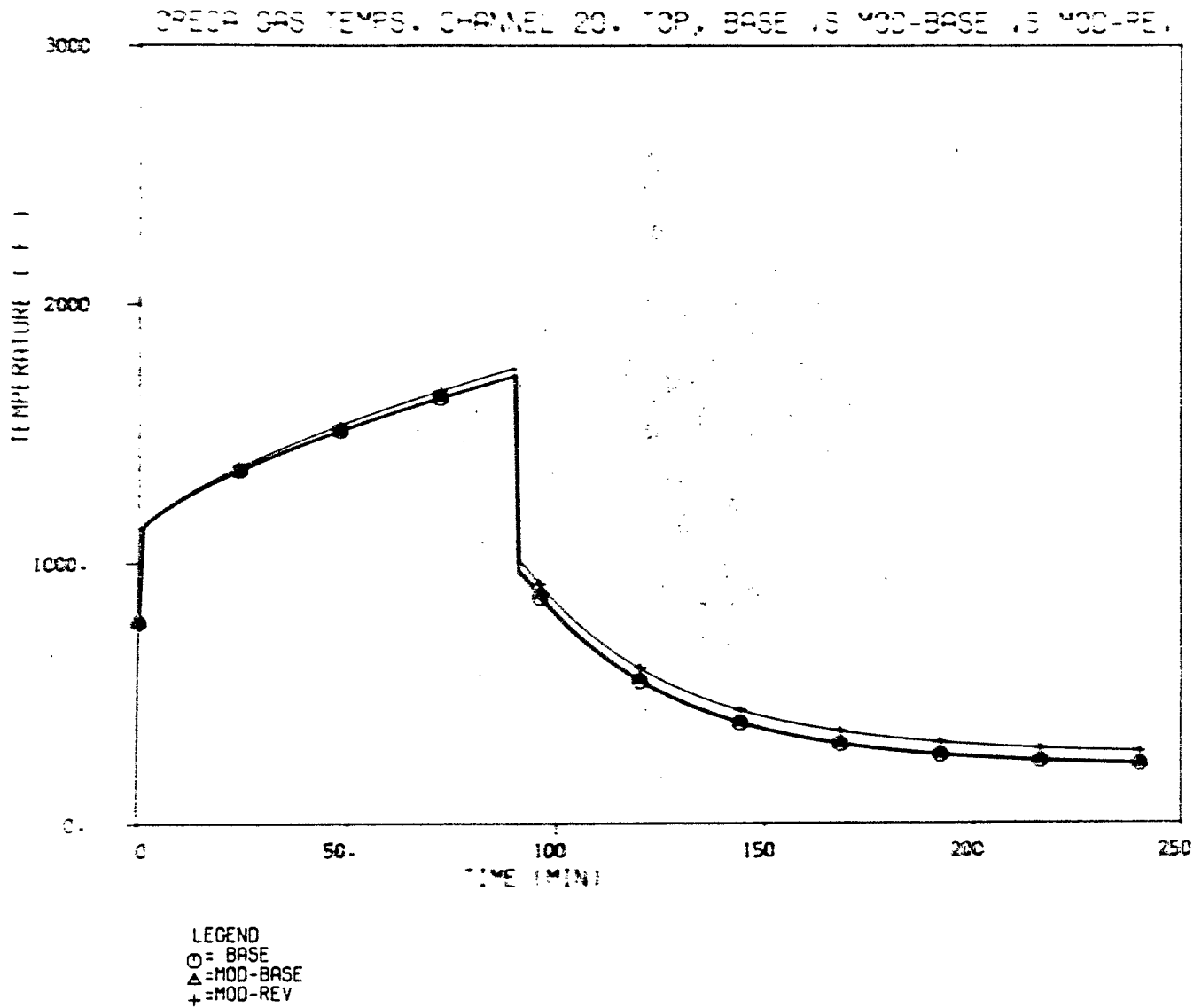


Figure B-8. Channel 20 gas outlet temperature at top node (J=1) for cases BASE, MOD-BASE, and MOD-REV.

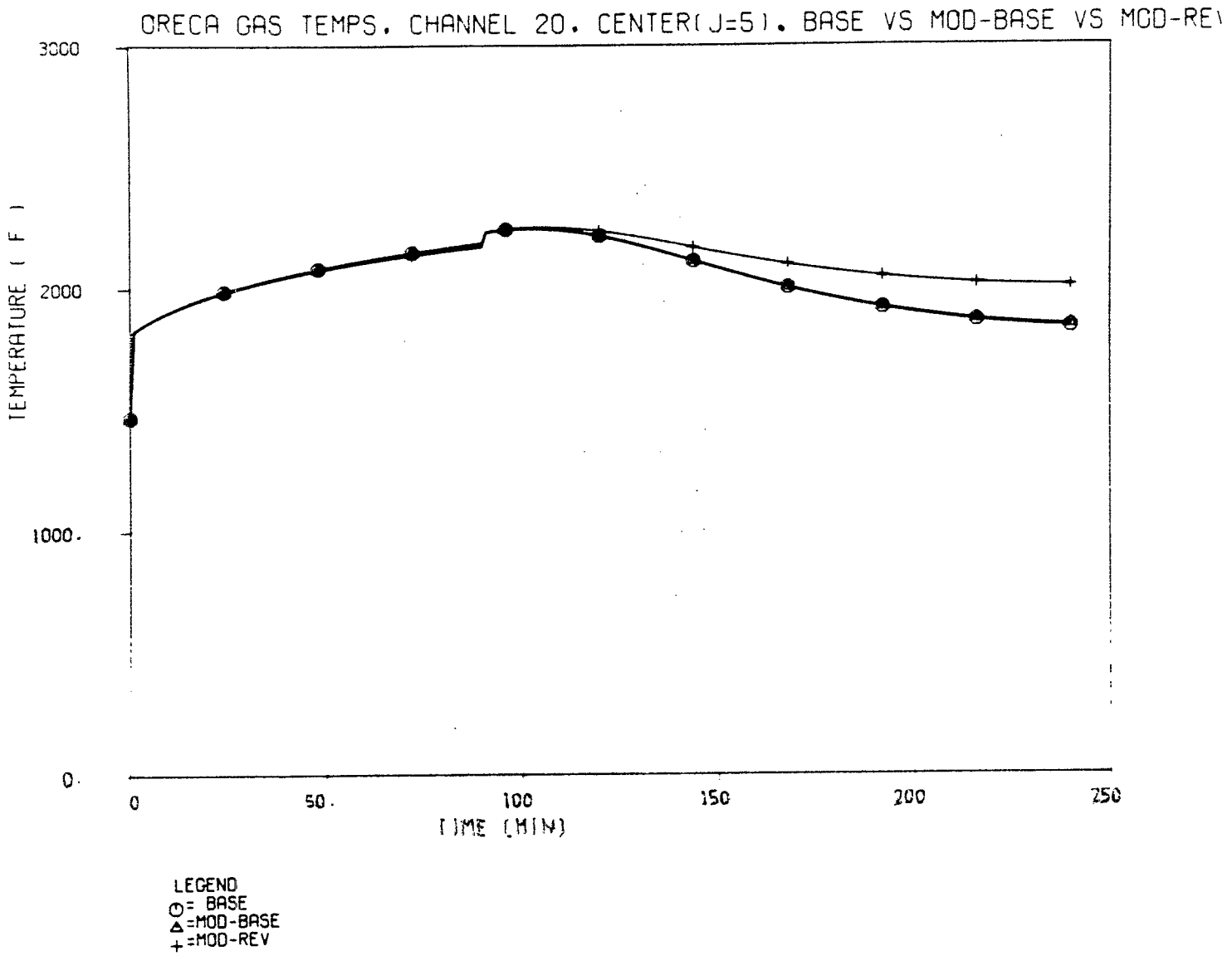


Figure B-9. Channel 20 gas outlet temperature at center node (J=5) for cases BASE, MOD-BASE, and MOD-REV.

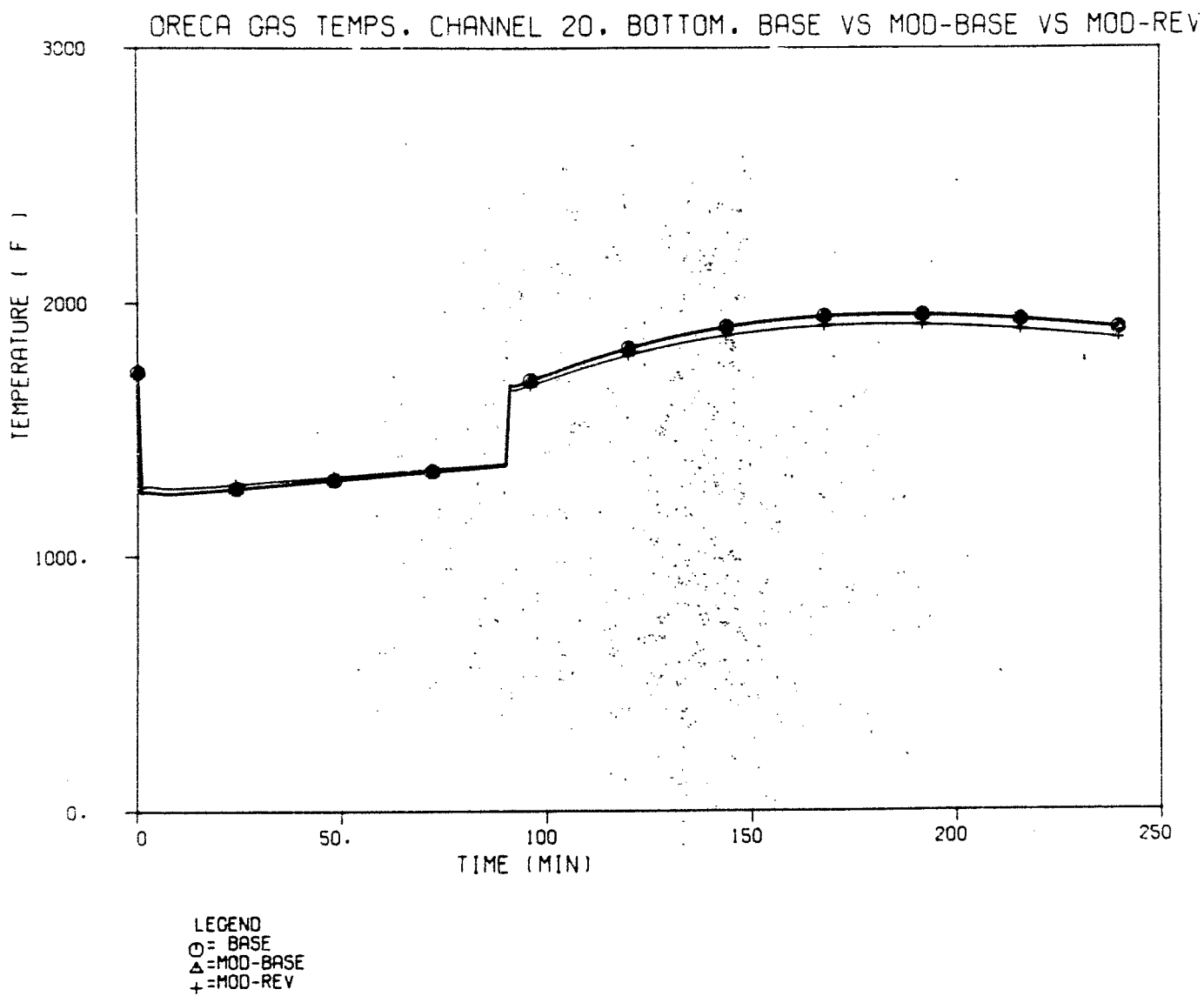


Figure B-10. Channel 20 gas outlet temperature at bottom node (J=8) for cases BASE, MOD-BASE, and MOD-REV.

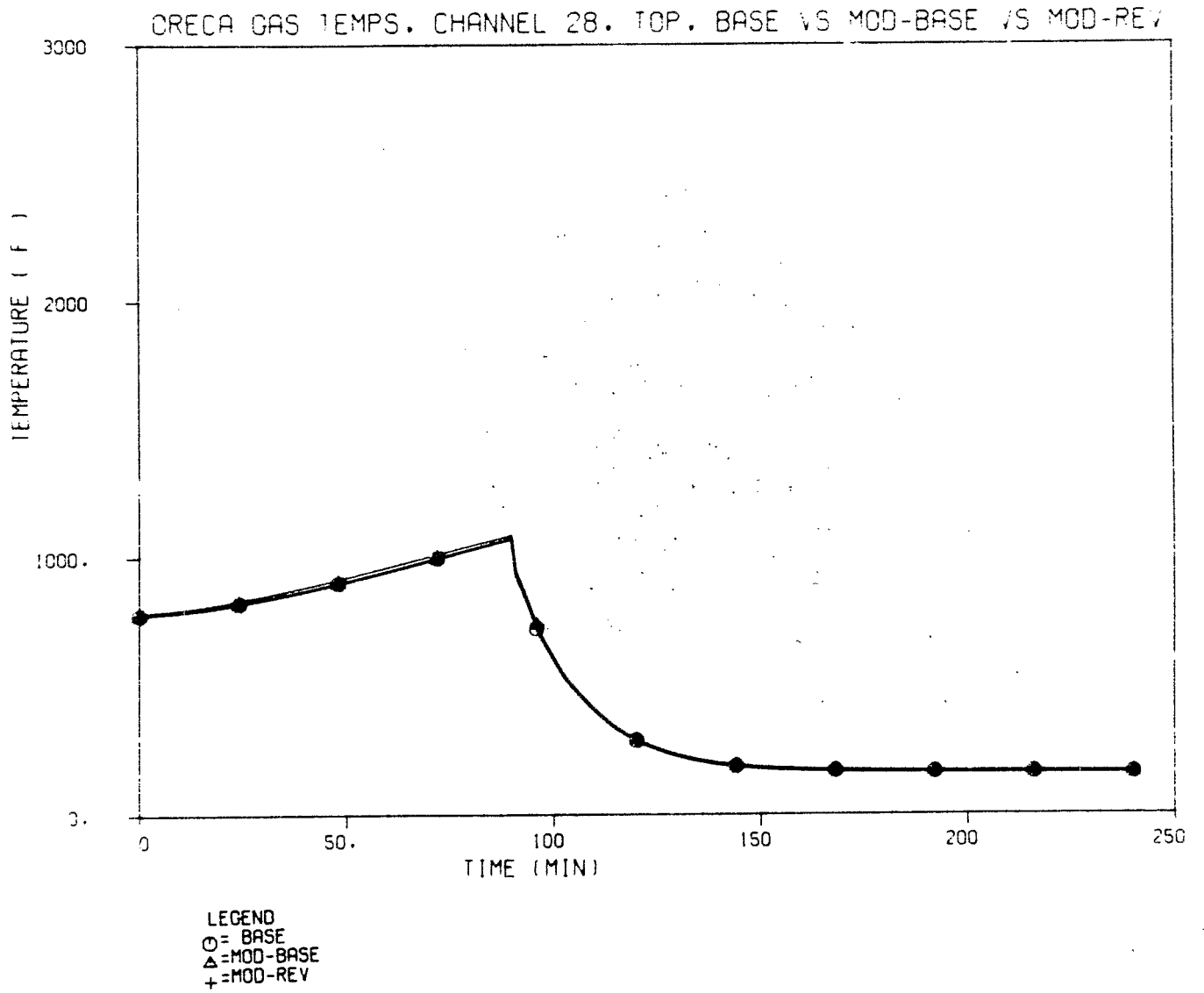


Figure B-11. Channel 28 gas outlet temperature at top node (J=1) for cases BASE, MOD-BASE, and MOD-REV.

ORECA GAS TEMPS. CHANNEL 28. CENTER (J=5). BASE VS MOD-BASE VS MOD-REV

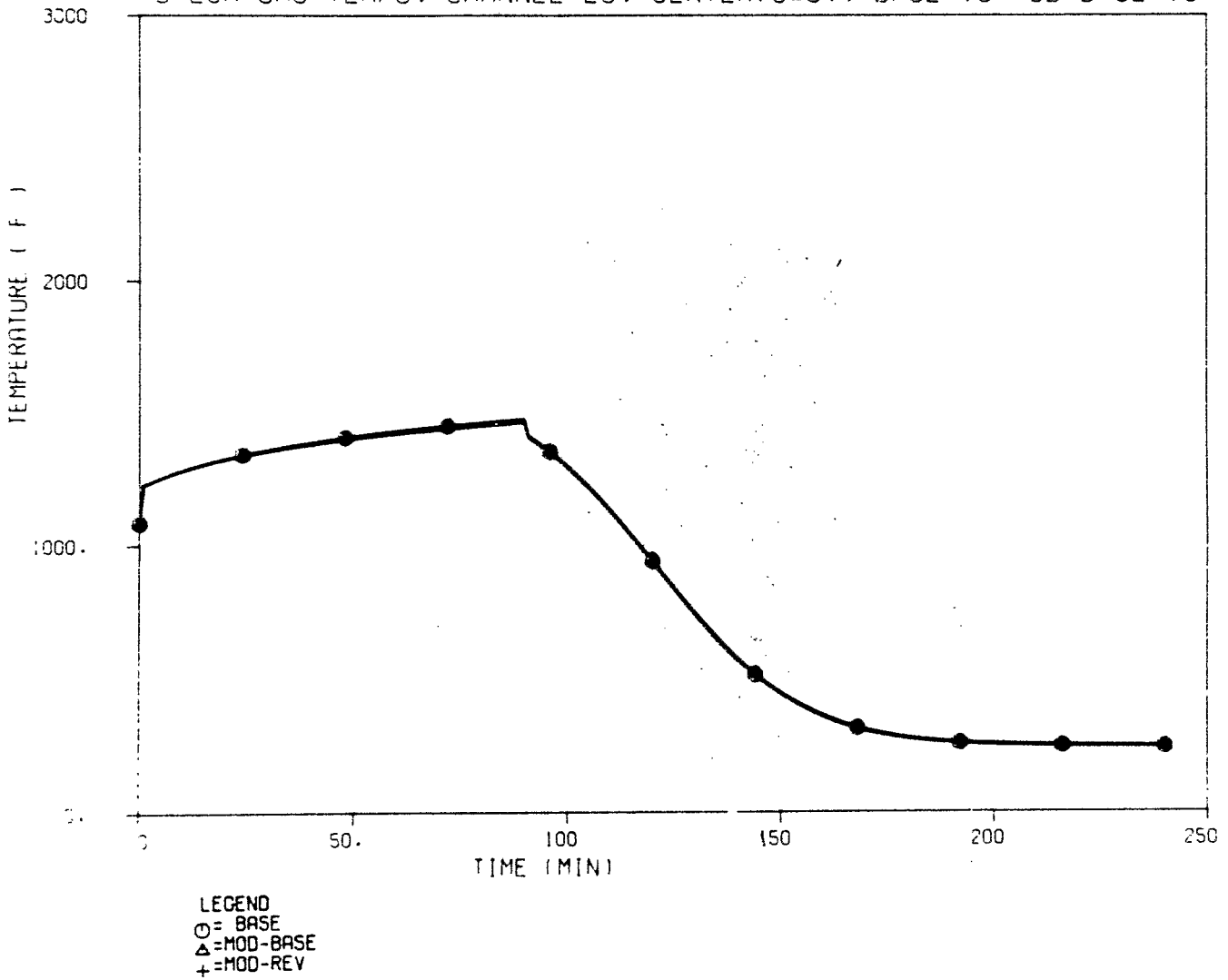


Figure B-12. Channel 28 gas outlet temperature at center node (J=5) for cases BASE, MOD-BASE, and MOD-REV.

OPERA GAS TEMPS. CHANNEL 28. BOTTOM. BASE VS MOD-BASE VS MOD-REV

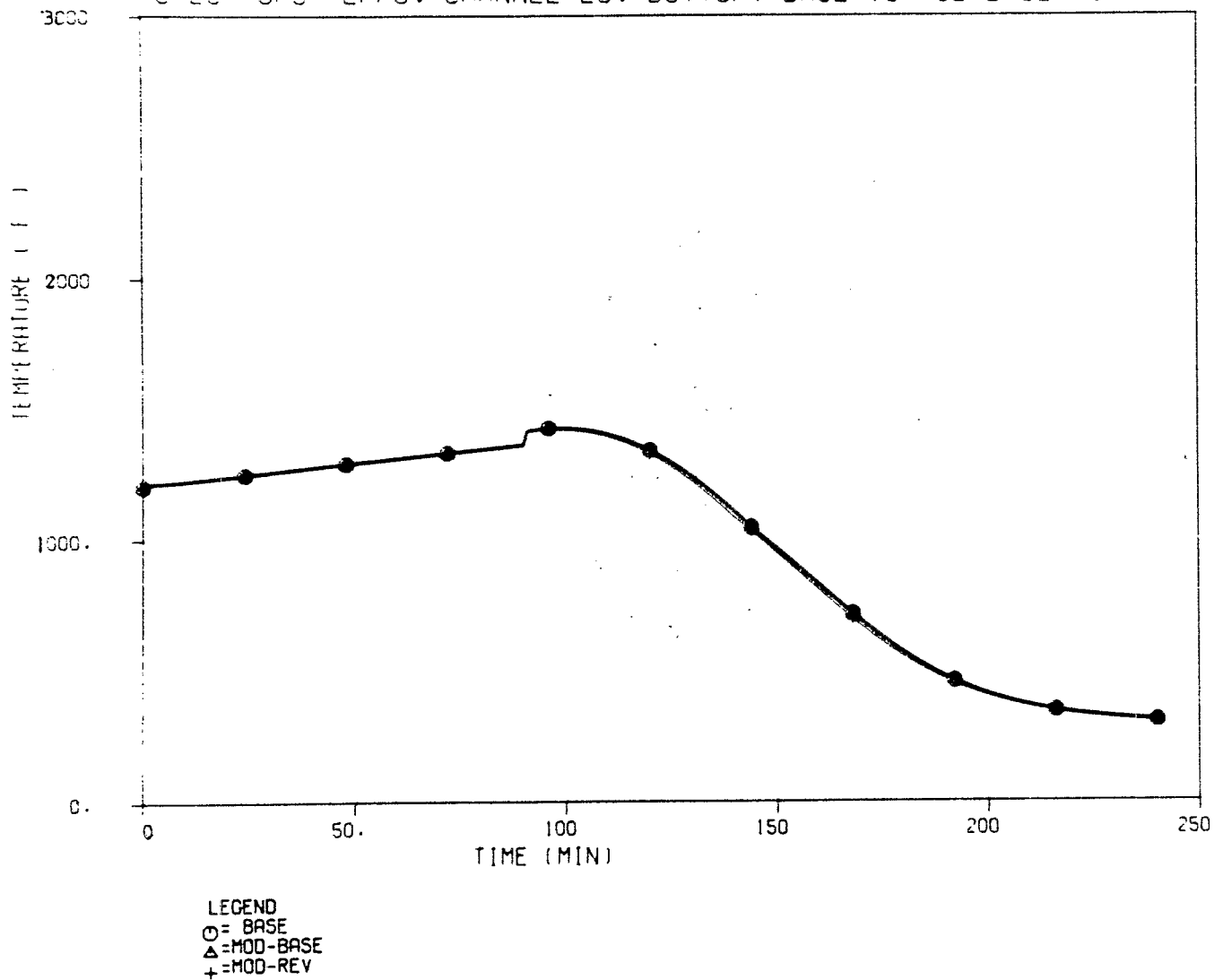


Figure B-13. Channel 28 gas outlet temperature at bottom node (J=8) for cases BASE, MOD-BASE, and MOD-REV.

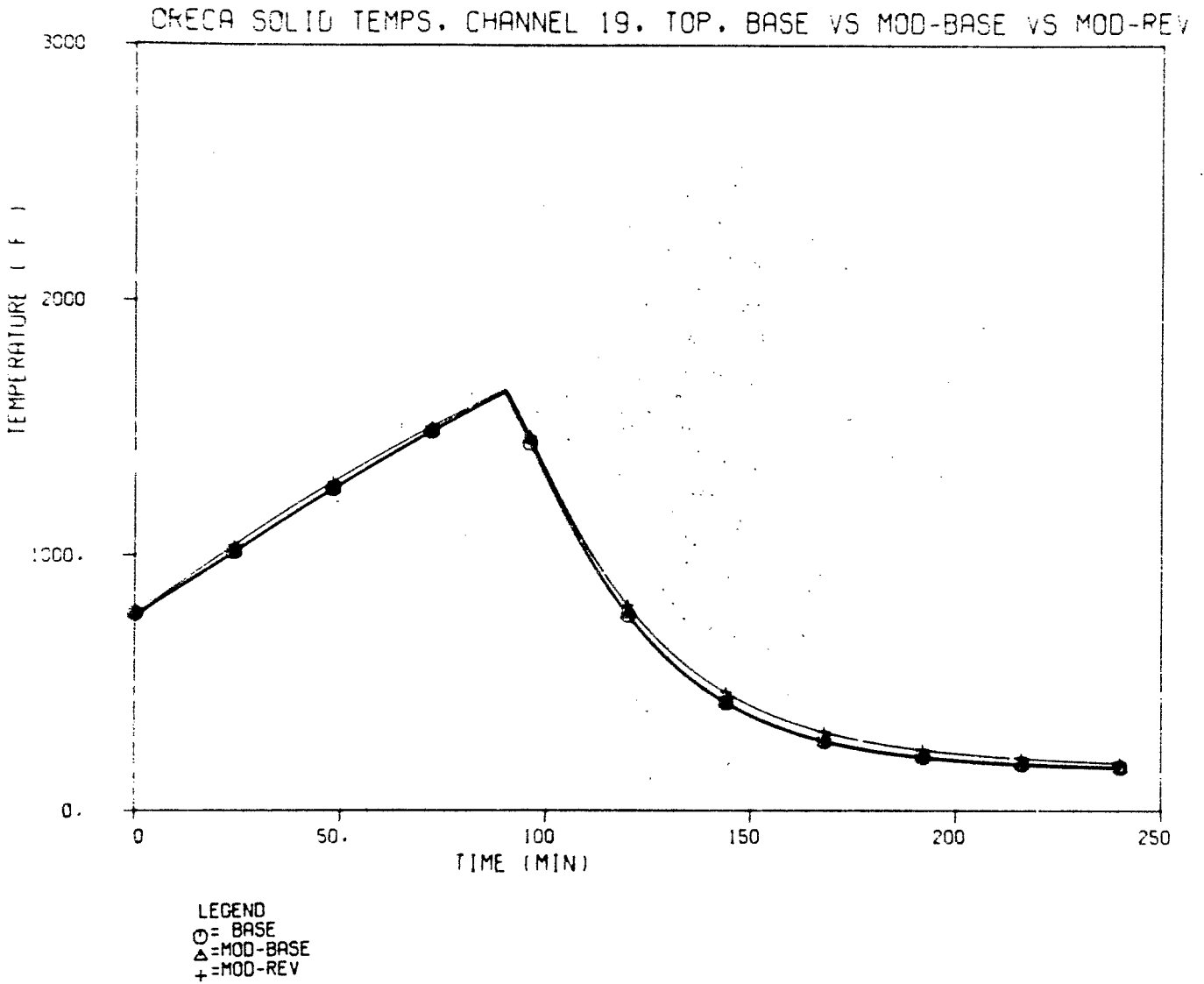


Figure B-14. Channel 19 core temperature at top node (J=1) for cases BASE, MOD-BASE, and MOD-REV.

CRECA SOLID TEMPS. CHANNEL 19. CENTER (J=5). BASE VS MOD-BASE VS MOD-

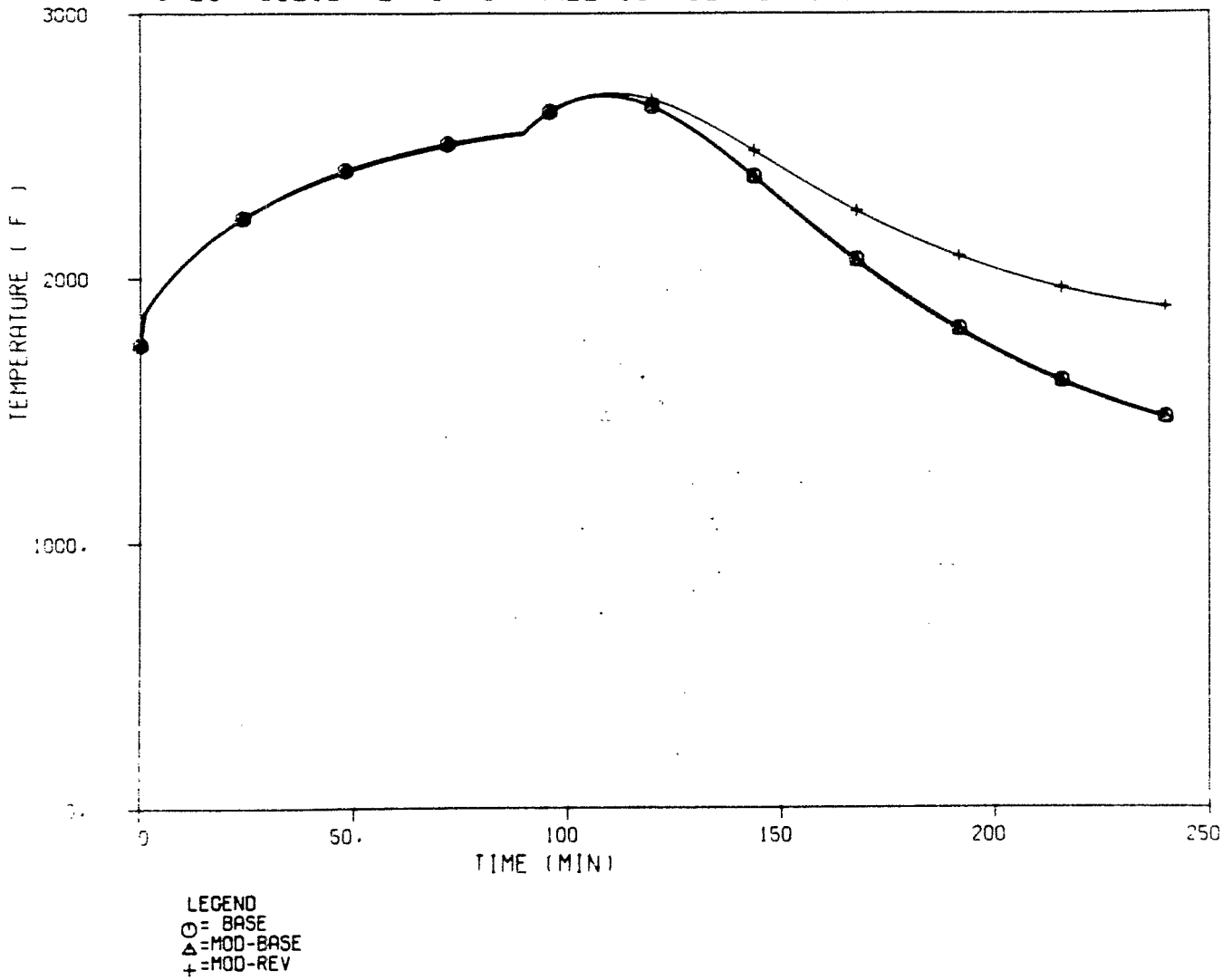


Figure B-15. Channel 19 core temperature at center node (J=5) for cases BASE, MOD-BASE, and MOD-REV.

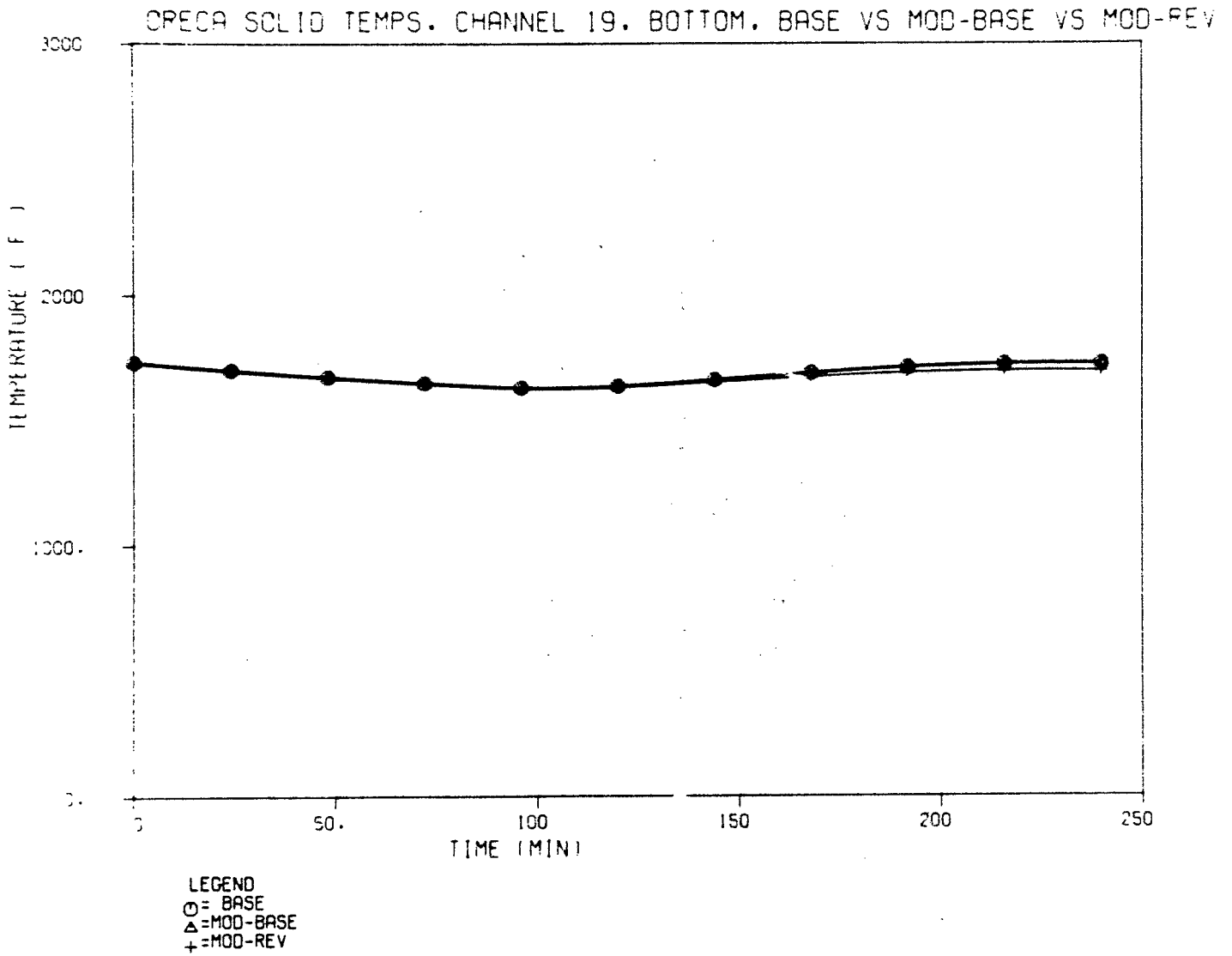


Figure B-16. Channel 19 core temperature at bottom node (J=8) for cases BASE, MOD-BASE, and MOD-REV.

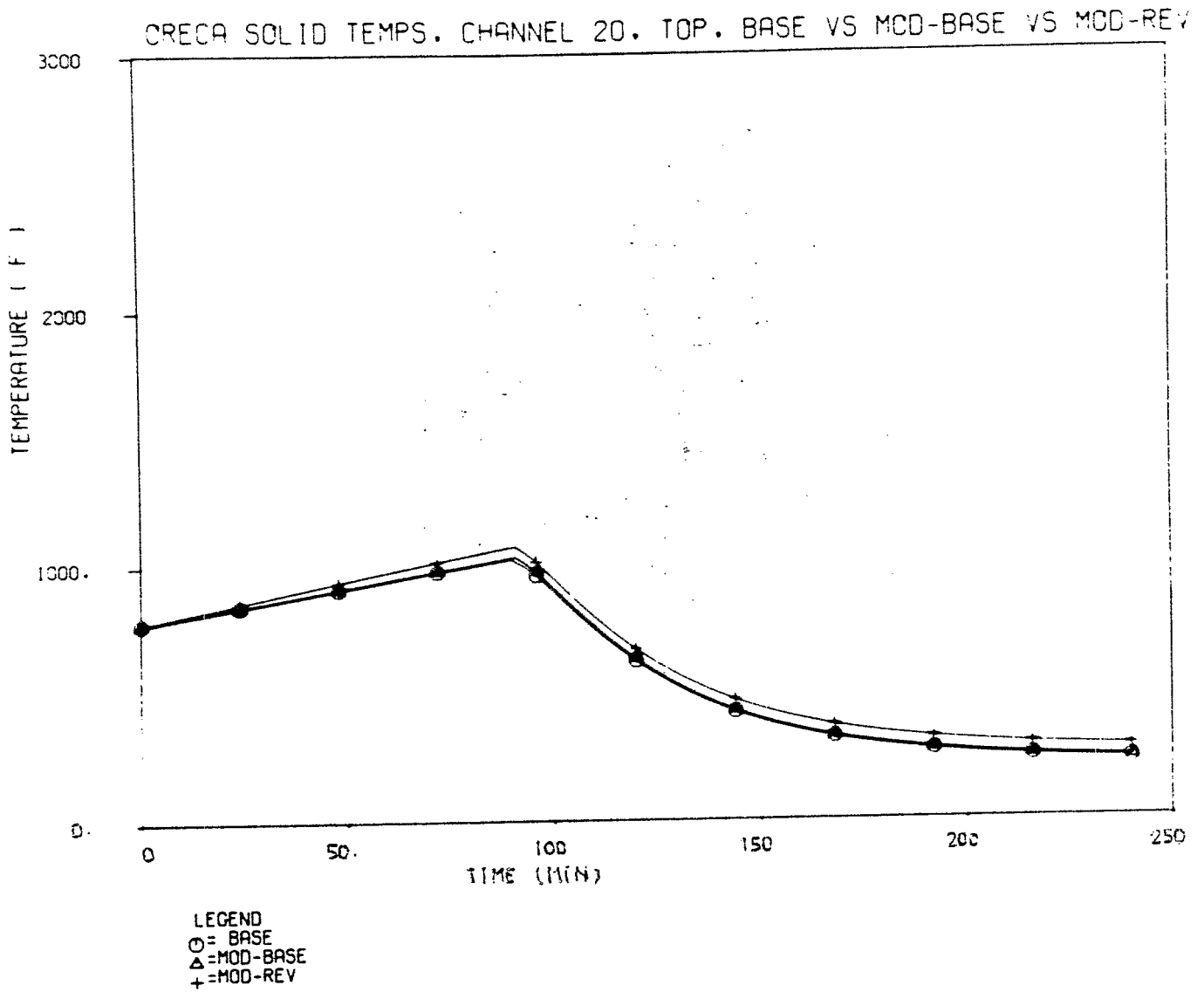
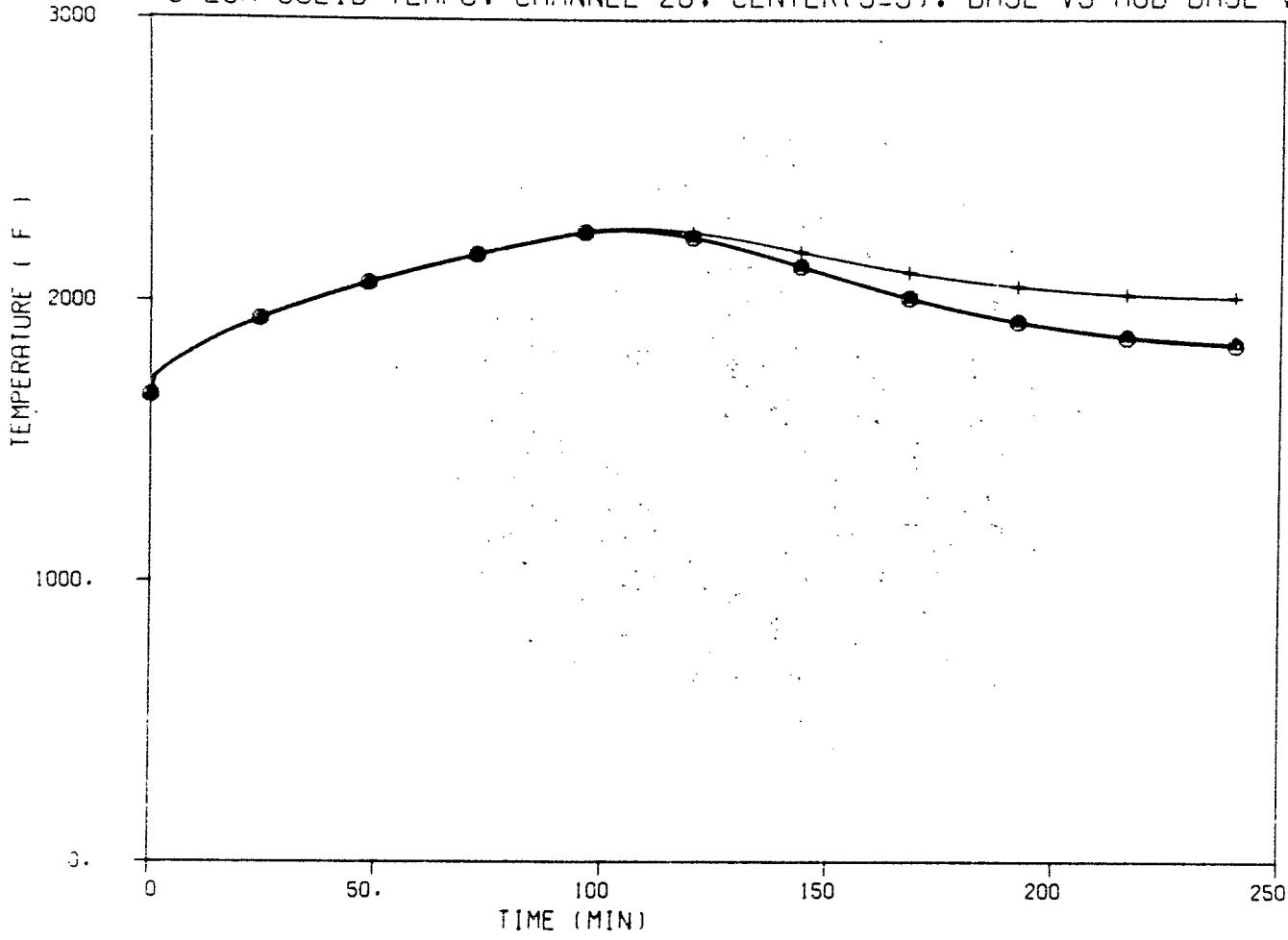


Figure B-17. Channel 20 core temperature at top node (J=1) for cases BASE, MOD-BASE, and MOD-REV.

OPECA SOLID TEMPS. CHANNEL 20, CENTER(J=5). BASE VS MOD-BASE VS MOD-REV



LEGEND
○ = BASE
△ = MOD-BASE
+ = MOD-REV

Figure B-18. Channel 20 core temperature at center node (J=5) for cases BASE, MOD-BASE, and MOD-REV.

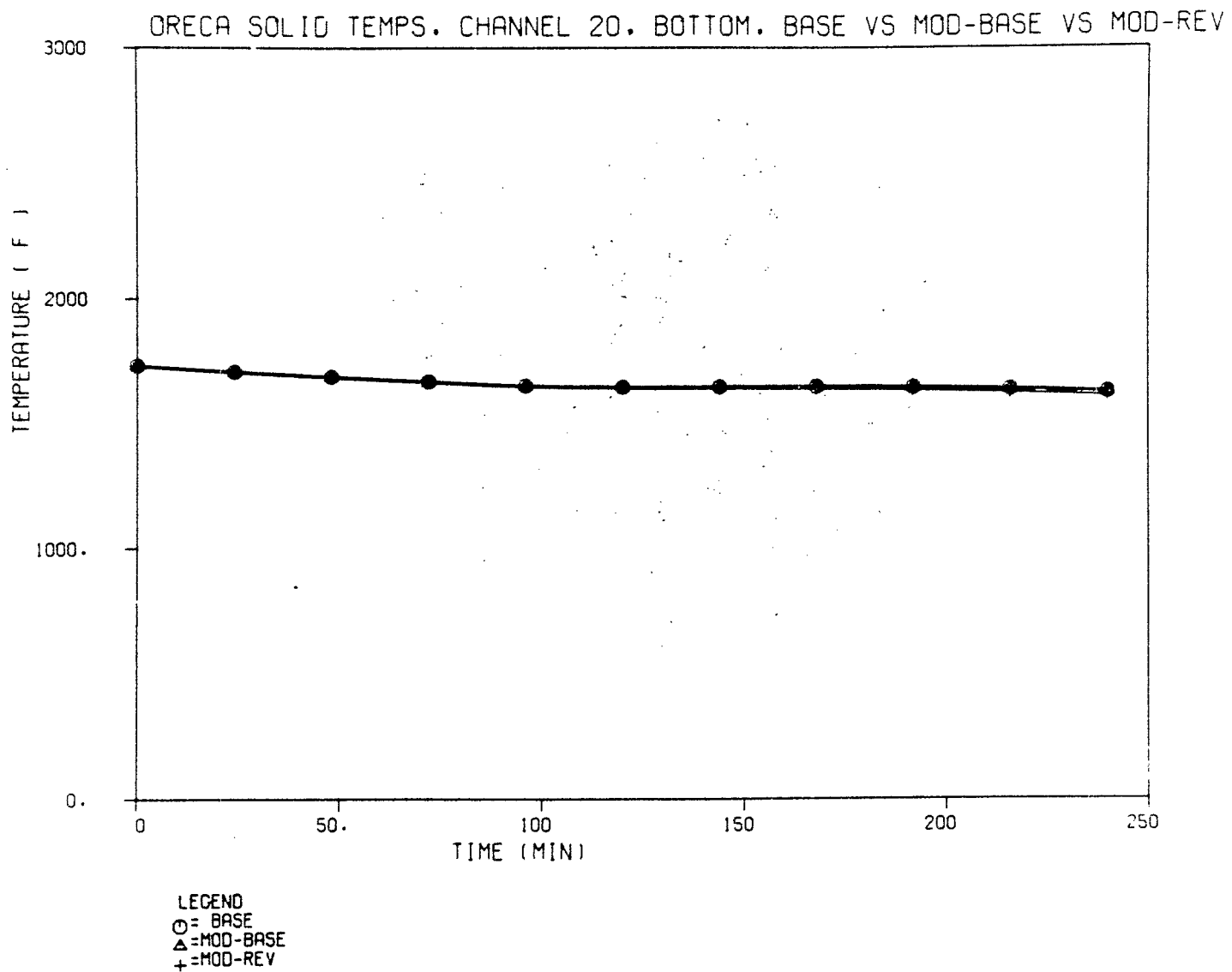


Figure B-19. Channel 20 core temperature at bottom node (J=8) for cases BASE, MOD-BASE, and MOD-REV.

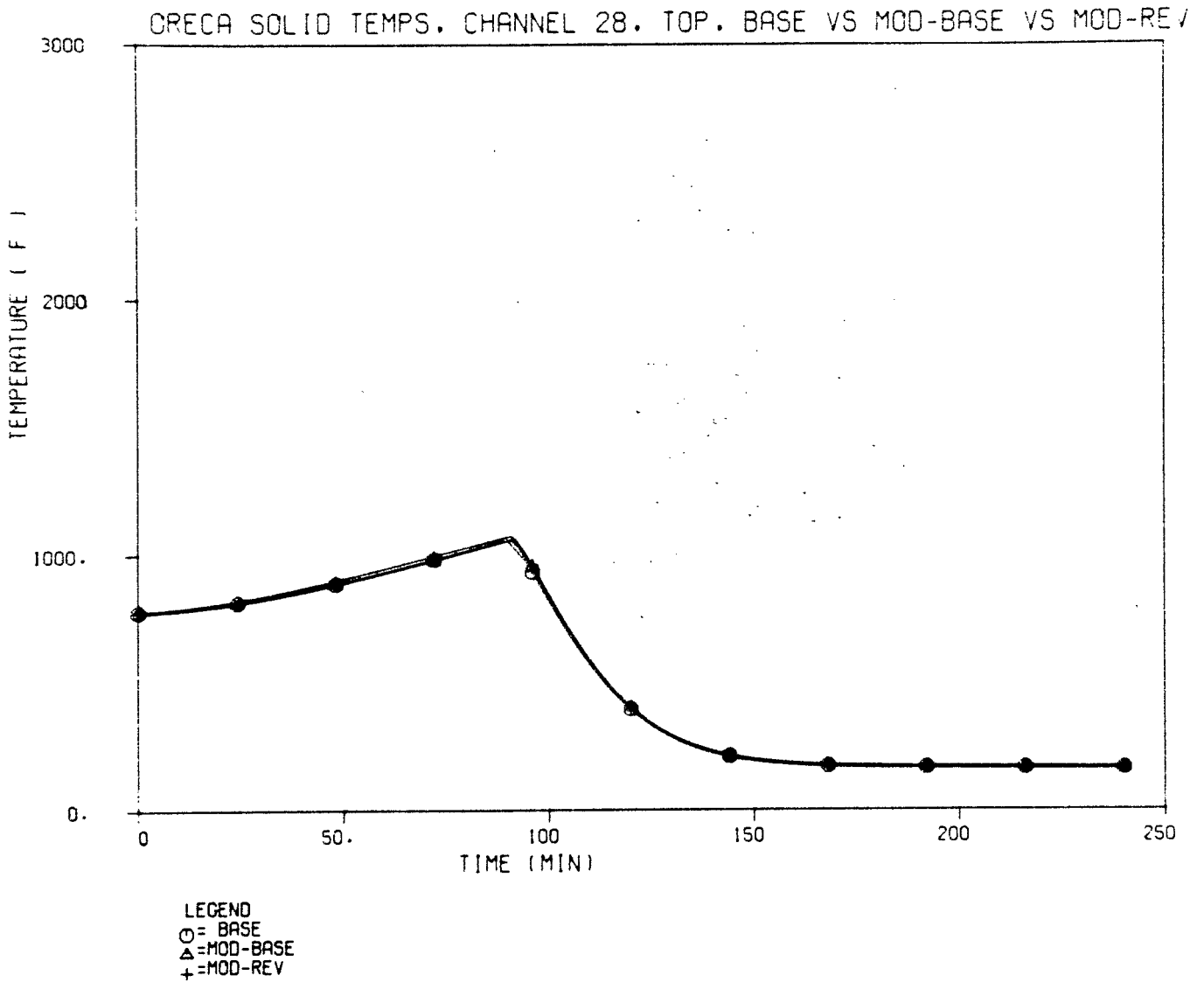
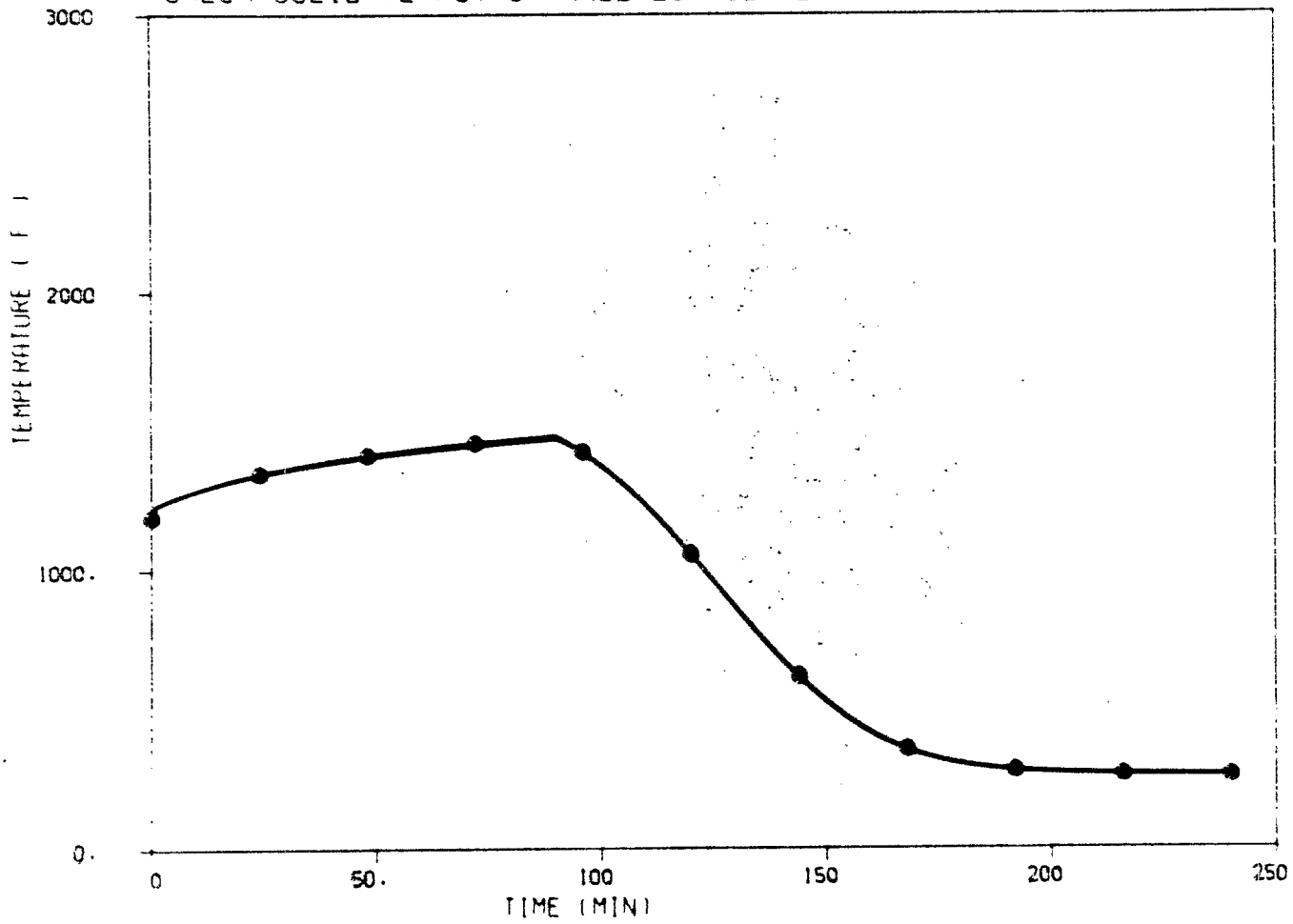


Figure B-20. Channel 28 core temperature at top node (J=1) for cases BASE, MOD-BASE, and MOD-REV.

CRECA SOLID TEMPS. CHANNEL 28. CENTER (J=5). BASE VS MOD-BASE VS MOD-REV



LEGEND
○ = BASE
△ = MOD-BASE
+ = MOD-REV

Figure B-21. Channel 28 core temperature at center node (J=5) for cases BASE, MOD-BASE, and MOD-REV.

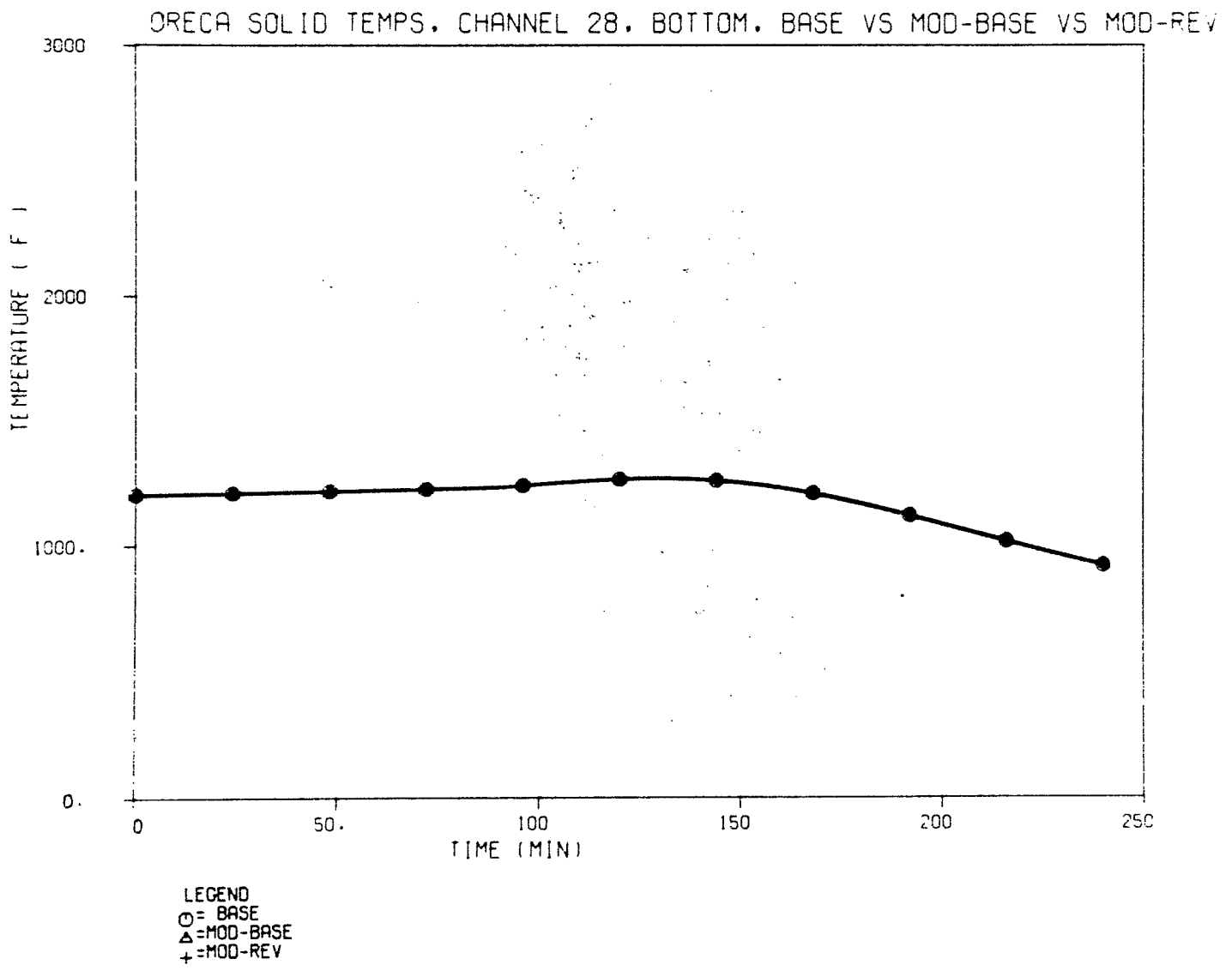


Figure B-22. Channel 28 core temperature at bottom node (J=8) for cases BASE, MOD-BASE, and MOD-REV.

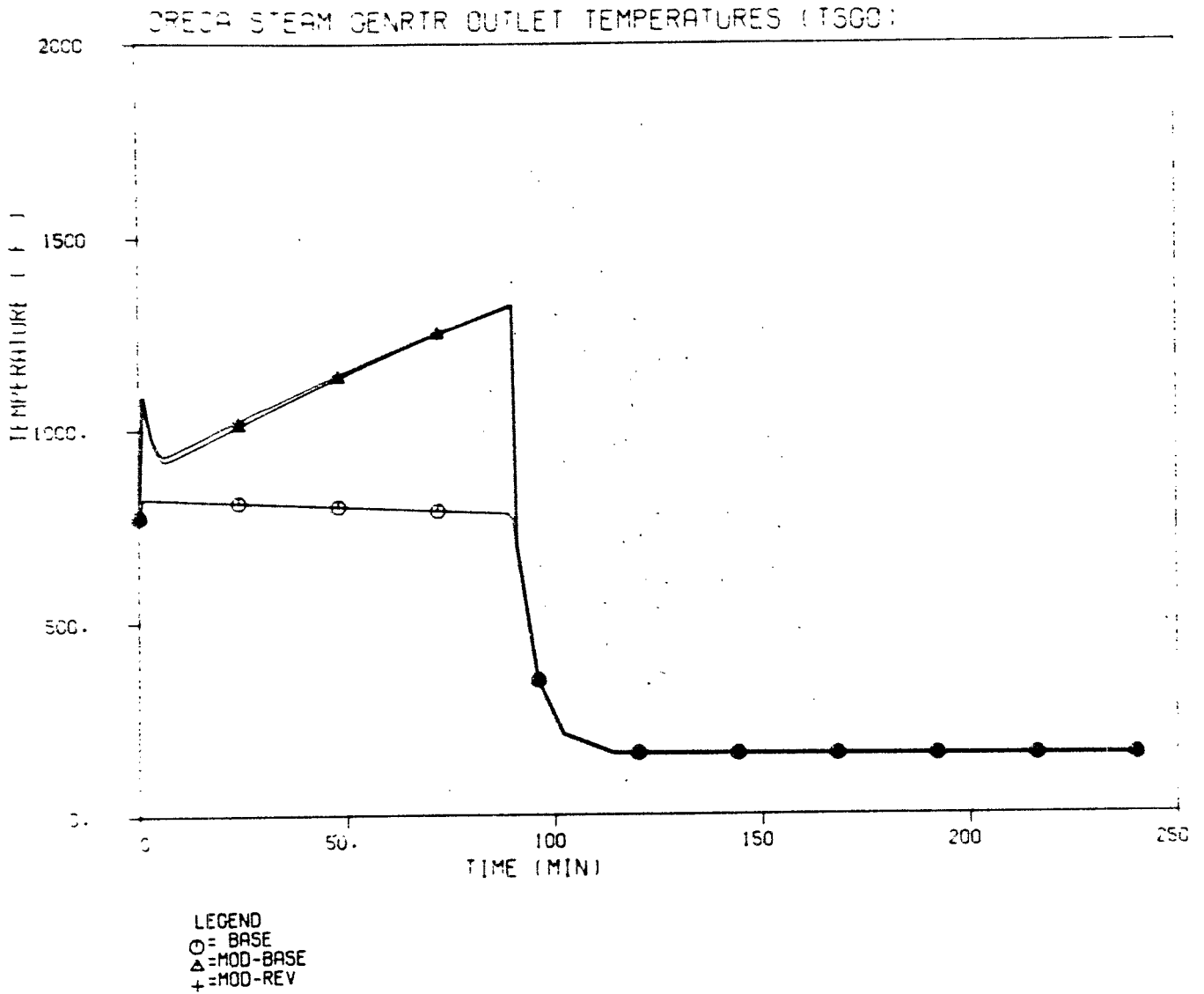


Figure B-23. Temperature at upper plenum inlet position for cases BASE, MOD-BASE, and MOD-REV.

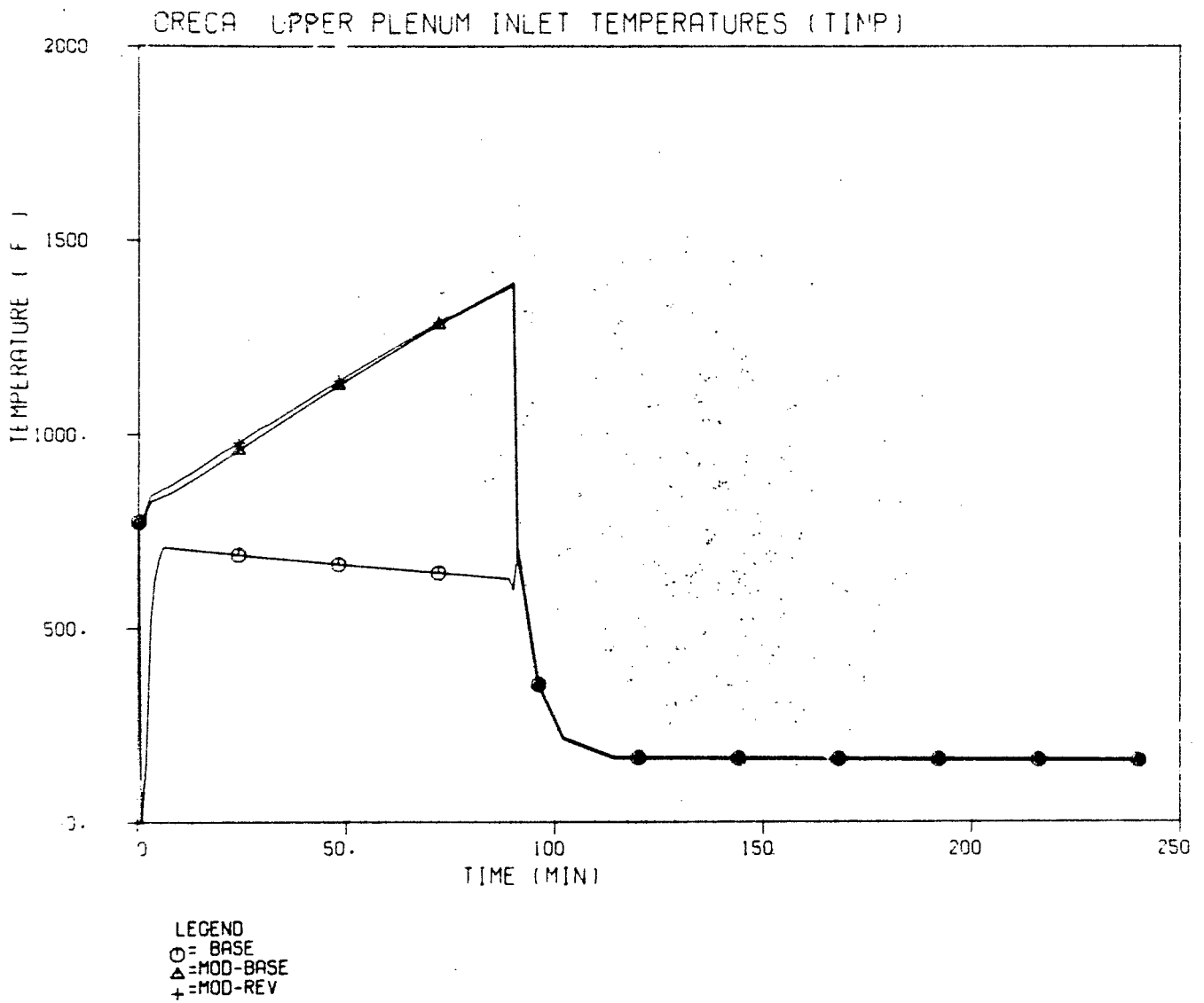


Figure B-24. Temperature at upper plenum inlet position for cases BASE, MØD-BASE, and MØD-REV.

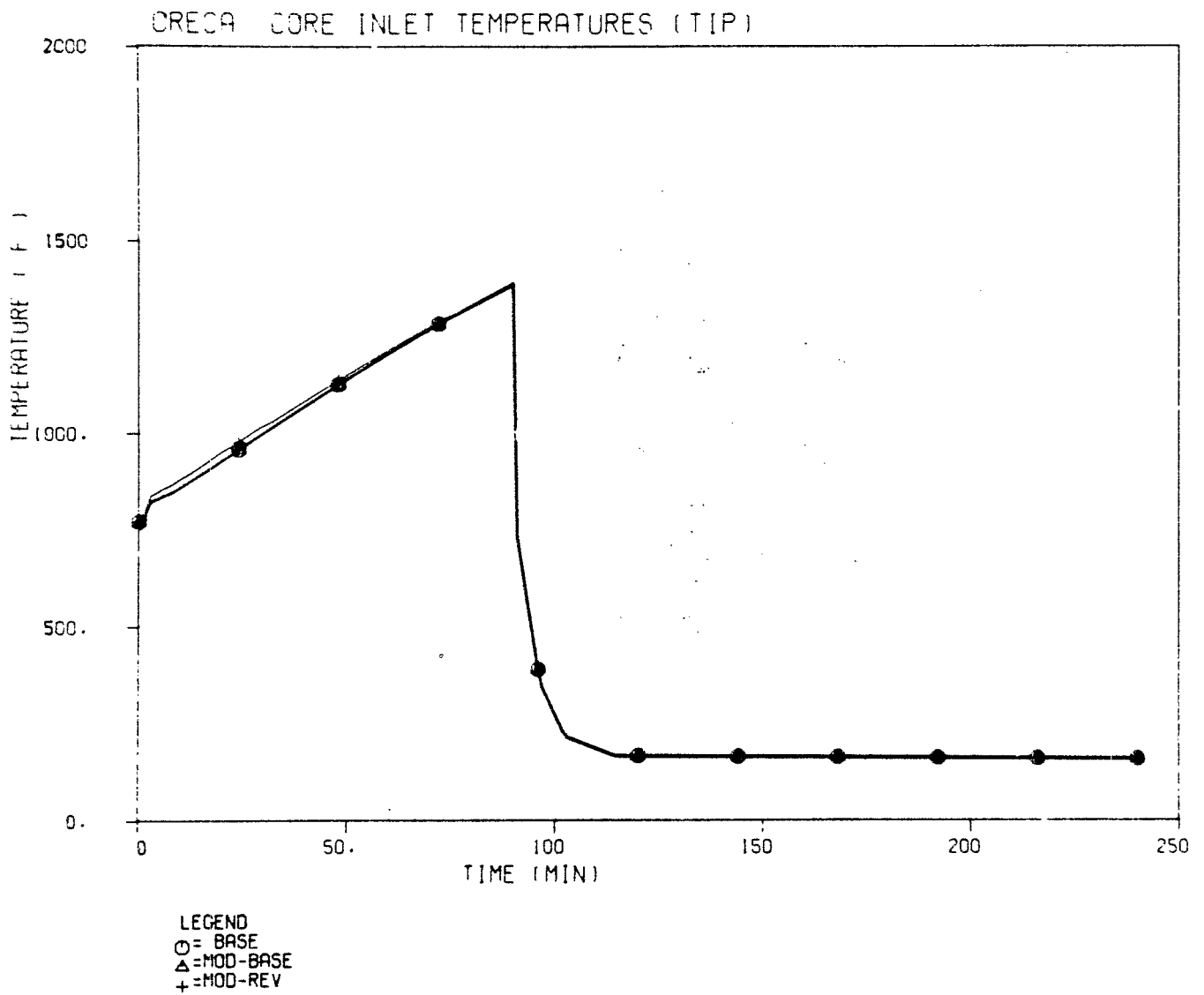


Figure B-25. Temperature at core inlet position for cases BASE, MOD-BASE, and MOD-REV.

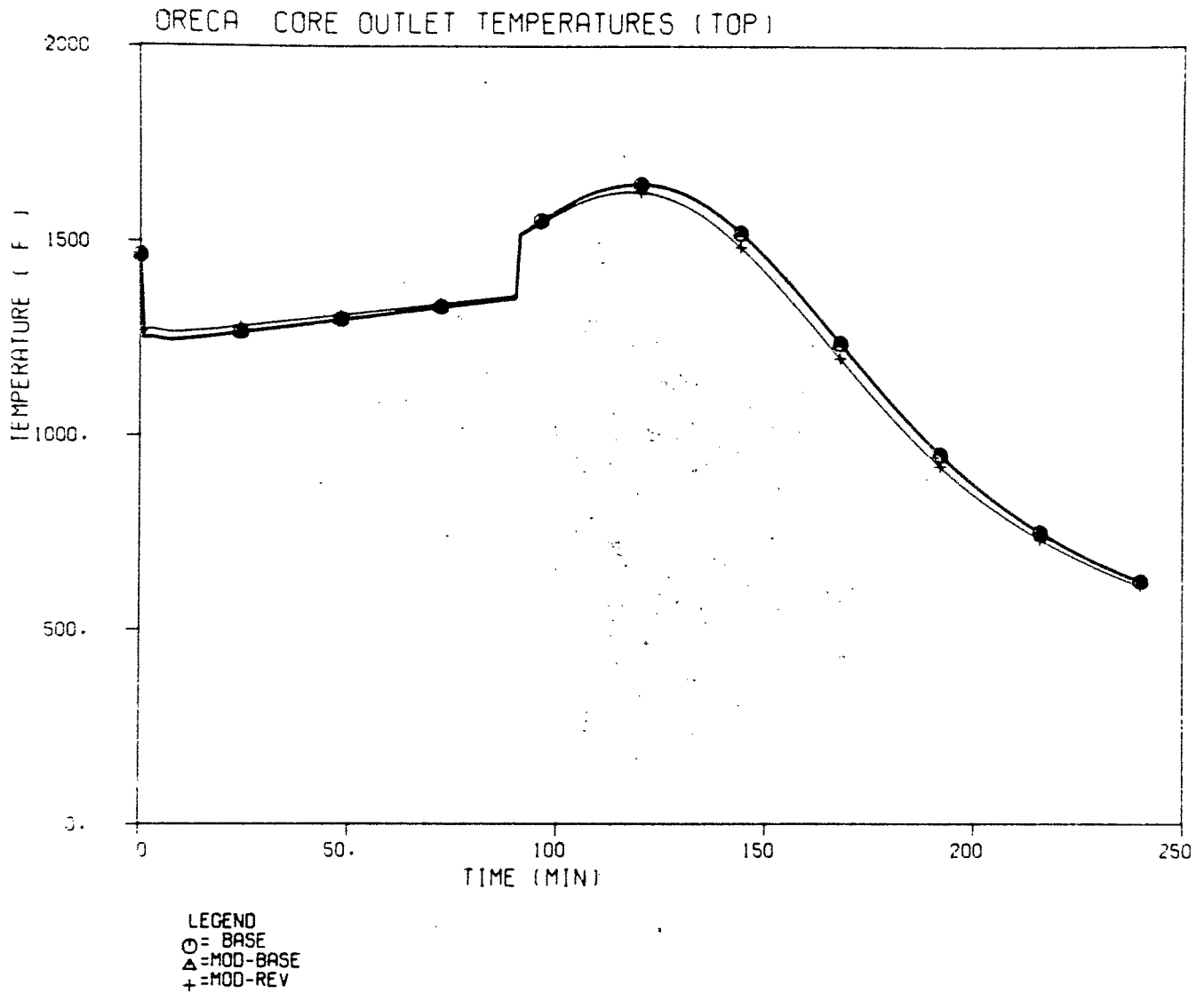


Figure B-26. Temperature at core outlet position for cases BASE, MOD-BASE, and MOD-REV.

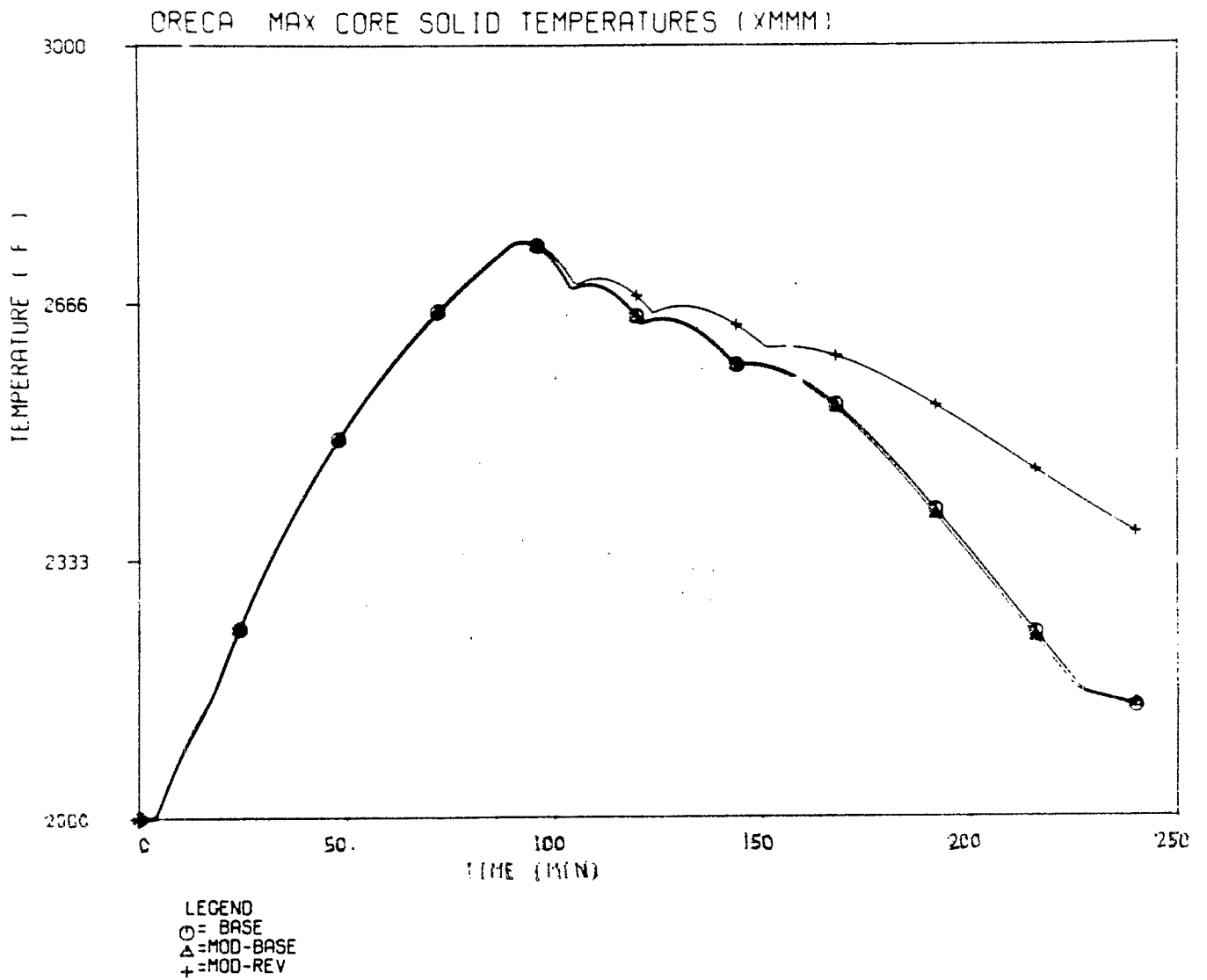


Figure B-27. Peak core temperature during transient for cases BASE, MOD-BASE, and MOD-REV.

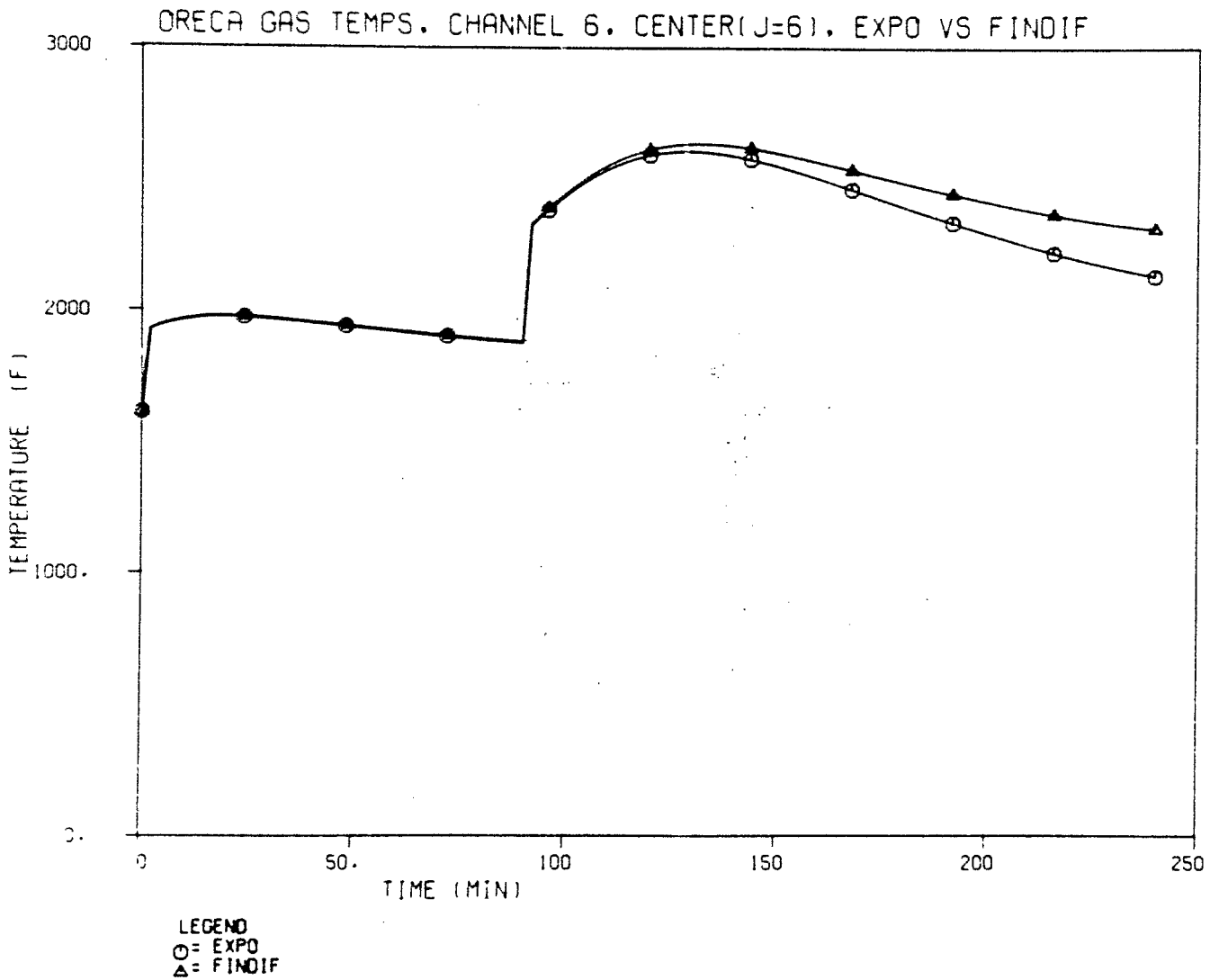


Figure B-28. Channel 6 gas outlet temperature at center node J=6 for cases EXPO and FINDIF.

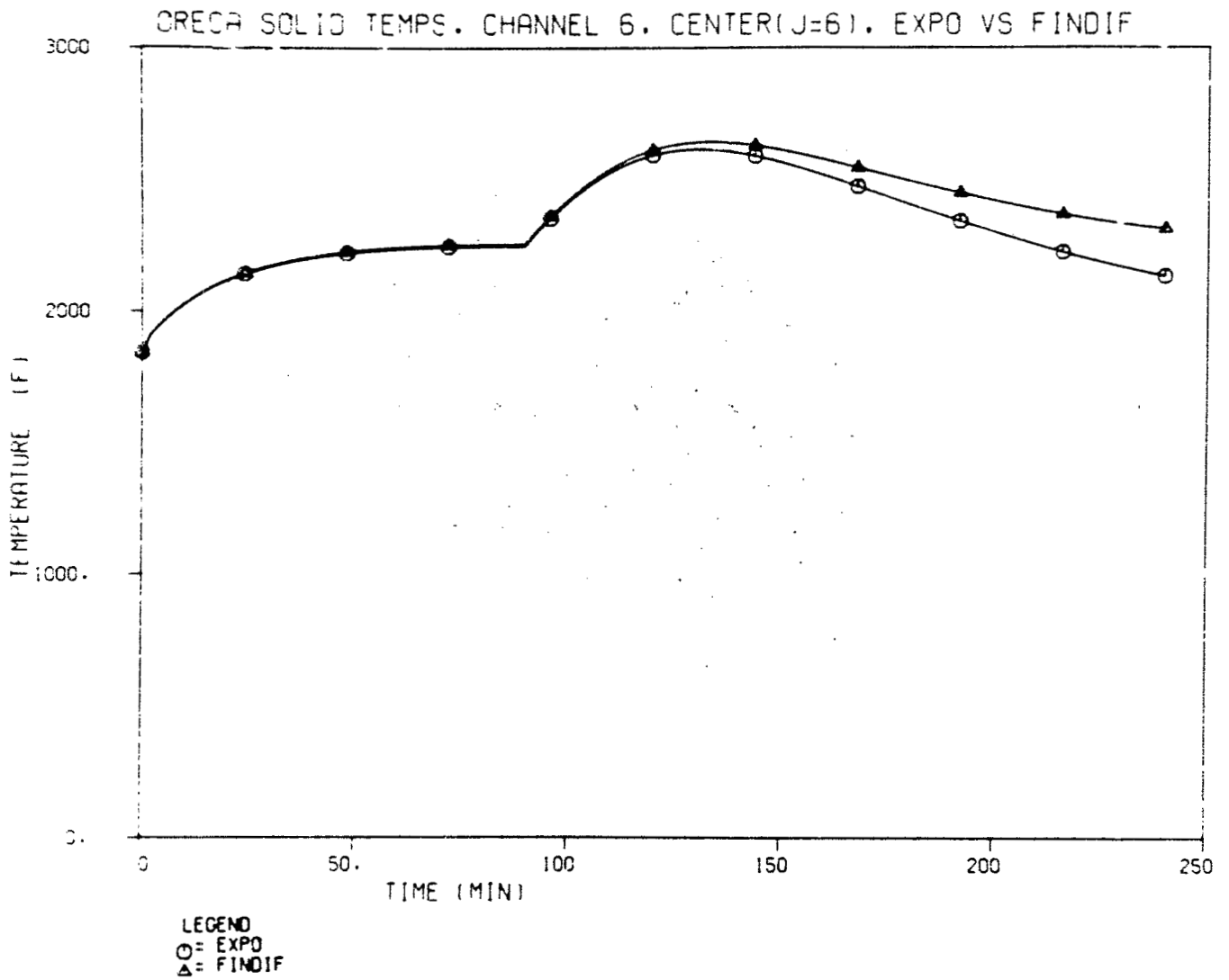


Figure B-29. Channel 6 core temperature at center node J=6 for cases EXPO and FINDIF.

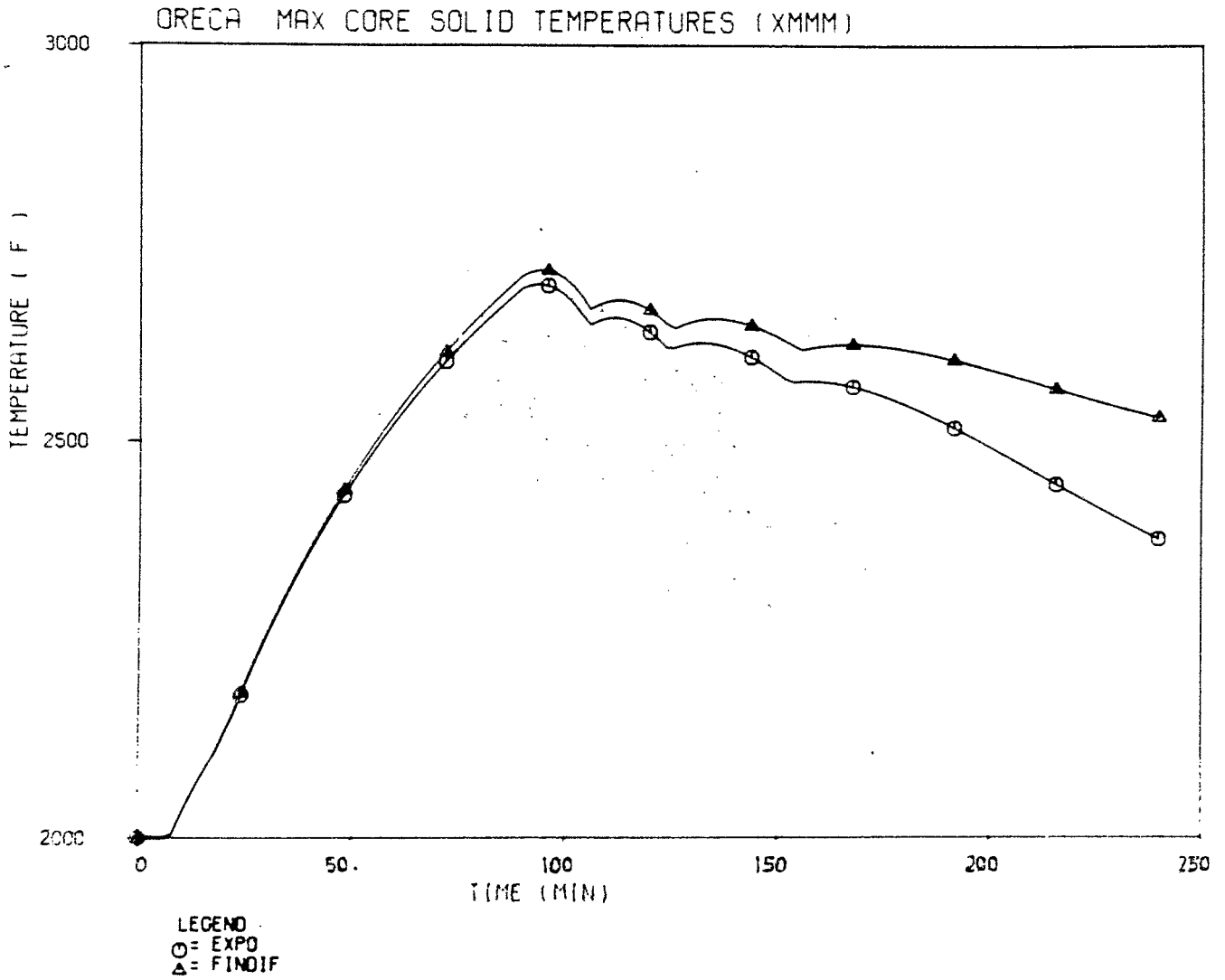


Figure B-30. Peak core temperature during transient for cases EXPO and FINDIF.

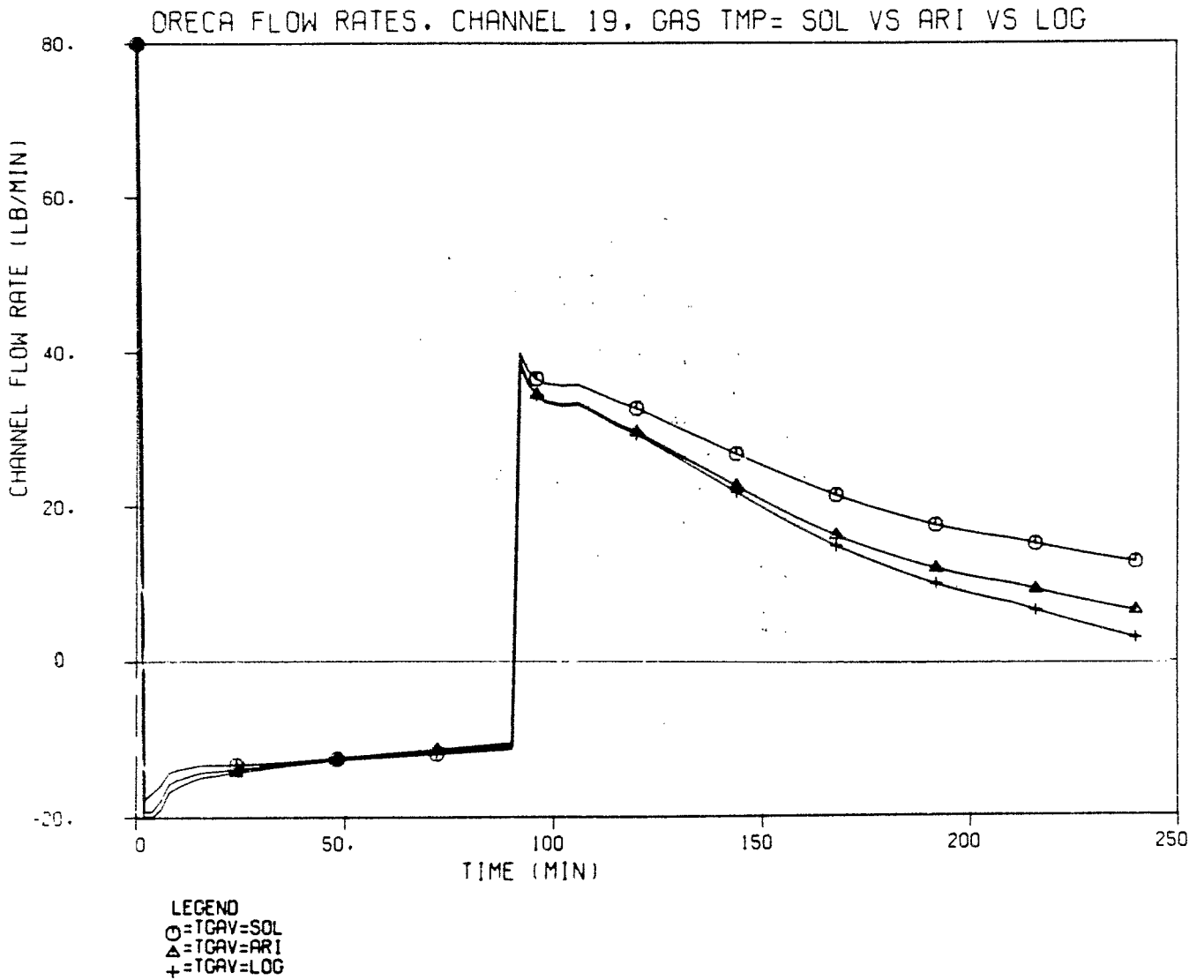


Figure B-31. Channel 19 flow rate for case of gas temperatures being varied in the evaluation of densities in pressure drop terms.

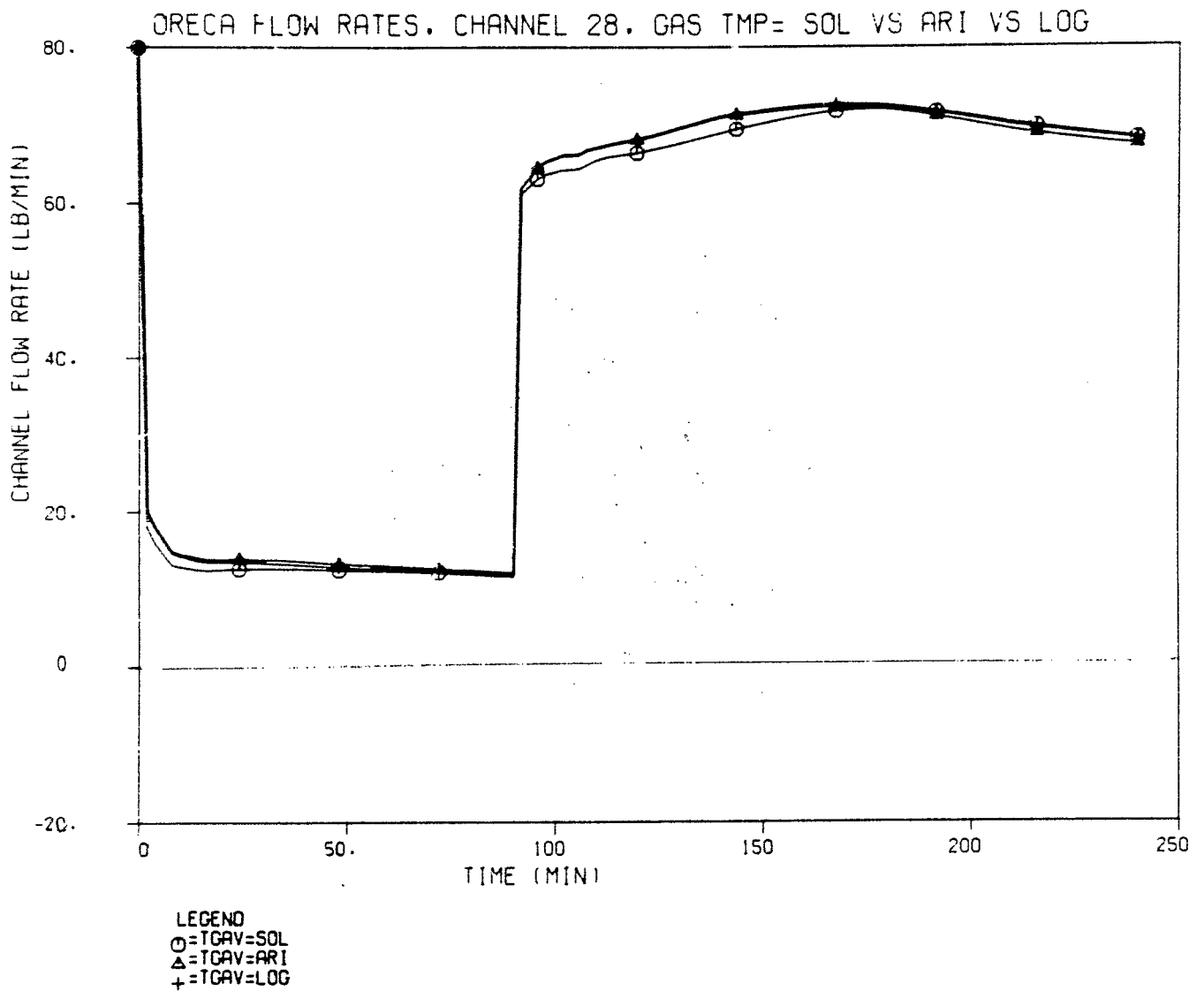


Figure B-32. Channel 28 flow rate for case of gas temperatures being varied in the evaluation of densities in pressure drop terms.

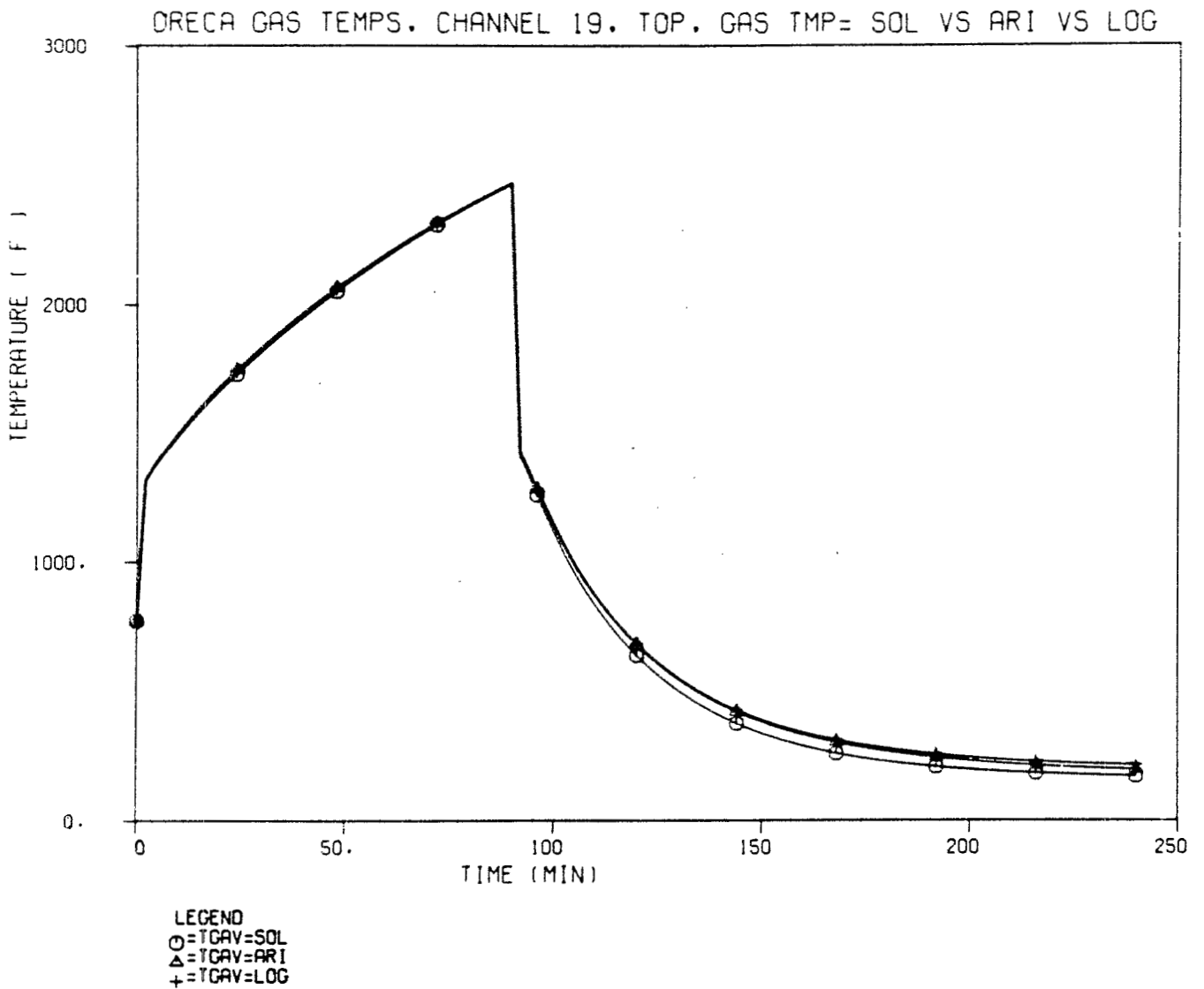


Figure B-33. Channel 19 gas outlet temperature at top node (J=1) for case of gas temperatures being varied in the evaluation of densities in pressure drop terms.

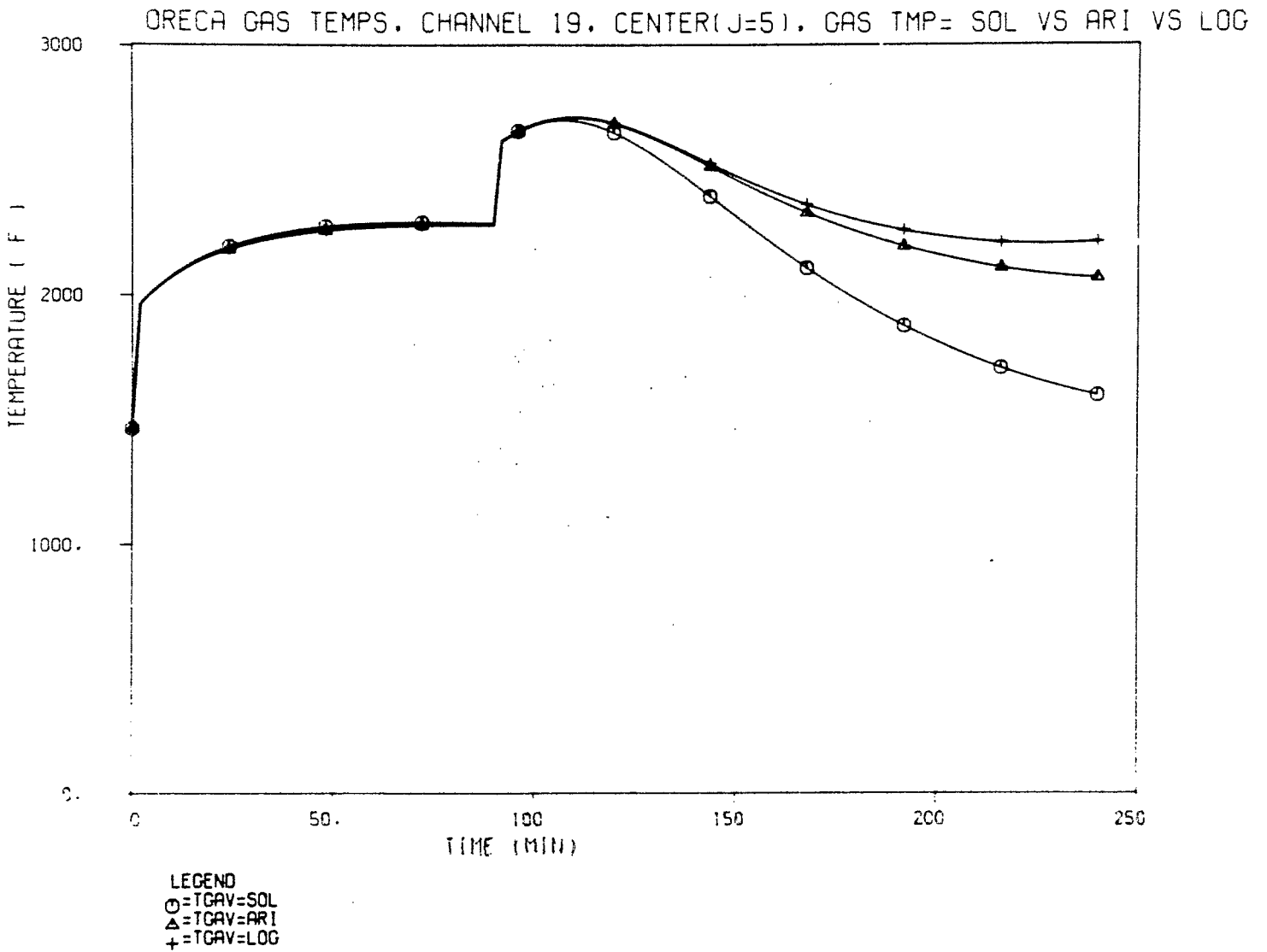


Figure B-34. Channel 19 gas outlet temperature at center node (J=5) for case of gas temperatures being varied in the evaluation of densities in pressure drop terms.

CRECA GAS TEMPS. CHANNEL 19, CENTER (J=6), GAS TMP= SOL VS ARI VS LOG

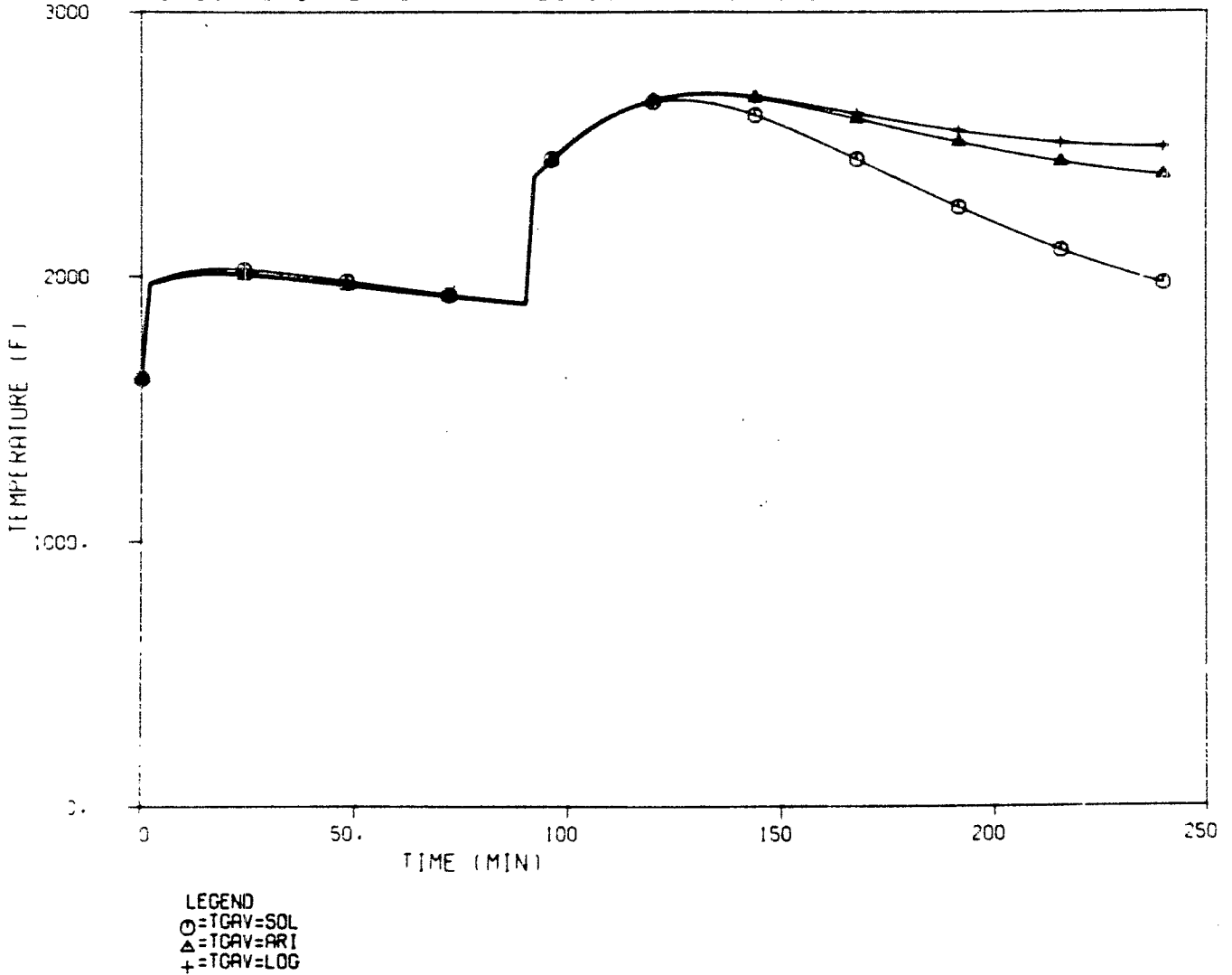
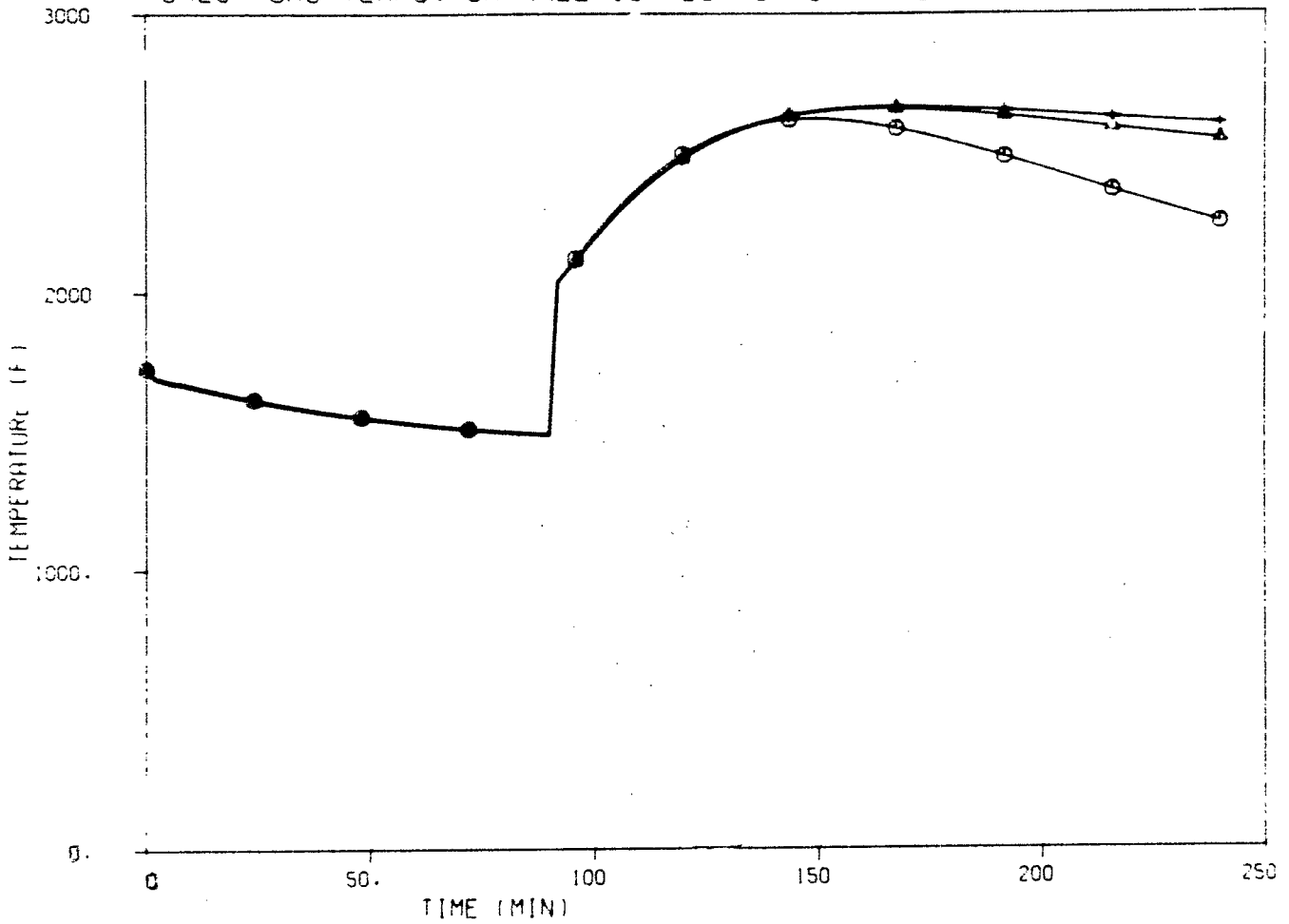


Figure B-35. Channel 19 gas outlet temperature at center node (J=6) for case of gas temperatures being varied in the evaluation of densities in pressure drop terms.

CRECA GAS TEMPS. CHANNEL 19, BOTTOM(J=7), GAS TMP= SOL VS ARI VS LOG



LEGEND
 ○=TCAV=SOL
 △=TCAV=ARI
 +=TCAV=LOG

Figure B-36. Channel 19 gas outlet temperature at center node (J=7) for case of gas temperatures being varied in the evaluation of densities in pressure drop terms.

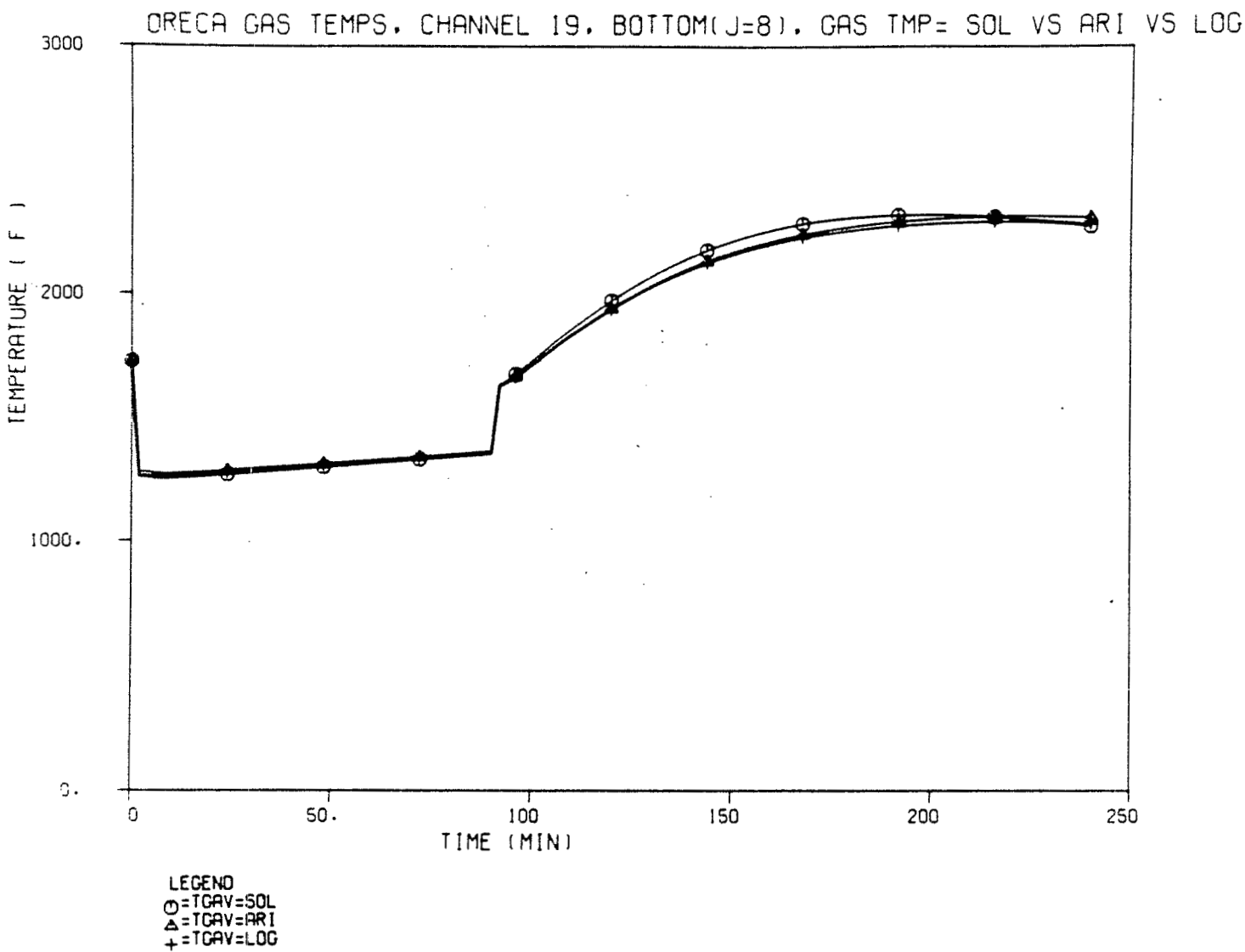


Figure B-37. Channel 19 gas outlet temperature at bottom node (J=8) for case of gas temperatures being varied in the evaluation of densities in pressure drop terms.

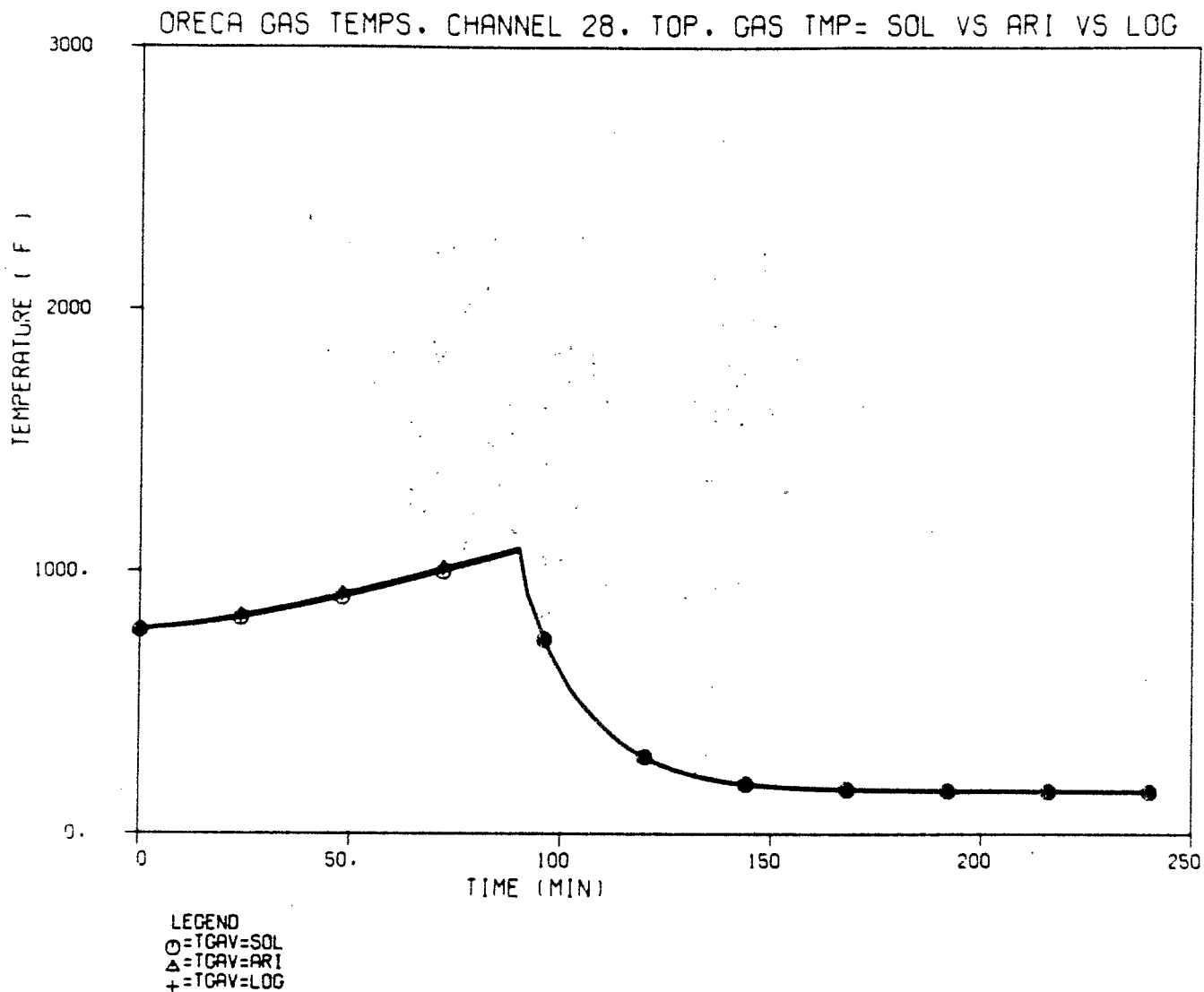


Figure B-38. Channel 28 gas outlet temperature at top node (J=1) for case of gas temperatures being varied in the evaluation of densities in pressure drop terms.

ORECA GAS TEMPS. CHANNEL 28. CENTER(J=5). GAS TMP= SOL VS ARI VS LOG

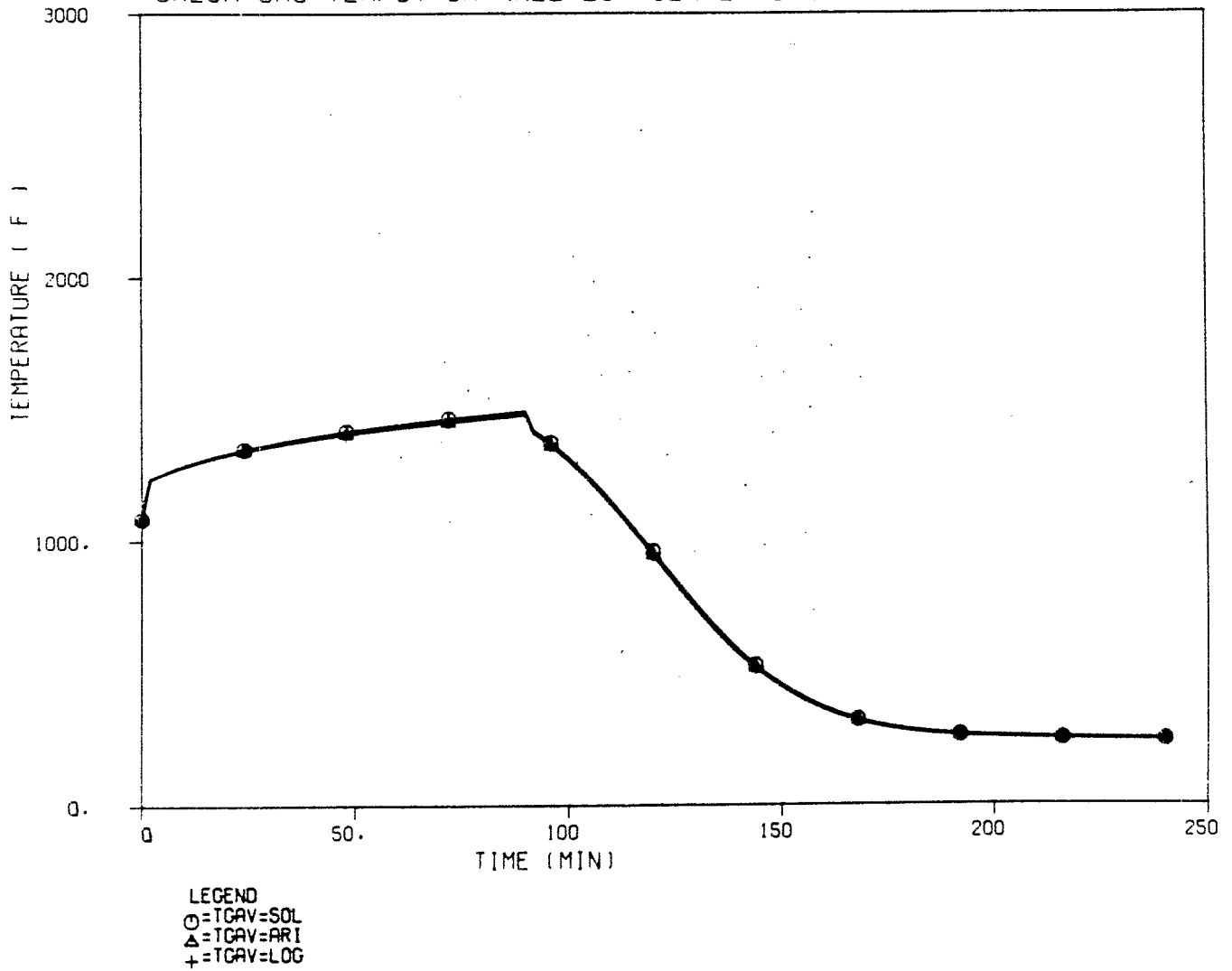


Figure B-39. Channel 28 gas outlet temperature at center node (J=5) for case of gas temperatures being varied in the evaluation of densities in pressure drop terms.

ORECA GAS TEMPS. CHANNEL 28, BOTTOM(J=8). GAS TMP= SOL VS ARI VS LOG

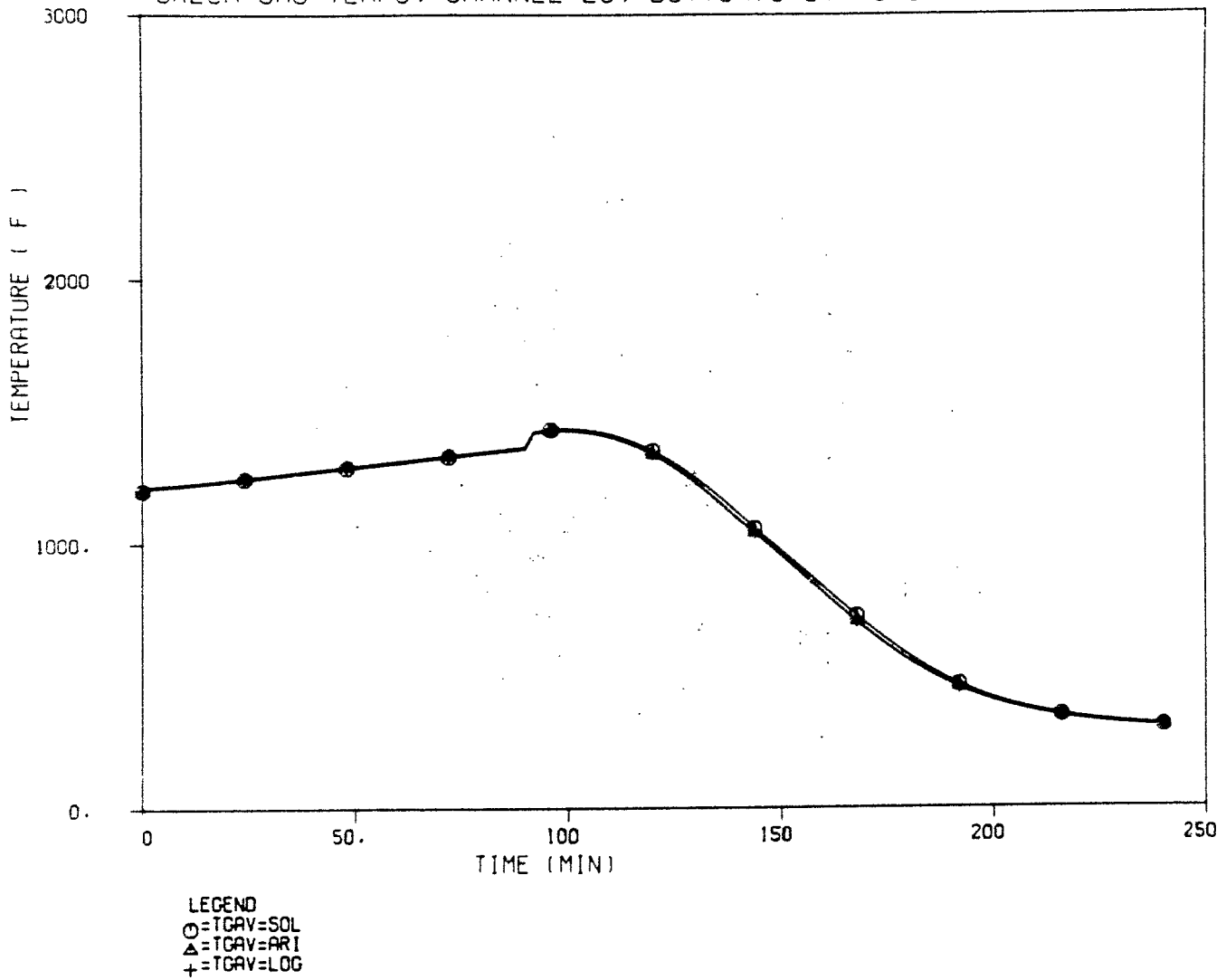


Figure B-40. Channel 28 gas outlet temperature at bottom node (J=8) for case of gas temperatures being varied in the evaluation of densities in pressure drop terms.

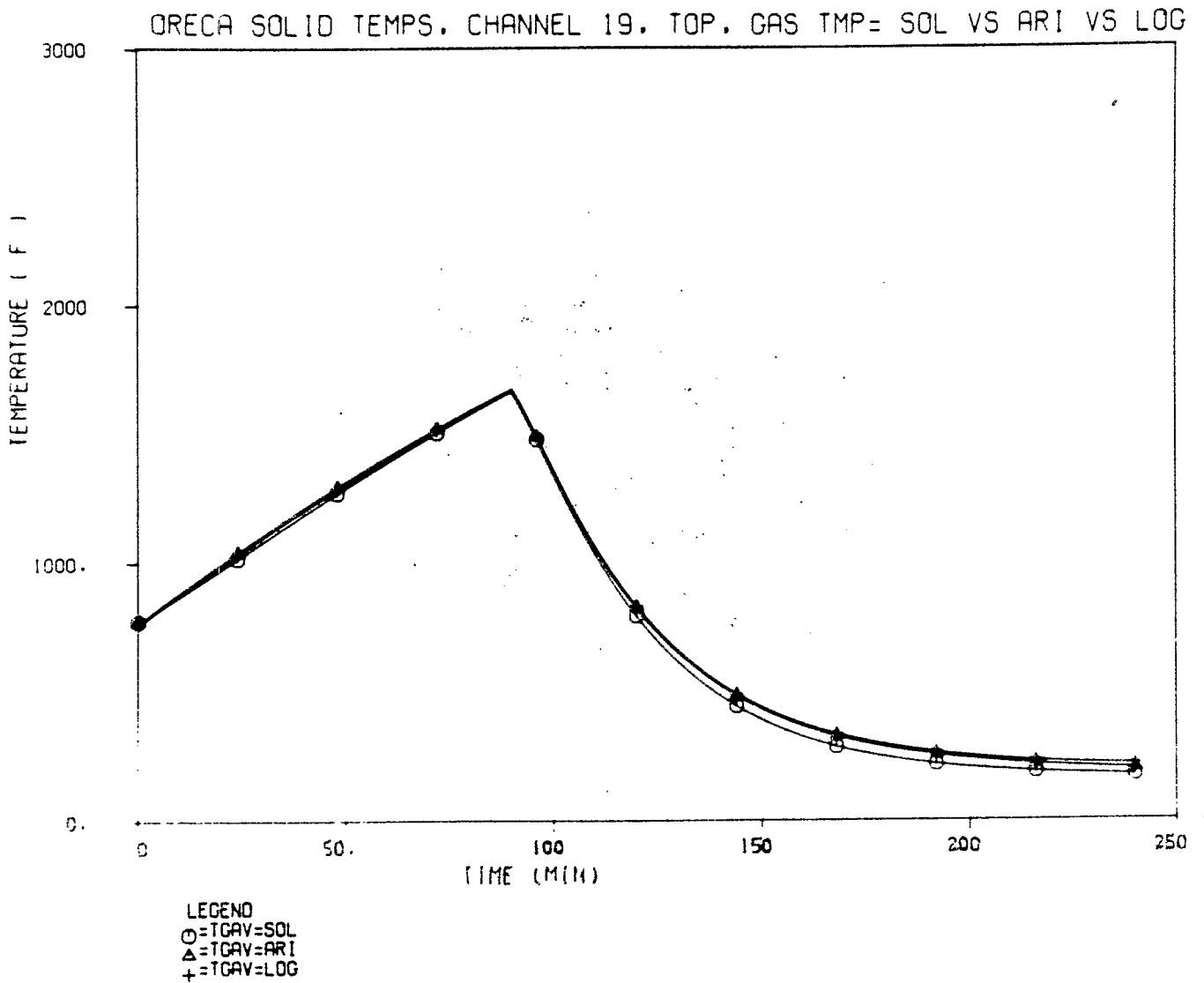


Figure B-41. Channel 18 core temperature at top node (J=1) for case of gas temperatures being varied in the evaluation of densities in pressure drop terms.

ORECA SOLID TEMPS. CHANNEL 19. CENTER (J=5). GAS TMP= SOL VS ARI VS LOG

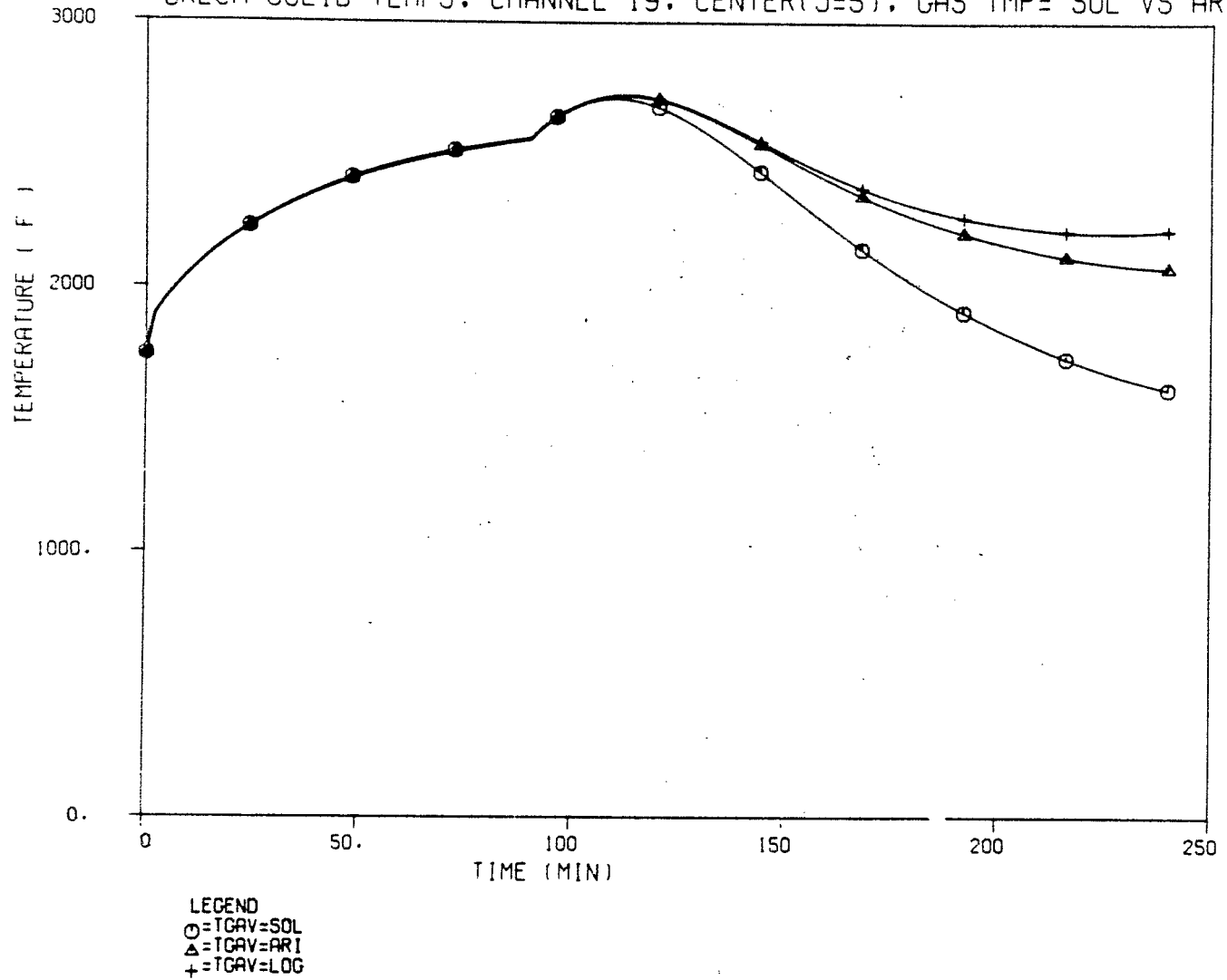


Figure B-42. Channel 19 core temperature at center node (J=5) for case of gas temperatures being varied in the evaluation of densities in pressure drop terms.

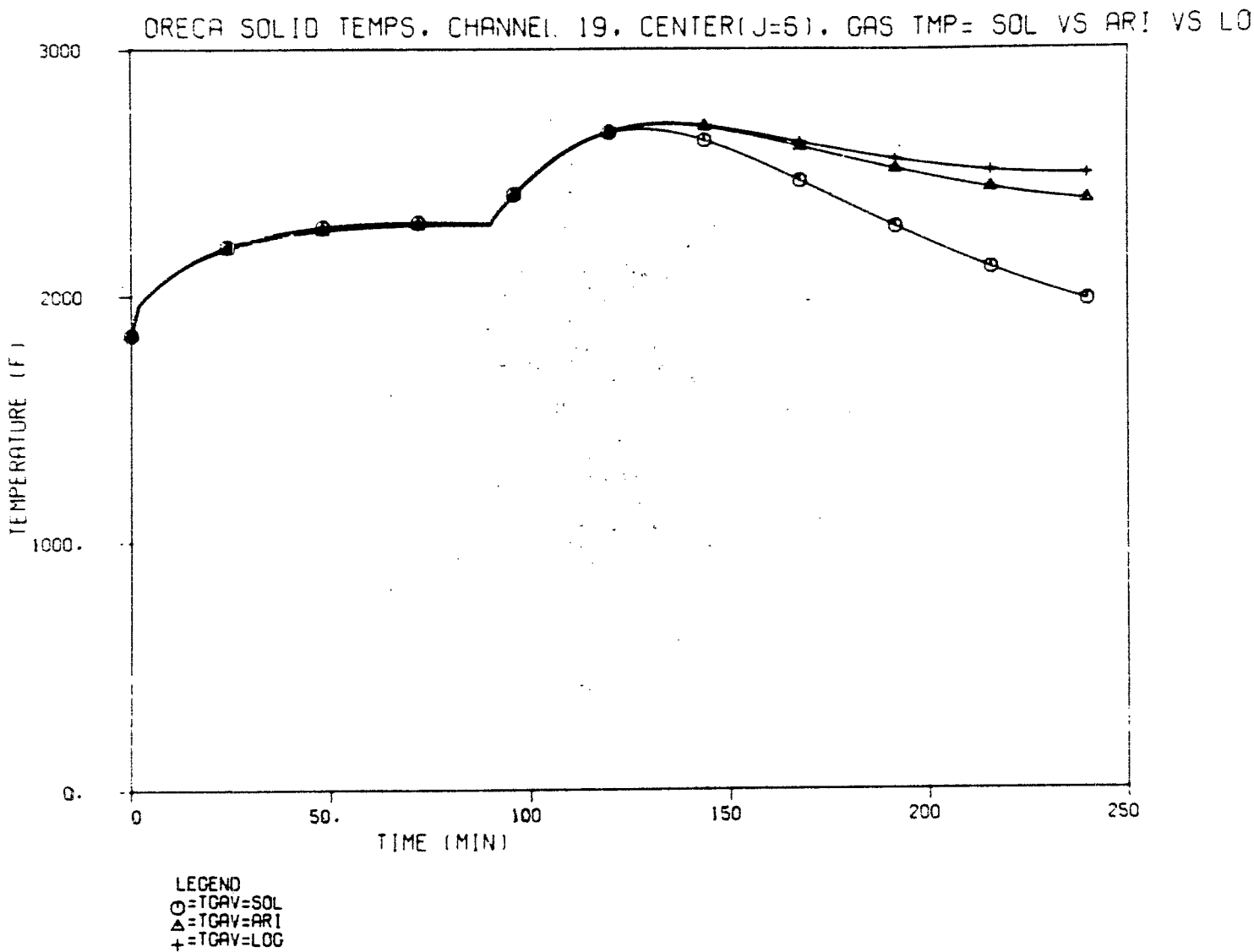


Figure B-43. Channel 19 core temperature at center node (J=6) for case of gas temperatures being varied in the evaluation of densities in pressure drop terms.

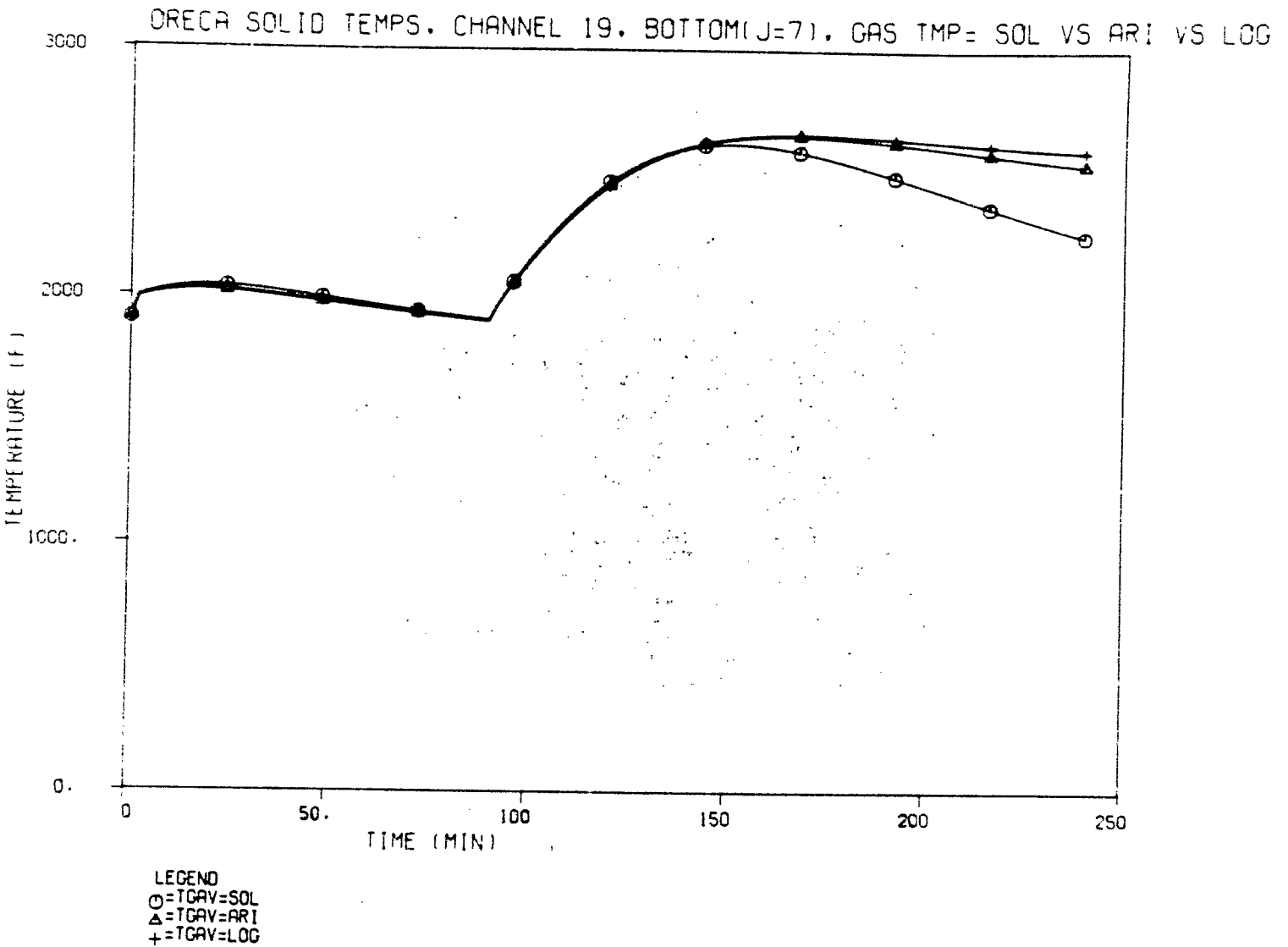


Figure B-44. Channel 19 core temperature at center node (J=7) for case of gas temperatures being varied in the evaluation of densities in pressure drop terms.

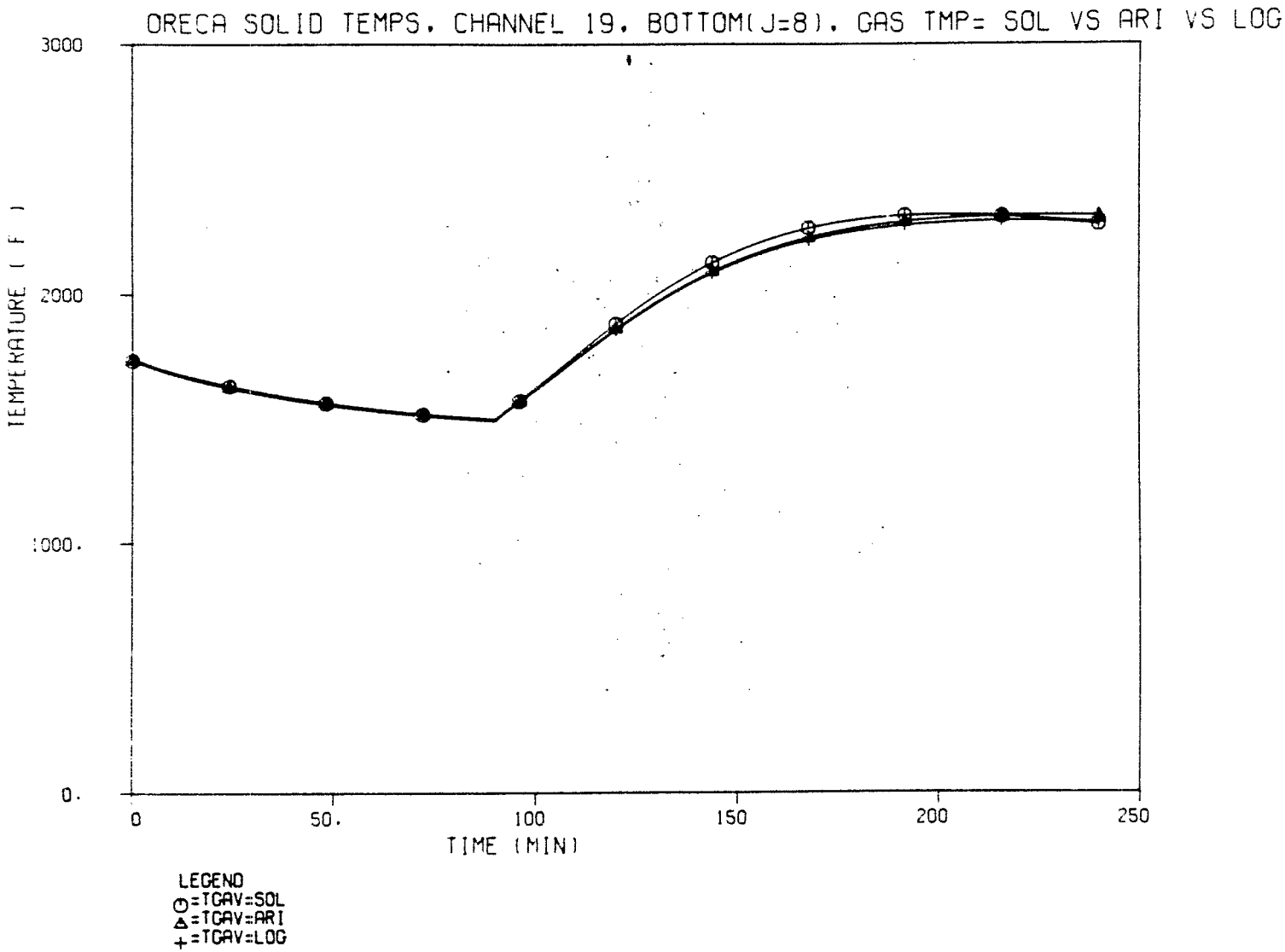


Figure B-45. Channel 19 core temperature at bottom node (J=8) for case of gas temperatures being varied in the evaluation of densities in pressure drop terms.

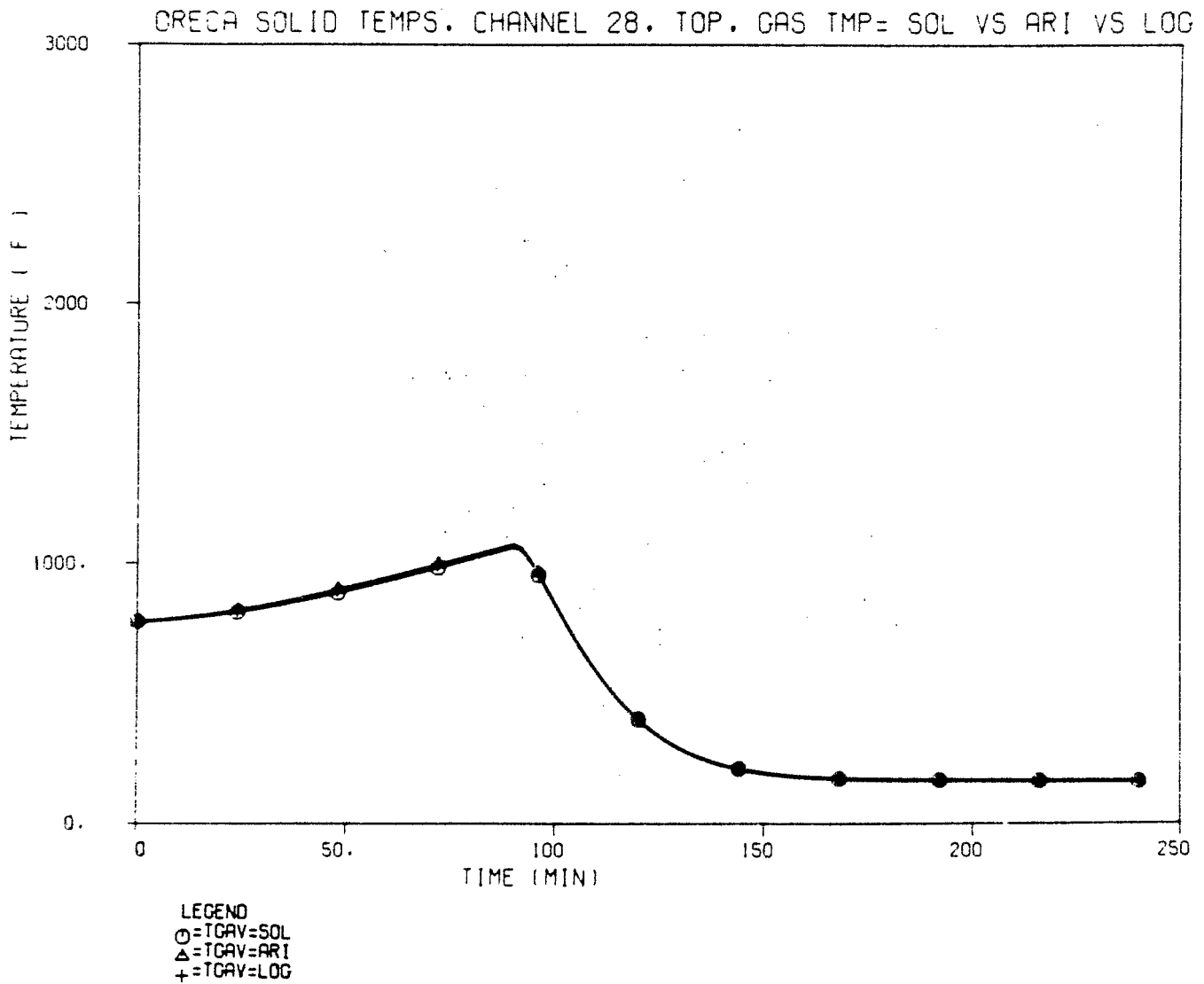


Figure B-46. Channel 28 core temperature at top node (J=1) for case of gas temperatures being varied in the evaluation of densities in pressure drop terms.

OPECA SOLID TEMPS. CHANNEL 28, CENTER(J=5). GAS TMP= SOL VS ARI VS LOG

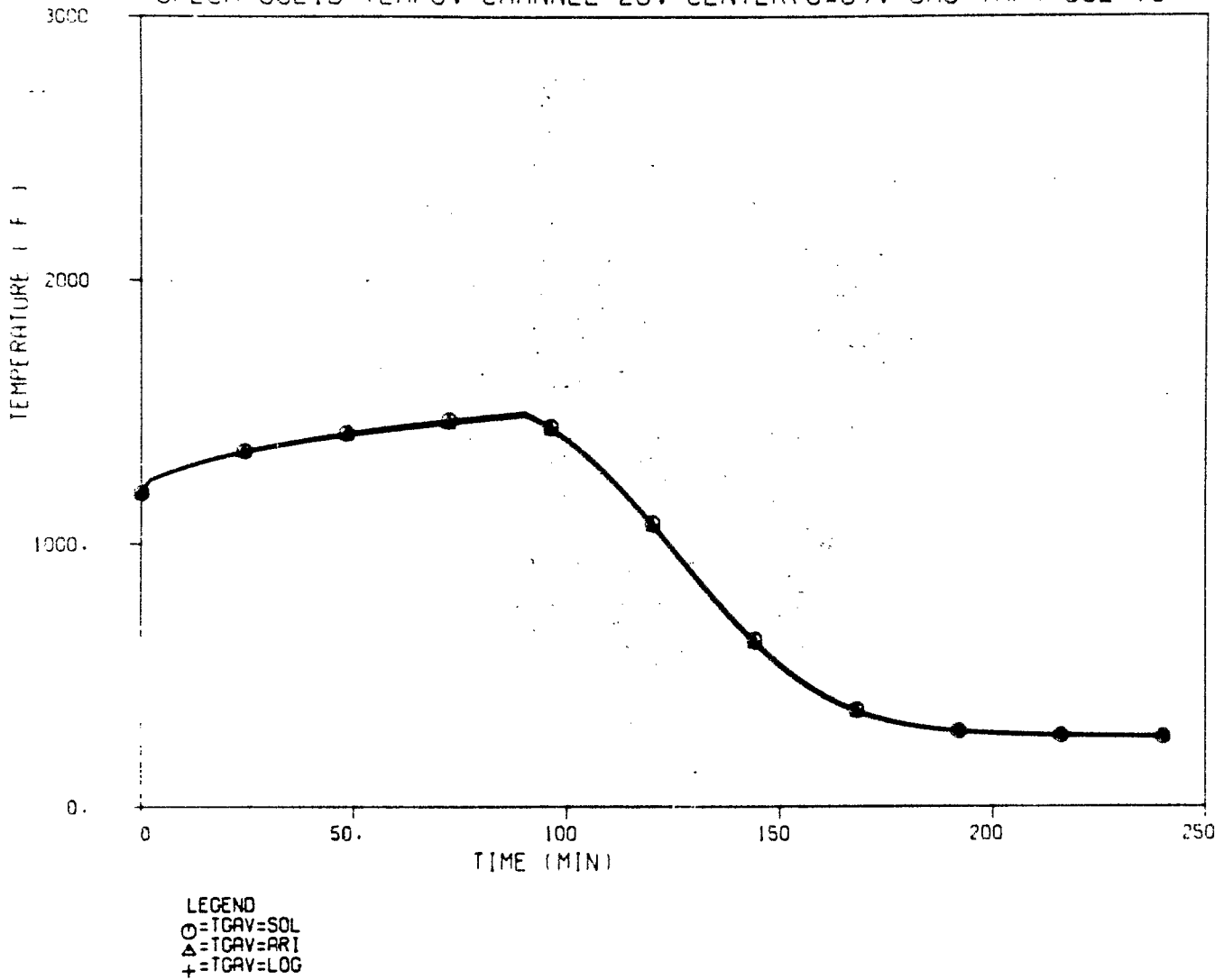


Figure B-47. Channel 28 core temperature at center node (J=5) for case of gas temperatures being varied in the evaluation of densities in pressure drop terms.

ORECA SOLID TEMPS. CHANNEL 28. BOTTOM(J=8). GAS TMP= SOL VS ARI VS LOG

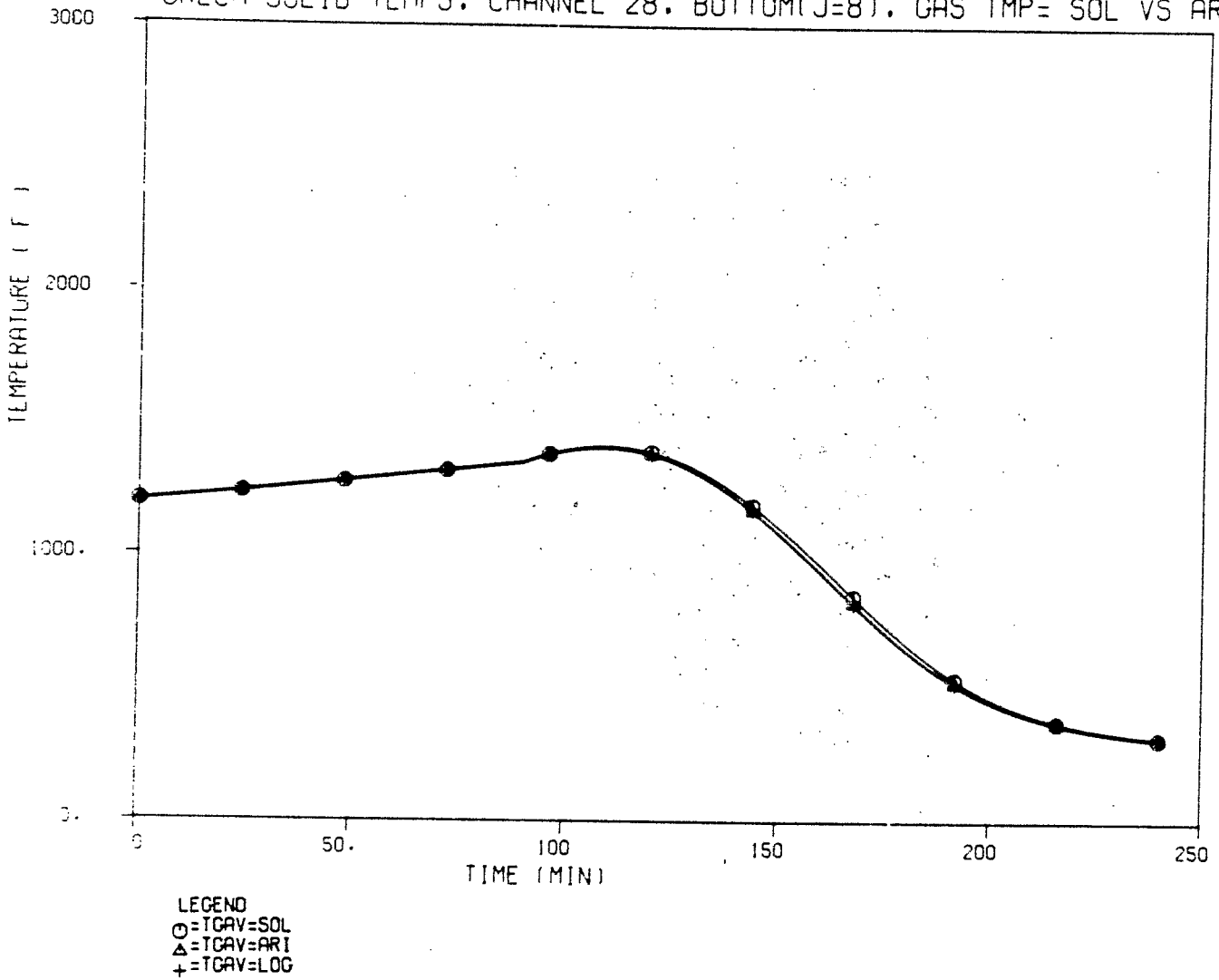
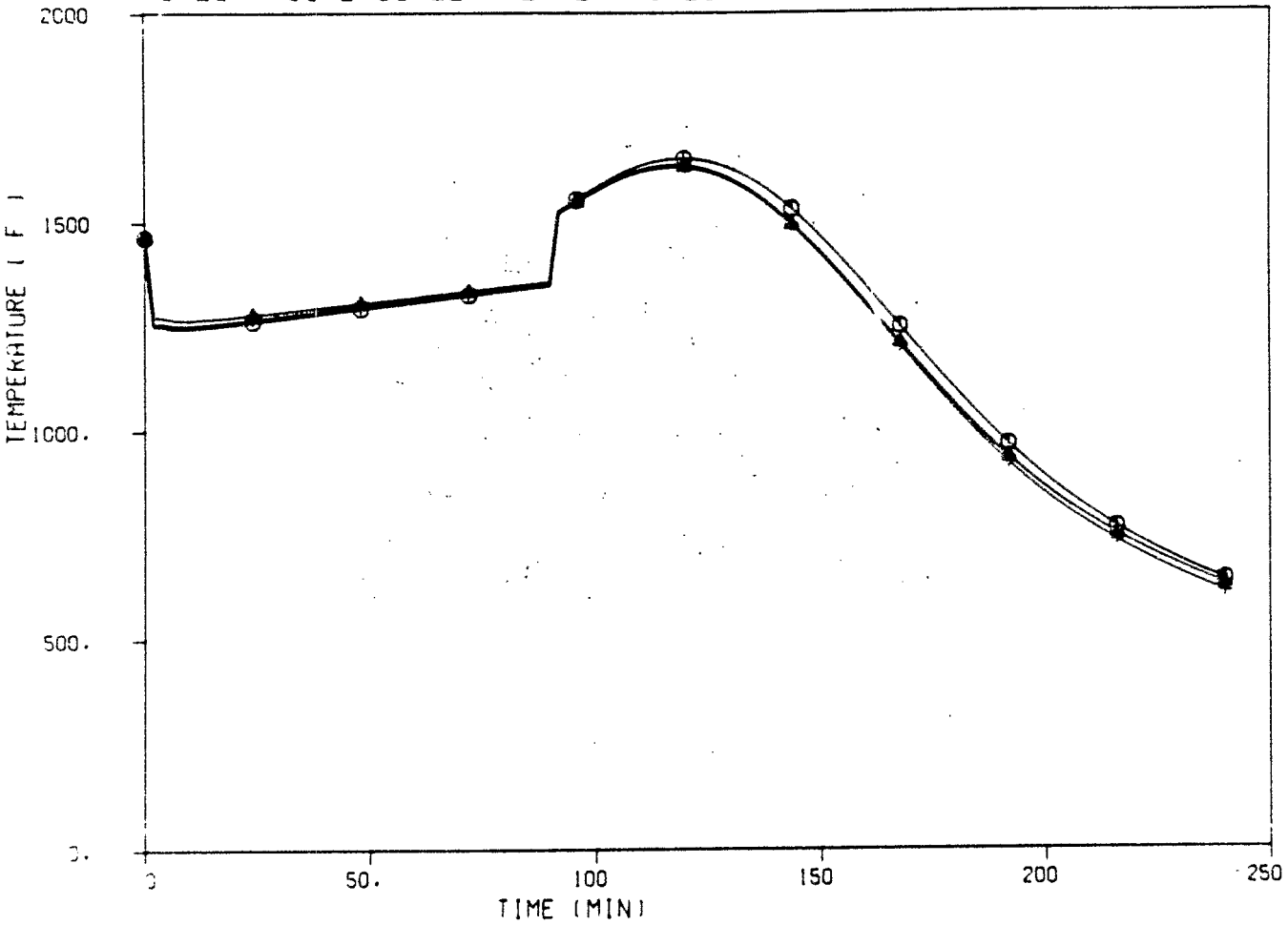


Figure B-48. Channel 28 core temperature at bottom node (J=8) for case of gas temperatures being varied in the evaluation of densities in pressure drop terms.

ORECA CORE OUTLET TEMPERATURES (TOP)



LEGEND
 ○=TGAV-SOL
 △=TGAV-ARI
 +=TGAV-LOG

Figure B-49. Temperature at core outlet position for case of gas temperatures being varied in the evaluation of densities in pressure drop terms.

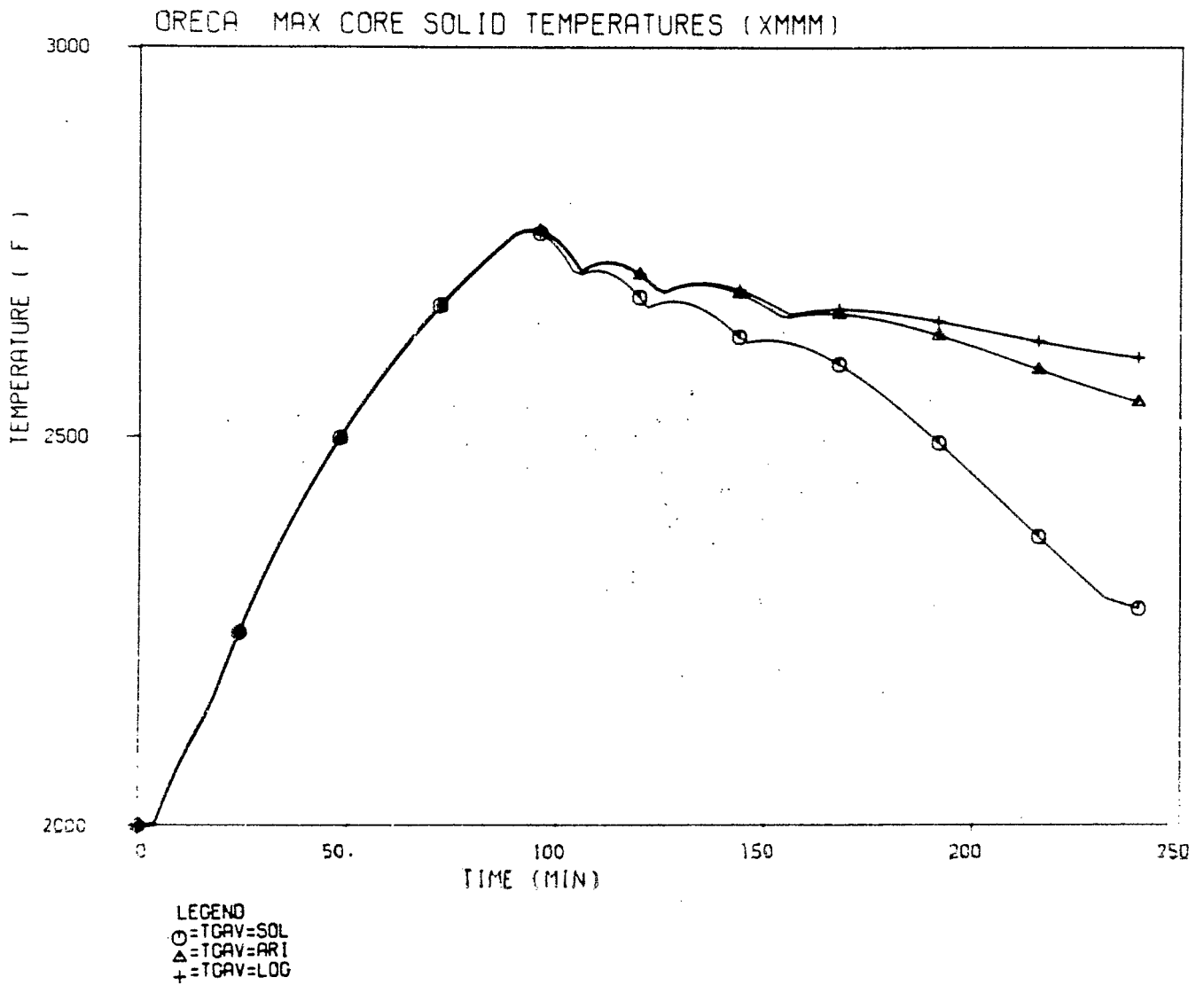


Figure B-50. Peak core temperature for case of gas temperatures being varied in the evaluation of densities in pressure drop terms.

Appendix C

Idealized Heat Conduction Problem in HTGR Core Configuration

The ORECA code provides for a three-dimensional core and includes three-dimensional heat conduction. With the properties and sizes of an HTGR core the characteristic times for conduction to be essential are very large. A Fourier number of unit order is only reached after 1900 hrs, see Section 3, above.

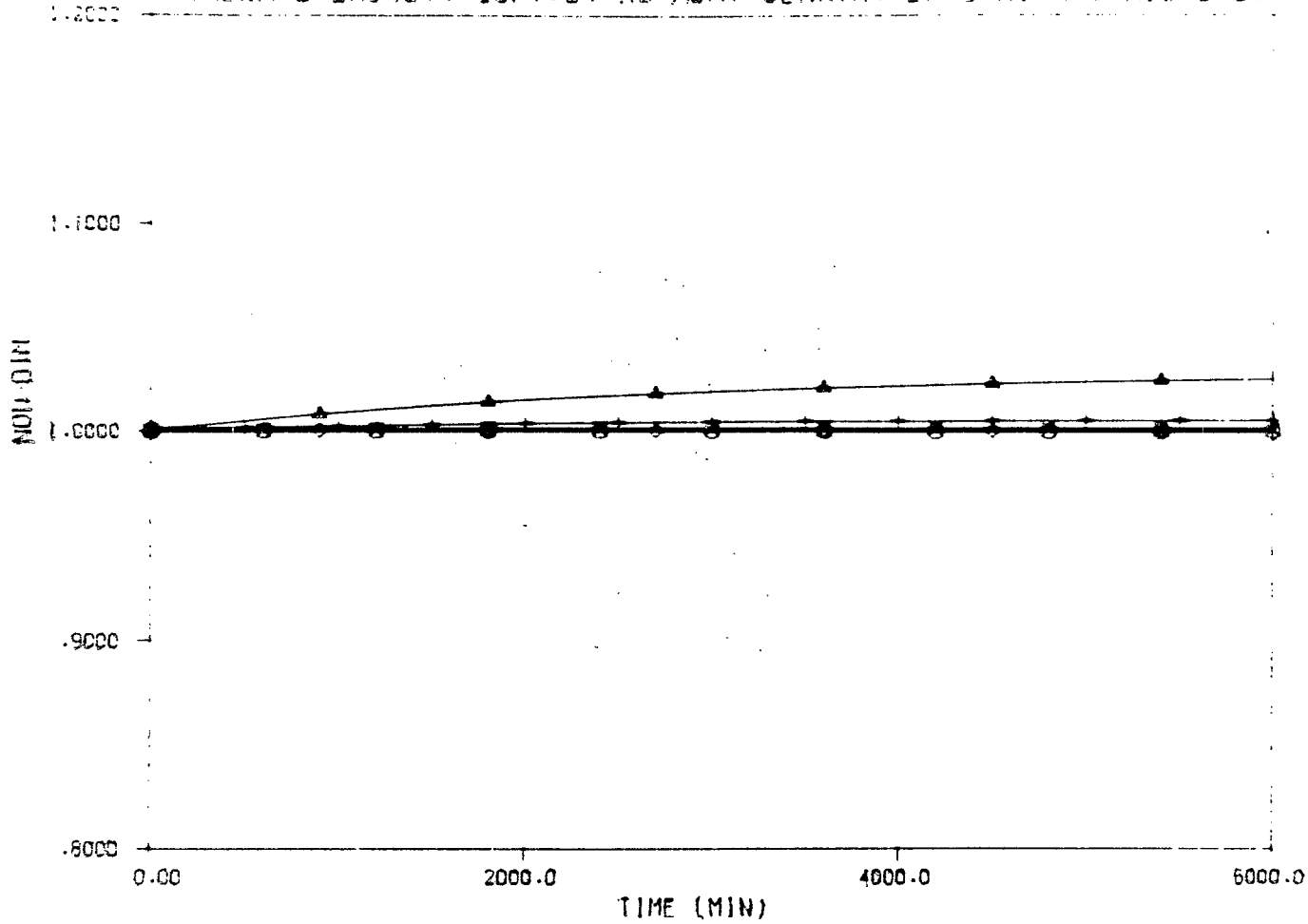
To assess the accuracy of the exponential algorithm used by ORECA in solving the three-dimensional heat conduction problem a simple homogeneous thermal conduction problem was solved in the HTGR core configuration of the code. The temperatures in the active core ($1 \leq i \leq 37$, $2 \leq j \leq 7$) are set to 3000°F, and the temperatures in the side-, top-, and bottom-reflectors are set to 1000°F. There is neither any coolant flow, nor any internal heat generation. The ultimate steady state temperature for this problem is only reached at $Fou > 1$, i.e. for times of the order of 2000 hrs. The transient was followed here for 100 hrs only using the exponential algorithm (mode=EXPO) or a conservative finite difference algorithm (mode=FINDIF). Three property options were permitted:

- IØPT = 0 all properties are constant
- IØPT = 1 the active core properties are temperature dependent;
 the side reflector properties are constant; the top
 and bottom reflector ($j = 1$ and 8) have a higher mass
 than the other active core regions (this is exactly
 corresponding to the ORECA code)
- IØPT = 2 all properties are temperature dependent; the same
 mass correction as in IØPT = 1 is applied for the
 top and bottom reflector ($j = 1$ and 8).

Trial runs showed that the FINDIF solutions of 50 min and 10 min time steps were within plotting accuracy. The 10 min time step results will be compared to the EXPØ results. Some results are shown in Figures C-1 to C-8.

Figures C-1 to C-4 show that for constant properties (IØPT = 0) the exponential solution approaches the conservative finite difference solution as the time step is reduced. However, in the case IØPT = 2 the EXPO model loses energy and converges with reduced time step size to a final steady state temperature which lies about 200°F lower than the conservative solution as shown in Figures C-5 to C-8. Thus, the simplified property treatment of the exponential algorithm can improve computational speed, but can also result in significant errors in the final solution of long term transients.

THERMAL ENERGY. IOPT=0. NO HEAT GENRTN. EXPC WITH VARIOUS DT



LEGEND
 ○=FD 10.
 △=EX 300.
 +=EX 50.
 x=EX 10.
 ◇=EX 2.

Figure C-1. Thermal energy in the system, IOPT = 0.

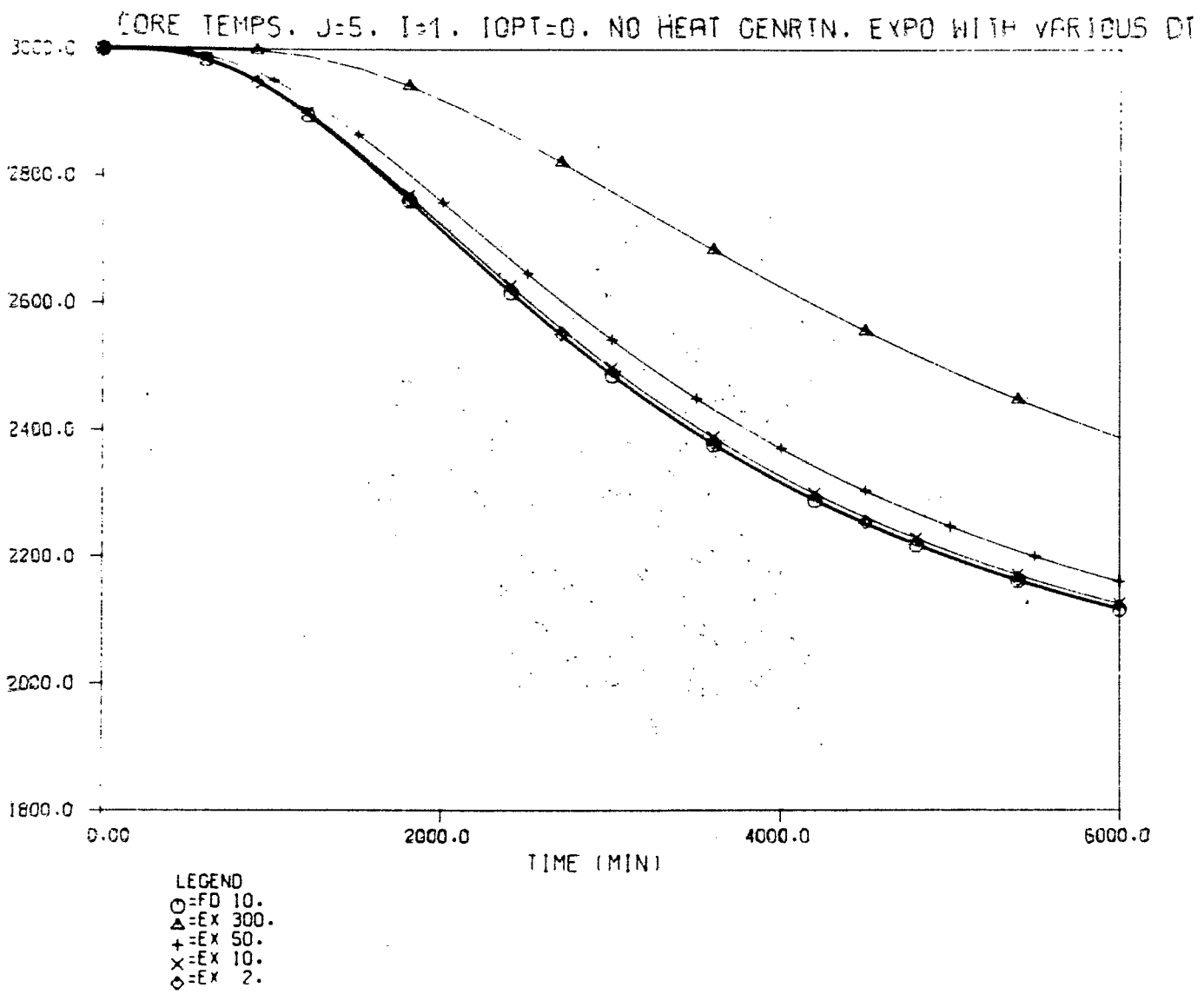


Figure C-2. Core center temperature (i=1, j=5), IOPT = 0.

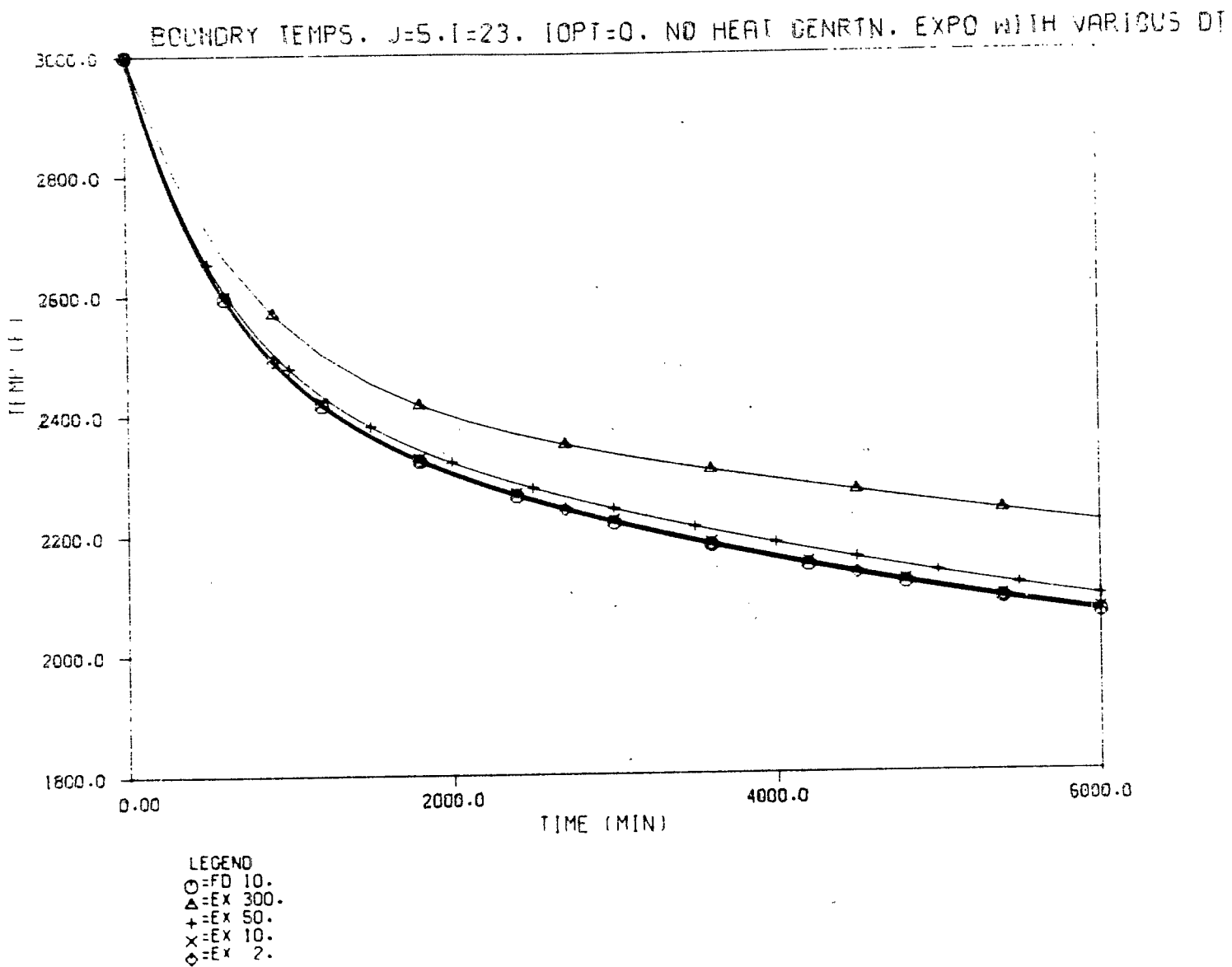


Figure C-3. Core boundary temperature ($i=23, j=5$), IOPT = 0.

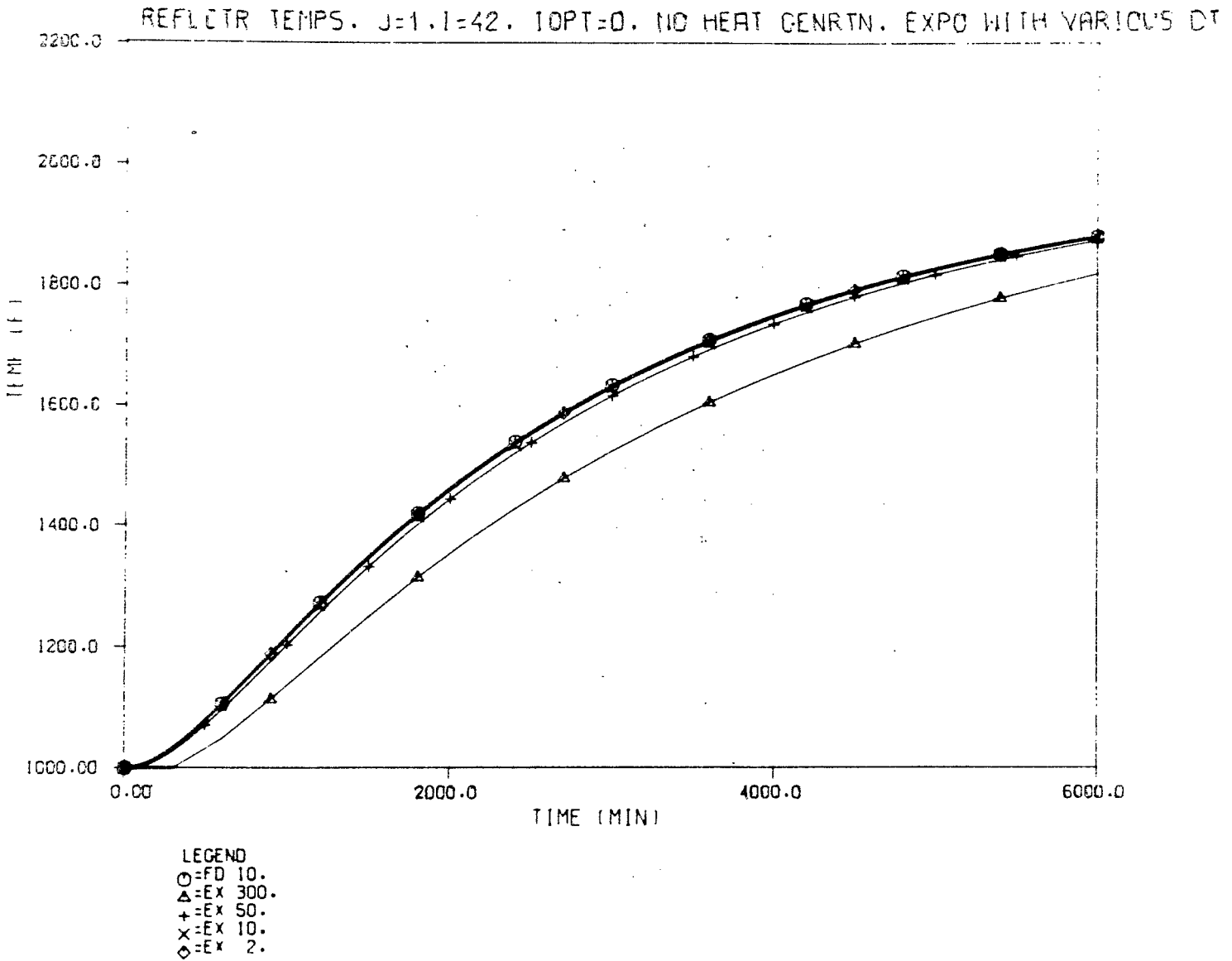


Figure C-4. Reflector lower temperature (i=42, j=1), IOPT = 0.

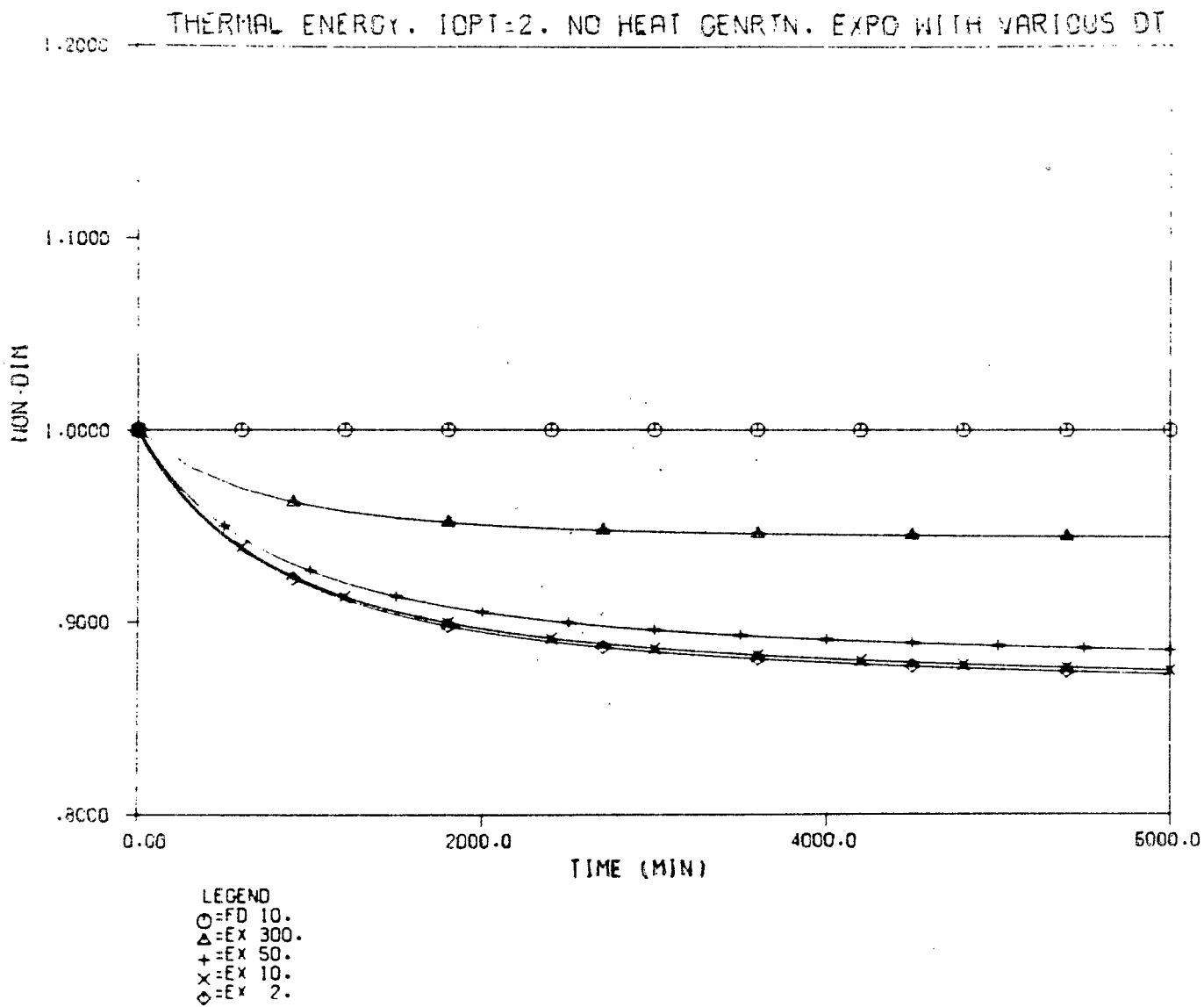


Figure C-5. Thermal energy in the system, IOPT = 2.

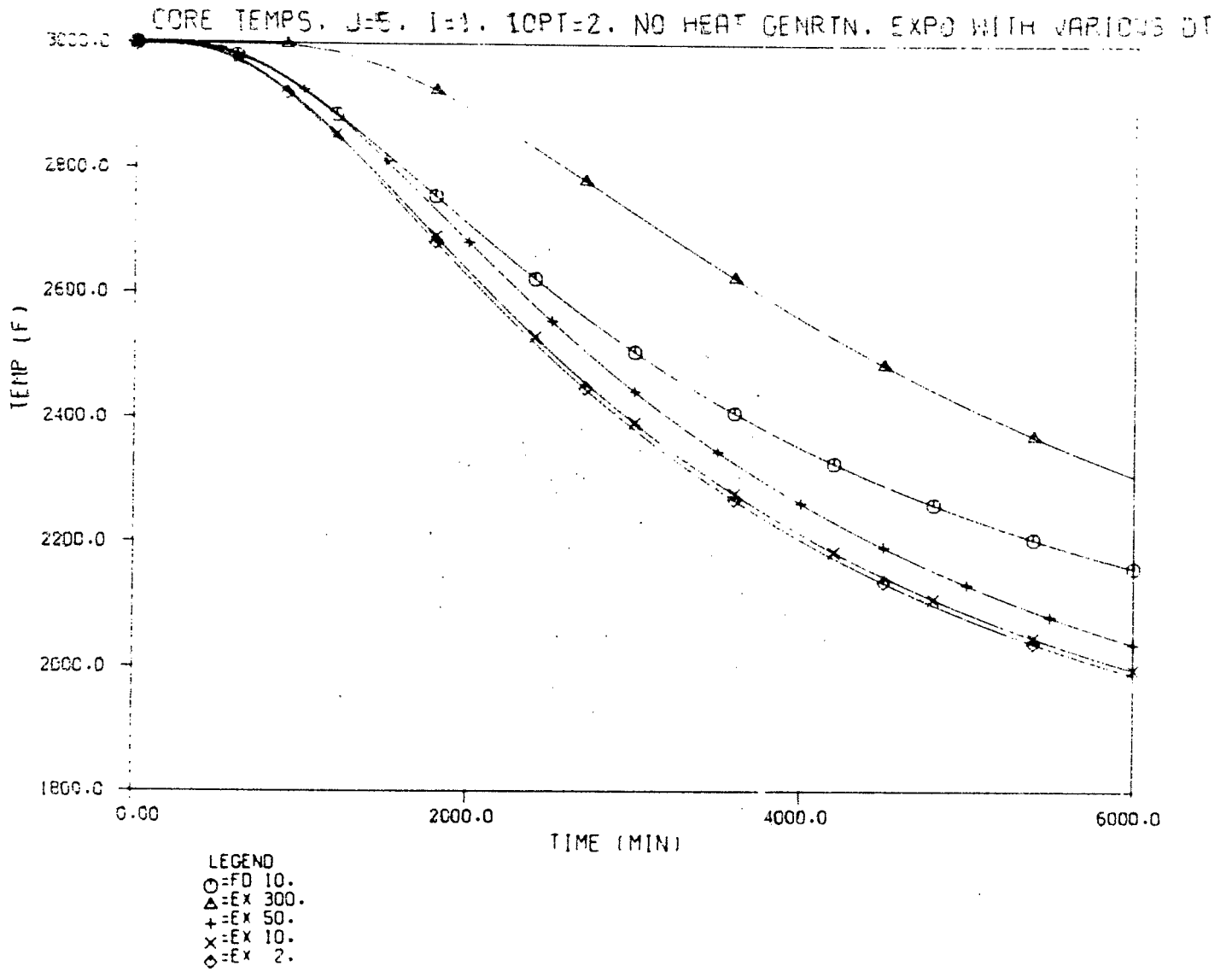


Figure C-6. Core center temperature (i=1, j=5), IOPT = 2.

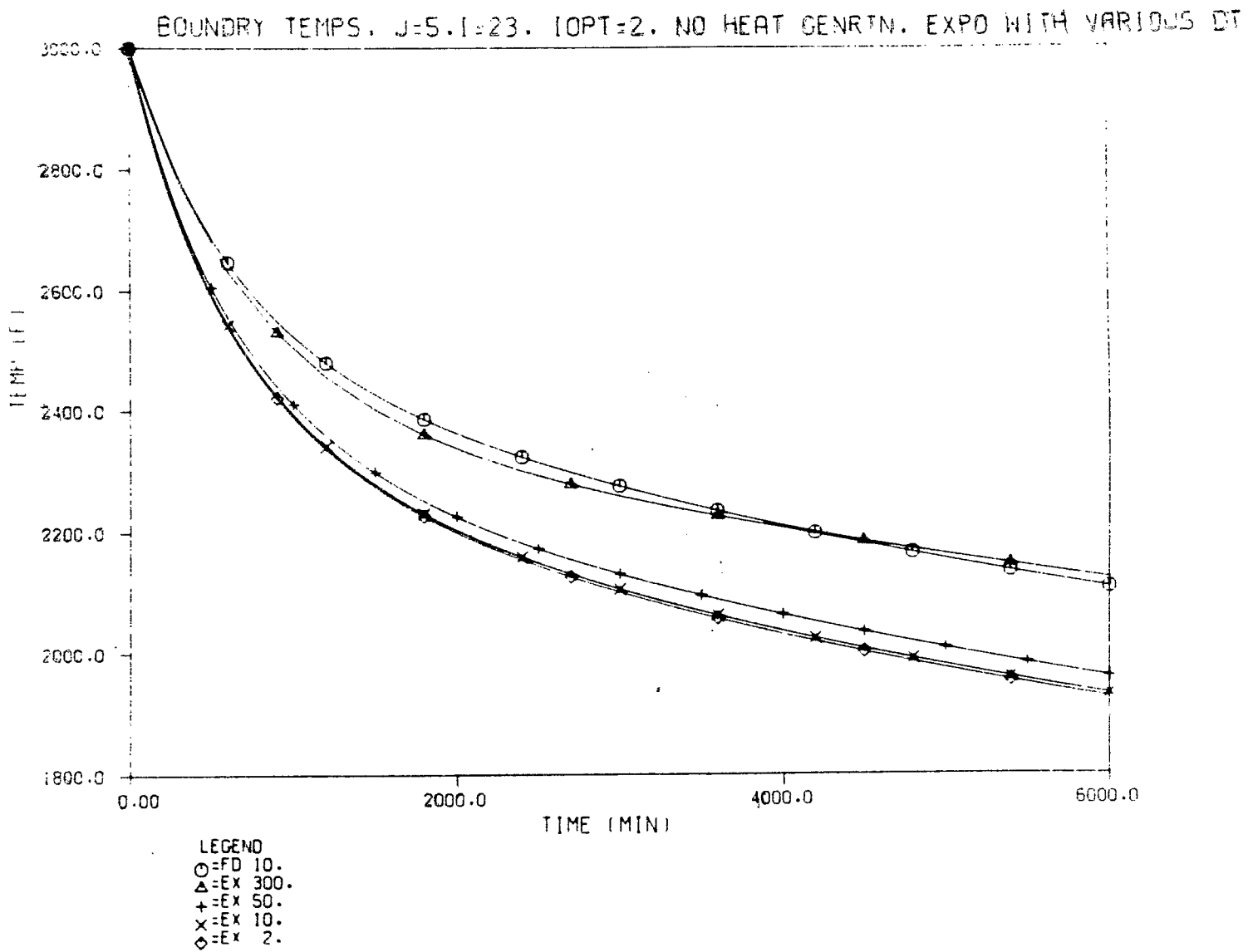


Figure C-7. Core boundary temperature (i=23, j=5), IOPT = 2.

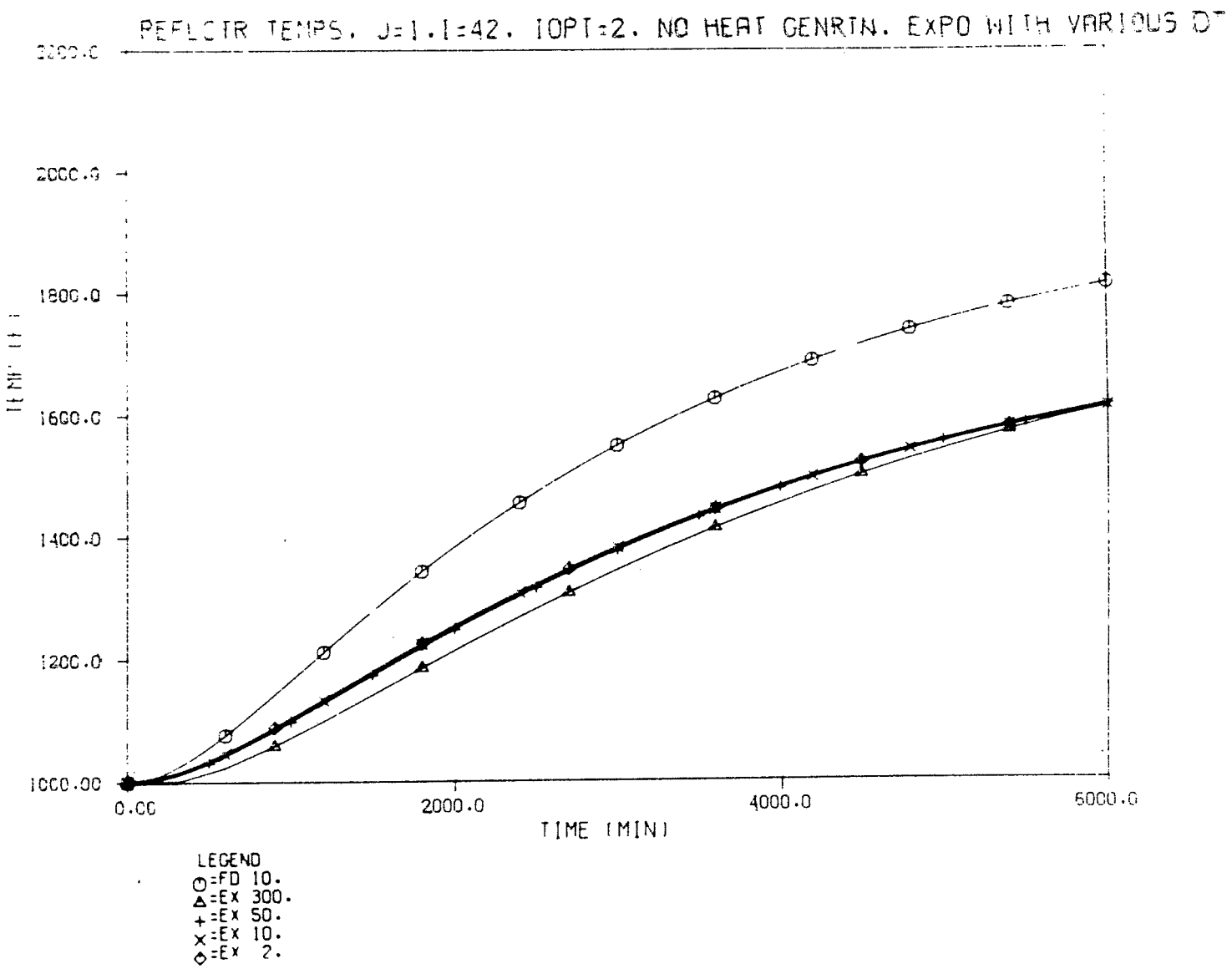


Figure C-8. Reflector lower temperature (i=42, j=1), IOPT = 2.

Notation

(Dimensions in L,M,T, θ System With

$$F = \frac{ML}{T^2} \text{ and } H = FL = \frac{ML^2}{T^2})$$

A	cross sectional area between nodes [L^2]
A'	heat transfer area per unit length [$\frac{L^2}{L}$]
c_p	specific heat [$\frac{H}{M\theta}$]
D	coolant channel hydraulic diameter [L]
f	friction factor [-]
G	mass flux [$\frac{M}{L^2T}$]
g	gravity constant [$\frac{L}{T^2}$]
k	thermal conductivity [$\frac{H}{TL\theta}$]
L	length of coolant passage (Eq. 1) [L] (also length of flow passage within node [Eqs. 3 to 5])
M	mass per node [M]
p	pressure [$\frac{F}{L^2}$]
ρ	density [$\frac{M}{L^3}$]
Q_{gen}	heat generated [$\frac{H}{T}$]
T	temperature [θ]
t	time [T]
U	overall heat transfer coefficient [$\frac{H}{L^2T\theta}$]
W	mass flow [$\frac{M}{T}$]

X running coordinate in flow direction [L]

Δx distance between nodes [L]

Subscripts

i lateral refueling region or coolant channel

j axial nodal position

f1 coolant

s solid core

Superscript

\sim averaged over coolant channel

References

1. S. J. Ball: "ORECA-1: A Digital Computer Code for Simulating the Dynamics of HTGR Cores for Emergency Cooling Analyses," ORNL/TM-5159, Oak Ridge National Laboratory, Oak Ridge, Tennessee, April, 1976.
2. A. M. Clausing: "Numerical Methods in Heat Transfer," p. 157, Advanced Heat Transfer, B. T. Chao, ed., University of Illinois Press, Urbana, Illinois, 1969.

Distribution List

S. Aronson
S. Ball
N. Corngold
D. Davis
J. Fassbender
E. A. Fletcher
R. Foulds
W. Y. Kato
H. C. Kouts
J. Lamarsh
A. McEvily
R. A. Meyer
D. Okrent
B. E. Olsen
D. G. Schweitzer
R. A. Strehlow
K. Stroh
P. Williams